수의학박사학위논문

동맥경화 칼슘 침착에서 Thioredoxin Interacting Protein 의 역할

Thioredoxin Interacting Protein in Atherosclerotic Calcification

2023 년 2 월

서울대학교 대학원

수의학과 수의병리학 전공

우 상 호

동맥경화 칼슘 침착에서
Thioredoxin Interacting Protein의 역할

Thioredoxin Interacting Protein
in Atherosclerotic Calcification

지도교수 김 대 용

이 논문을 수의학 박사 학위논문으로 제출함

2022 년 11 월

서울대학교 대학원 수의학과 수의병리학 전공

우 상 호

우상호의 박사 학위 논문을 인준함

2023 년 01 월

위 원 장 _____ 김용백 (인)

부 위 원 장 _____ 김대용 (인)

위 원 _____ 이소영 (인)

위 원 _____ 최양규 (인)

위 원 _____ 최재훈 (인)

ABSTRACT

Thioredoxin Interacting Protein in Atherosclerotic Calcification

(Supervisor: Dae-Yong Kim, D.V.M., Ph.D.)

Sang-Ho Woo

Department of Veterinary Pathology, College of Veterinary Medicine, Graduate School, Seoul National University

The osteochondrogenic switch of vascular smooth muscle cells (VSMCs) is a pivotal cellular process in atherosclerotic calcification. However, the exact molecular mechanism governing this process remains to be elucidated. Previous studies have suggested that multifunctional protein thioredoxin-interacting protein (TXNIP) play a role in the pathophysiology of VSMCs and calcification in atherosclerosis. In this study, I explored the regulatory role of TXNIP in the phenotypical transitioning of VSMCs toward osteochondrogenic cells responsible for atherosclerotic calcification.

The atherosclerotic phenotypes of *Txnip*$^{-/-}$ mice were analyzed in combination with single-cell RNA-sequencing (scRNA-seq). The atherosclerotic phenotypes of *Tagln*-Cre; *Txnip*$^{flox/flox}$ mice (SMC-specific

Txnip ablation model), and bone marrow transplanted mice (hepatopoietic ablation of *Txnip* model) were analyzed. Public scRNA-seq dataset GSE159677 was reanalyzed to define the gene expression of *TXNIP* in the VSMCs of human calcified atherosclerotic plaques. The expression patterns of TXNIP in endarterectomized human atherosclerosis samples were analyzed by immunohistochemistry. *In vitro* mechanism study was performed using primary cultured VSMCs.

Atherosclerotic lesions of $Txnip^{-/-}$ mice presented significantly increased calcification and deposition of collagen content compared to $Txnip^{+/+}$ mice. Subsequent single-cell RNA-sequencing (scRNA-seq) analysis identified the modulated VSMC and osteochondrogenic clusters, which were VSMC-derived populations. The osteochondrogenic cluster was markedly expanded in $Txnip^{-/-}$ mice compared to $Txnip^{+/+}$ mice. The pathway analysis of the VSMC-derived cells revealed enrichment of bone and cartilage formation related pathways and BMP signaling in $Txnip^{-/-}$ mice. Reanalyzing GSE159677 revealed that *TXNIP* was downregulated in the modulated VSMC and osteochondrogenic clusters of human calcified atherosclerotic lesions. Atherosclerotic lesions of *Tagln*-Cre; $Txnip^{flox/flox}$ mice recapitulated the calcification and collagen-rich phenotypes of $Txnip^{-/-}$ mice, whereas hematopoietic absence of TXNIP did not affect atherosclerotic calcification. Primary VSMC culture experiments revealed that suppression of TXNIP accelerates osteodifferentiation and upregulates both canonical and non-

canonical BMP signaling. Treatment with the BMP signaling inhibitor K02288 abrogated the effect of TXNIP suppression on osteodifferentiation.

In conclusion, TXNIP is a regulator of atherosclerotic calcification by suppressing BMP signaling to inhibit the transition of VSMCs toward an osteochondrogenic phenotype. This study broadened the understanding of atherosclerosis, and importantly, discovered a novel role of TXNIP as an inhibitor of atherosclerotic calcification.

Keywords: atherosclerosis, calcification, vascular smooth muscle cell, phenotypic transition, TXNIP, osteochondrogenic, bone morphogenetic protein

Student Number: 2016-21767

CONTENTS

ABSTRACT i
CONTENTS iv
ABBREVIATIONS 1
LITERATURE REVIEW 3
Atherosclerosis: general introduction 3
Calcification in atherosclerosis 7
Vascular smooth muscle cells in atherosclerosis 11
The role of VSMCs in atherosclerotic calcification 17
The roles of BMP signaling in osteoblast differentiation and implications in atherosclerotic calcification 19
Thioredoxin-interacting protein 23
Objective 26
INTRODUCTION 28
MATERIALS and METHODS 32
Animal models 32
Bone marrow transplantation 33
Necropsy, tissue preparations, and histological staining of atherosclerotic lesions 34
qRT-PCR 35
Preparation of scRNA-seq experiment 37

Pre-processing of the scRNA-seq data 38
Analysis of scRNA-seq data 38
In situ hybridization 40
Analysis of human scRNA-seq data GSE159766 41
Immunostaining of human atherosclerotic lesion samples 42
Primary VSMC culture experiment 43
Immunoblotting 44
Statistical analysis 45
RESULTS 47
Genetic ablation of *Txnip* in mice markedly increased the deposition of calcium and collagen in the lesion. 47
ScRNA-seq analysis revealed that the "osteochondrogenic" cluster enriched with bone- and cartilage-related genes was markedly expanded in *Txnip* KO mice. 52
Hematopoietic deficiency of TXNIP did not affect the atherosclerotic lesion phenotype. 60
The osteochondrogenic cluster is derived from VSMCs. 64
Analyzing VSMC-derived cell clusters revealed the enhancement of bone and cartilage formation pathways in *Txnip* KO mice. 68
TXNIP is downregulated in the modulated VSMCs and osteochondrogenic cells of human calcified atherosclerotic plaques. 76
VSMC-specific *Txnip* ablation recapitulates the calcification and collagen-rich plaque phenotype of global *Txnip* KO mice. 79

TXNIP suppression in VSMCs accelerate osteodifferentiation and augments BMP signaling. 85
TXNIP inhibits osteodifferentiation of VSMCs by suppressing both canonical and non-canonical BMP signaling. 91
Wnt/β-catenin signaling is not involved in the effect of TXNIP on VSMC osteodifferentiation. 96
DISCUSSION 98
CONCLUSION 106
국문 초록 107
REFERENCES 110
감사의 글 126

ABBREVIATIONS

BM: Bone marrow

BMP: Bone morphogenetic protein

CAC: Coronary artery calcium

CHO: Cholesterol

CKD: Chronic kidney disease

Co-Smad: Common Smad

CT: Computed tomography

DEG: Differentially expressed gene

DIT: Diffuse intimal thickening

ECM: Extracellular matrix

ERK: Extracellular signal-regulated kinase

HAT: Histone acetyltransferase

HDAC: histone deacetylase

HDL: High density lipoprotein

HFD: High-fat diet

Id: Inhibitor of DNA binding

I-Smad: Inhibitory Smad

KO: Knock out

LDL: Low-density lipoprotein

MAPK: Mitogen activated protein kinase

MSC: Mesenchymal stem cell

MYOCD: Myocardin

NK: Natural killer cell

PDGF: Platelet-derived growth factor

qRT-PCR: Quantitative reversed transcriptase polymerase chain reaction

ROS: Reactive oxygen species

R-Smad: Receptor-activated Smad

ScRNA-seq: Single cell RNA-sequencing

SMC: Smooth muscle cells

SRF: Serum response factor

TGFβ: Transforming growth factor β

TXNIP: Thioredoxin-interacting protein

UMAP: Uniform Manifold approximation and projection

VSMC: Vascular smooth muscle cell

WT: Wild type

LITERATURE REVIEW

Atherosclerosis: general introduction

Atherosclerosis is a major pathological process underlying most cardiovascular diseases such as heart disease, stroke, angina pectoris, and aneurysms, which are the leading causes of global death (Libby, Buring et al. 2019). Once limited to Western countries in the past, atherosclerosis now affects people worldwide, including those living in developing countries, mainly due to population growth and increased life expectancy (Murray and Lopez 2013). Atherosclerosis reproducibly affects the multifocal sites of arterial trees. It typically affects the inner curvatures and branch points such as the coronary arteries, iliofemoral arteries, abdominal arteries, and carotid bifurcations, which are areas with low or oscillatory endothelial shear stress (Bentzon, Otsuka et al. 2014). Atherosclerosis is primarily driven by native or aggregated low-density lipoproteins (LDLs) in combination with other risk factors, including diabetes mellitus, smoking, hypertension, and male sex. Once accumulated in the arterial intima, LDLs are modified by oxidation and aggregation and act as chronic stimulators that provoke innate and adaptive immune responses. In turn, endothelial cells and vascular smooth muscle cells (VSMCs) express adhesion molecules, chemoattractants, and variable cytokines that home and attract monocytes, which then differentiate into macrophages and dendritic cells. Lipid-phagocytized macrophages become foam cells, and various pathological events, such as apoptosis, necrosis,

VSMC proliferation, matrix synthesis, and calcification, occur in complex interactions (Bentzon, Otsuka et al. 2014).

Atherosclerotic lesions can be classified into several histological subtypes according to their progression (Virmani, Kolodgie et al. 2000): adaptive intimal thickening, intimal xanthoma, pathological intimal thickening, fibroatheroma, and fibrocalcific plaque. Adaptive intimal thickening is the earliest lesion characterized by intimal accumulation of VSMCs. Intimal xanthomas indicate the intimal accumulation of foam cells. Then the lesion progresses to pathological intimal thickening, characterized by the extracellular accumulation of lipid pools without apparent necrosis. Fibroatheroma indicates an advanced stage of atherosclerosis, characterized by the formation of a fibrous cap, necrotic core, and accumulation of a collagenous extracellular matrix (ECM). The lesion eventually accumulates calcified areas in the necrotic core and surrounding tissues and becomes a fibrocalcific plaque.

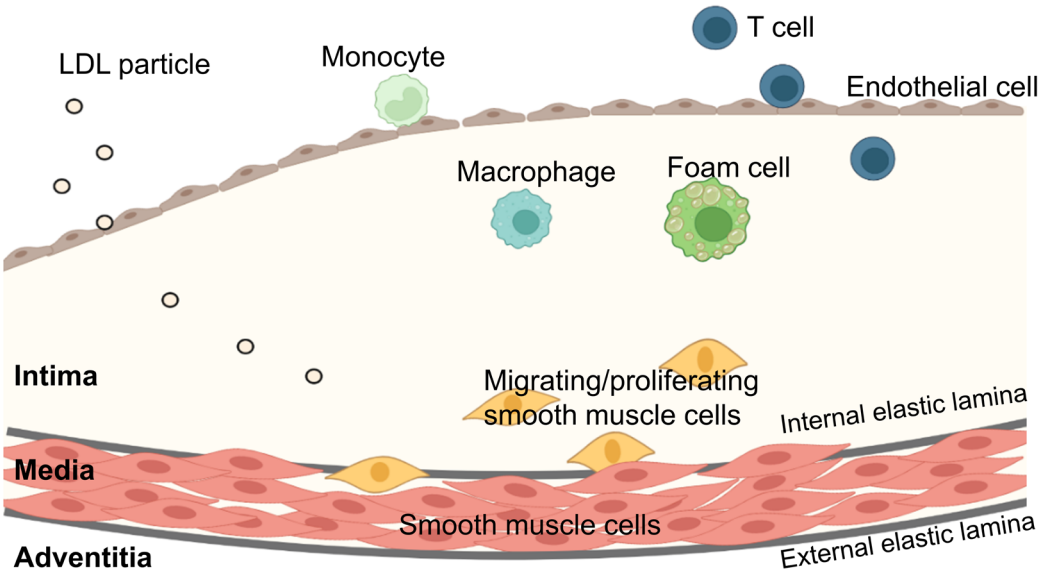

Fig 1. Initiation and progression of atherosclerosis. (Modified from Libby, Buring et al. 2019)

Atherosclerosis causes clinical complications mainly by limiting blood flow or thrombosis. Various clinical sequelae can occur depending on the affected vascular beds, such as angina and myocardial infarction in the coronary arteries, or stroke in the carotid arteries (Basatemur, Jørgensen et al. 2019). In the past, plaque rupture was considered a major mechanism for atherosclerotic thrombosis. In this context, the concept of "vulnerable plaque," which is histologically characterized by a lipid and macrophage-rich, large necrotic core and thin fibrous cap, had been receiving lots of attention. Hence, a large number of mouse atherosclerosis model studies have focused on the abovementioned histological criteria, although mouse atherosclerotic plaques seldom rupture to cause thrombosis (Bentzon, Otsuka et al. 2014; Libby and

Pasterkamp 2015). Recent studies have reported that “vulnerable plaques” seldom rupture, provoking thrombosis. In addition, generalized lipid-lowering therapy, such as statin administration, changes atherosclerotic plaques toward less-lipid-laden, less-inflamed, and more fibrous phenotypes. In this context, a new mechanism called “plaque erosion,” which is histologically characterized by the formation of thrombosis on an ECM-rich without a thin fibrous cap, less-inflamed, and lipid-laden plaque, was proposed as the principal cause of atherosclerosis-induced thrombosis (Libby and Pasterkamp 2015). In addition to plaque rupture and erosion, a “calcified nodule,” which is formed by atherosclerotic calcification and shows a distinct morphological entity, is reported to contribute to a minor portion (~5%) of atherosclerosis-induced thrombosis (Sugane, Kataoka et al. 2021; Virmani, Kolodgie et al. 2000).

Animal models have been extensively used to discover therapeutic agents or targets for atherosclerosis, and mice are most commonly utilized due to their ease of management and manipulation. However, atherosclerotic lesions between human and animal models have some important differences, which must be considered for the translation of animal study results. For example, human aortas harbor VSMCs in the intima even before the development of atherosclerosis, known as diffuse intimal thickening (Nakashima, Wight et al. 2008). Compared to that of medial VSMCs, these preexisting intimal VSMCs are reported to have different transcriptomic profiles and show more synthetic characteristics when exposed to stress signals (Mosse, Campbell et al. 1985). It is still unclear whether intimal VSMCs have a greater capacity to contribute

to the progression of human atherosclerotic lesions than that of medial VSMCs (Grootaert and Bennett 2021). Another important difference is that fibroatheroma in animal models rarely ruptures, and human atherosclerotic lesions develop relatively slowly compared with those in mice (Basatemur, Jørgensen et al. 2019; Bentzon, Otsuka et al. 2014).

Calcification in atherosclerosis

Atherosclerotic lesions can contain various noncellular components such as collagen, elastin, proteoglycans, glycosaminoglycan, and calcium. As atherosclerotic lesions progress, these noncellular components, especially fibrous and calcium, tend to gradually accumulate and often constitute most of the plaque components (Bentzon, Otsuka et al. 2014). Coronary artery calcification can be readily measured and quantified through computed tomography (CT). The resulting coronary artery calcium (CAC) score has a strong positive relationship with the total burden of atherosclerosis, indicating that calcification is a characteristic phenomenon of atherosclerosis (Alexopoulos and Raggi 2009). The CAC score can sensitively and specifically predict clinically significant coronary artery disease and identify patients at risk for adverse cardiac events. Currently, the general agreement is that high CAC scores can predict a high-risk patient rather than a vulnerable plaque or vessel. The possible roles of atherosclerotic calcification in plaque stability were proposed based on the size, location, and shape of the calcification. For instance, micro- and spotty calcifications are regarded as pro-inflammatory

processes and have a negative effect on plaque stability. On the other hand, macrocalcifications formed at the deep intima or necrotic core are considered to stabilize the plaque (Shi, Gao et al. 2020). However, there is still considerable debate regarding whether atherosclerotic calcification can serve as a marker for plaque stability or instability (Alexopoulos and Raggi 2009).

Atherosclerotic calcification can lead to a distinct type of lesion called "calcified nodule," which is histologically characterized by erupted and fractured calcified plates on a disrupted fibrous cap, accompanied by a luminal thrombus (Sato, Finn et al. 2021). Although calcified nodules account for a minority (~5%) of the causes of thrombosis related to atherosclerosis, its clinical implications were highlighted in a retrospective study. Calcified nodules were associated with a higher incidence of hypertension, chronic kidney disease (CKD), and maintenance hemodialysis. In a follow-up study, calcified nodules were highly correlated with major adverse cardiac events, which were defined by a combined outcome of death related to cardiac failure, recurrence of acute coronary syndrome, and target lesion revascularization. In addition, the recurrence rate of calcified nodules in patients implanted with drug-eluting stents who subsequently underwent target lesion revascularization was 82.4% (Sugane, Kataoka et al. 2021). These observations suggest that calcified nodules can hinder the neointimal-suppressing ability of drug-eluting stents, suggesting that different treatment approaches may be required when treating atherosclerotic lesions that harbor calcified nodules. To date, drugs that prevent or treat atherosclerotic

calcification, including statins, which have been a major treatment option for atherosclerosis, are unavailable (Durham, Speer et al. 2018).

Atherosclerotic calcification usually appears first at the necrotic core, implying that cell death (e.g., necrosis and apoptosis) and inflammatory processes are involved in the calcification process. Studies have reported that apoptotic bodies and matrix vesicles from intralesional cells (e.g., macrophages/foam cells and VSMCs) can act as nucleating agents to promote calcification. Various environmental cues, such as inflammatory cytokines (TNFα and IL-6), oxidative stress, bone morphogenetic proteins (BMPs) 2/4, changes in pyrophosphate levels, and osteocalcin, can accelerate atherosclerotic calcification (Johnson, Leopold et al. 2006). Conversely, various cytokines and molecules such as osteopontin, MGP, OPG, sclerostin, FGF-23, fetuin, or BMP7 can inhibit atherosclerotic calcification. Systemic factors, such as CKD, parathyroid hormone, vitamin D, glucocorticoids, diabetes, menopause, and osteoporosis, are also known to affect vascular calcification (Durham, Speer et al. 2018; Johnson, Leopold et al. 2006).

In the past, vascular calcification was regarded as a passive, degenerative, and unregulated process. Calcifications of both the intima (atherosclerotic calcification) and media (medial calcification) are considered to be tightly regulated active processes that recapitulate bone morphogenesis (Durham, Speer et al. 2018). Studies have shown the existence of osteo- and chondrocyte-like cells that express bone- and cartilage-related transcription factors such as MSX2, RUNX2, and SP7 during vascular calcification. Studies

have suggested that various cell types, such as VSMCs, nascent resident pericytes, circulating stem cells, or adventitial cells, can differentiate into osteoblastic cells in vascular calcification (Johnson, Leopold et al. 2006). Among these various cell types, VSMCs are considered to be the major cell type responsible for the osteochondrogenic cells in the atherosclerotic milieu (Durham, Speer et al. 2018).

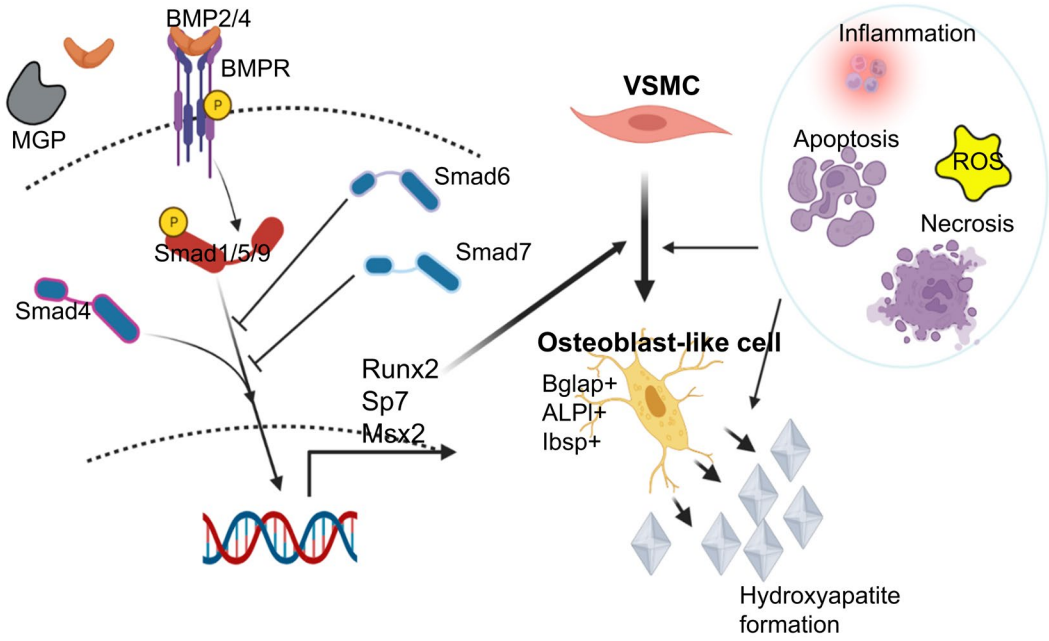

Fig 2. Proposed mechanisms of vascular calcification (Modified from Johnson, Leopoldn et al. 2006)

Vascular smooth muscle cells in atherosclerosis

VSMCs occupy the largest cell portion of the aorta, constituting the medial layer in a tightly woven fashion with elastic fibers. Under steady state, VSMCs are densely packed, exhibit spindle-shaped morphology, and express typical contractile markers, such as ACTA2, TAGLN, and MYH11, to exert their contractile properties to control vascular tone and blood pressure (VSMC role). Since the ultrastructural studies of medial VSMCs in the early 1970s, the remarkable plasticity of VSMCs has been well recognized. During vascular injury or atherosclerosis, VSMCs undergo "phenotypic switching," which is initially characterized by the downregulation of contractile genes (Grootaert and Bennett 2021). In the early days of VSMC research, the loss of such typical contractile markers hampered the accurate assessment of VSMC-derived cells in atherosclerotic lesions. However, the development of a lineage-tracing reporter system method (e.g., mouse model harboring the Myh11-CreERT2 transgene with the Cre-inducible fluorescent reporter transgene) enabled accurate tracking of VSMC-derived cells, even when VSMC-specific contractile marker expression was lost. Lineage-tracing studies have provided solid evidence that VSMC-derived cells constitute a substantial proportion (30%–70%) of all plaque cells and have also shown that VSMCs can produce multiple phenotypes such as macrophage-like, myofibroblast-like, or osteochondrogenic cells (Feil, Fehrenbacher et al. 2014; Jacobsen, Lund et al. 2017; Pan, Xue et al. 2020; Shankman, Gomez et al. 2015). In addition, mouse studies using a lineage-tracing system with a multicolor reporter system, such

as a confetti or rainbow system, revealed an interesting phenomenon: only a few VSMCs from the medial layer make up whole lesional VSMC-derived cells through clonal expansion (Chappell, Harman et al. 2016; Jacobsen, Lund et al. 2017). The underlying mechanisms of this phenomenon are currently under investigation.

Various in vivo and in vitro studies have reported that VSMCs can adopt multiple phenotypes such as synthetic, foam cell, macrophage-like, adipocyte-like, myofibroblast-like, mesenchymal stem cell (MSC)-like, endothelial cell-like, and osteochondrogenic cells (Grootaert and Bennett 2021). Recently, mouse studies using a combination of single-cell RNA sequencing (scRNA-seq) and VSMC-specific lineage-tracing system unbiasedly characterized several atherosclerotic VSMC-derived cell types at the transcriptomic level. On the scRNA-seq data, VSMCs generated transcriptomically distinct clusters, namely, "modulated VSMC," "osteochondrogenic cells," and foam cells/macrophage-like cells (Alencar, Owsiany et al. 2020; Kim, Zhao et al. 2020; Pan, Xue et al. 2020; Wirka, Wagh et al. 2019).

The modulated VSMC, or named differently depending on the groups albeit showing similar transcriptomic profiles, such as intermediate cell state (Pan, Xue et al. 2020), fibromyocytes (Wirka, Wagh et al. 2019), and Lgals3+ VSMC (Alencar, Owsiany et al. 2020), expressed the stem cell markers Ly6a and Lgals3 with decreased contractile gene expression. The modulated VSMC cluster appears to act as a pioneer cell population that eventually transdifferentiates into the osteochondrogenic cluster. Pan et al. showed that,

by reference-based integration of mouse and human scRNA-seq data, modulated VSMC and osteochondrogenic clusters also exist in human atheroma (Pan, Xue et al. 2020).

The regulation of dedifferentiation and phenotypic switching of VSMCs is primarily achieved at the transcriptional level (Grootaert and Bennett 2021). The contractile properties of VSMCs are transcriptionally controlled by the serum response factor (SRF) and its coactivator myocardin (MYOCD) (Li, Wang et al. 2003; Yoshida, Sinha et al. 2003). SRF binds to the DNA consensus sequence CC(A/T)6GG, called the CArG box, within the promoters of contractile genes. SRF is ubiquitously expressed, whereas MYOCD is specifically expressed in smooth muscle cells (SMCs) and cardiomyocytes. Because SRF must be bound to MYOCD to express contractile genes, the combination of SRF and MYOCD enables the SMC-specific expression of contractile genes. MYOCD serves as a primary regulator of VSMC differentiation, as many factors related to the phenotypic change of VSMCs directly or indirectly alter the expression or activity of MYOCD (Grootaert and Bennett 2021). Other relatively well-studied factors that regulate the phenotypic transition of VSMCs include stem cell pluripotency factor Krüppel-like factor 4 (KLF4), octamer-binding transcription factor 4 (OCT4), and transcription factor 21 (TCF21). Using SMC-specific deletion of KLF4 in atherosclerotic mice model, Gary K. Owens groups showed that KLF4 promotes transdifferentiation of VSMCs toward macrophage-like and $Ly6a^{+}$ MSC-like phenotypes (Shankman, Gomez et al. 2015) and also toward $Lagls3^{+}$

osteogenic cells (Alencar, Owsiany et al. 2020). Several mechanisms by which KLF4 suppresses the contractile phenotype of VSMCs have been proposed (Yoshida and Hayashi 2014). KLF4 binds to the G/C repressor element of contractile gene promoters or recruits histone deacetylase (HDAC2/5) to suppress contractile gene expression. In addition, KLF4 antagonizes the binding of SRF to the CArG box through direct interaction with SRF, or can form a complex with p-ELK1 and SRF to hinder the binding of MYOCD to SRF. In addition, it is also reported that KLF4 can bind to RUNX2 to enhance the activity (Yoshida, Yamashita et al. 2012). Another stem cell pluripotency factor, OCT4, also regulates VSMC phenotypic modulation but has an opposite effect to that of KLF4. The atherosclerotic phenotype of VSMC-specific KLF4 and OCT4 deletions showed inverse phenotypes (Cherepanova, Gomez et al. 2016). The activation of OCT4 in VSMCs was related to the hydroxymethylation of the OCT4 promoter and was KLF4- and HIF-1α-dependent (Cherepanova, Gomez et al. 2016). TCF21, which is known to be a causal gene of the coronary artery disease-associated locus at 6q23.2, also promotes VSMC differentiation by decreasing both SRF and MYOCD gene expression and interferes with SRF-MYOCD complex formation (Nagao, Lyu et al. 2020).

MicroRNAs, epigenetic modifications, and various environmental stimuli can post-transcriptionally regulate the VSMC phenotype (Grootaert and Bennett 2021). Among the miRNAs, miRNA143 and miRNA145 are known to be involved in the regulation of the VSMC contractile phenotype. SRF and

MYOCD induce the expression of miRNA143/145, which in turn reinforce the VSMC contractile phenotype and suppress proliferation. It has been reported that miRNA143/145 shows reduced expression in injured or atherosclerotic aortas, and cholesterol loading promotes VSMC transdifferentiation via the miRNA143/145-MYOCD axis, collectively suggesting that downregulation of miRNA143/145 may promote VSMC dedifferentiation (Boettger, Beetz et al. 2009; Cordes, Sheehy et al. 2009). Other known miRNAs involved in the phenotypic switching of VSMCs are miRNA221, miRNA222, and miRNA124 (Grootaert and Bennett 2021). Of note, miRNA221/222 has been reported to promote the osteochondrogenic transition of VSMCs, leading to calcification (Mackenzie, Staines et al. 2014).

Epigenetic regulation is another important mechanism regulating the contractile phenotype of VSMCs. Histone modifications (such as acetylation or methylation) regulate chromatin accessibility for transcription factors by modifying the chromatin structure (Gomez, Swiatlowska et al. 2015). Studies have reported that during VSMC differentiation, histone acetylation of ACTA2 and MYH11 enables their activation by allowing the binding of the SRF/MYOCD complex (Manabe and Owens 2001). The transcriptional activity of MYOCD can be enhanced by histone acetylation through P300 histone acetyltransferase (HAT), or inhibited by HDACs (Cao, Wang et al. 2005). In addition, HATs and HDACs have also been reported to regulate VSMC characteristics, such as matrix production, proliferation, and migration (Grootaert and Bennett 2021). Lastly, histone methylation is also involved in

the binding of MYOCD/SRF to the CarG box loci (McDonald, Wamhoff et al. 2006). During VSMC differentiation, enrichment of H3K4me2 histone modification at the contractile gene promotor occurs, which in turn increases MYOCD binding. Interestingly, H3K4me2 methylation persists even when VSMCs lose contractile marker expression during phenotypic modulation. Researchers have exploited this phenomenon to track VSMC-derived cells in human atherosclerotic lesions, where lineage-tracing techniques are unavailable (Gomez, Shankman et al. 2013).

In the atherosclerotic milieu, VSMCs receive various cytokines from environmental cues that can promote or inhibit the phenotypic modulation of VSMCs. Platelet-derived growth factor (PDGF)-BB promotes the differentiation and proliferation of VSMCs (Mack 2011). PDGF-BB can stimulate the phosphorylation of ELK1 through the PDGFRβ receptor, which in turn competitively inhibits the interaction between MYOCD and SRF (Wang, Wang et al. 2004). KLF4 and miRNA221 can in part mediate the effect of PDGF-BB on phenotypic modulation (Davis, Hilyard et al. 2008; Deaton, Gan et al. 2009). Wnt/β-catenin signaling is reported to promote the proliferation of VSMC, leading to intimal hyperplasia (Tsaousi, Mill et al. 2011), and is also involved in the process of osteodifferentiation of VSMCs through the activation of RUNX2 (Cai, Sun et al. 2016). Transforming growth factor-β (TGFβ) is involved in various VSMC properties, such as contractile phenotype, proliferation, hypertrophy, matrix synthesis, and proteolytic activities (Grootaert and Bennett 2021). TGFβ is one of the few growth factors

that promote the VSMC contractile phenotype. This is achieved by binding of the TGFβ signaling molecule SMAD2/3 to the contractile gene promoter or by CArG-dependent interaction with SRF (Qiu, Feng et al. 2003). In addition, TGFβ can downregulate KLF4 via miRNA143/145 to suppress VSMC phenotypic switching (Diavis, Chan et al. 2011). Integrinβ3 has been reported to be involved in the transdifferentiation, proliferation, and migration of VSMCs in the atherosclerotic milieu through cell-autonomous and paracrine effects (Misra, Feng et al. 2018).

The role of VSMCs in atherosclerotic calcification

Numerous studies have shown that VSMCs are the major cell type responsible for vascular calcification through their phenotypic transition toward osteogenic cells. VSMC-specific deletion of the osteogenic transcription factors Msx1 and Msx2 attenuated arteriosclerotic calcification in *LDLR*$^{-/-}$ mice with a diabetogenic background (Cheng, Behrmann et al. 2014). Transgenic mice that are forced to express the pro-osteogenic factors BMP2 or S100A12 in VSMCs show increased osteoblastic differentiation, leading to atherosclerotic calcification (Bowman, Gawdzik et al. 2011; Nakagawa, Ikeda et al. 2010). VSMC-specific deletion of the osteogenic inhibitory molecules PPARγ or LRP6 increased osteochondrogenic differentiation of VSMCs by augmenting Wnt signaling (Cheng, Ramachandran et al. 2015; Woldt, Terrand et al. 2012). The most convincing evidence came from a lineage-tracing study using VSMC-specific reporter mice, which demonstrated that approximately 98% of

osteochondrogenic cells expressing Runx2 in atherosclerotic plaques were derived from VSMCs (Naik, Leaf et al. 2012). Notably, Kramann et al. showed that Gil1^{+} adventitial MSC-like progenitor cells can substantially contribute osteoblast-like cells of atherosclerotic lesions under CKD conditions (Kramann, Goesttsch et al. 2016). In contrast, Wang et al. demonstrated that Ly6a+ adventitial stem cells barely contribute to the VSMC population of atherosclerotic lesions in the absence of other systemic diseases (e.g., CKD) (Wang, Zhao et al. 2021). Although the Gil1+ and Ly6a+ cells of the adventitia may not be completely identical to each other, multiple lineage-tracing studies collectively suggest that VSMCs are the principal cell type responsible for the osteochondrogenic cells in atherosclerosis.

The development of the scRNA-seq technique has enabled unbiased characterization of multiple heterogeneous cell populations in tissues or organs of interest. In addition, combining scRNA-seq with a lineage-tracing system allowed for unambiguous tracking of the transition of specific cells, even when the typical marker expression of the cells was lost. Recent scRNA-seq studies on mouse atherosclerotic lesions using a combination of fluorescence reporters (e.g., ZsGreen1 or tdTomato) with the inducible Cre recombinase on SMC-specific contractile gene promoter (e.g., Myh-CreERT2) revealed generally consistent findings with regard to the process of VSMCs transitioning toward the osteochondrogenic clusters (Alencar, Owsiany et al. 2020; Kim, Zhao et al. 2020; Pan, Xue et al. 2020). VSMCs first give rise to the “pioneer” cell population (showing similar transcriptomic profiles, albeit named differently

by each group such as intermediate cell state, fibromyocyte, or *Lgals3*$^{+}$ VSMC) and then transform into the osteochondrogenic population (fibrochondrocyte, chondromyocytes, or osteogenic). The osteochondrogenic population was enriched with multiple collagen-producing and osteochondrogenic genes, representing the cell population responsible for calcification and chondroid metaplasia in atherosclerotic lesions. Among these studies, Thomas Quertermous group and Gary K. Owens group also showed that the VSMC-derived osteochondrogenic population can be manipulated by SMC-specific ablation of a specific gene, *Ahr* or *Klf4* (Alencar, Owsiany et al. 2020; Kim, Zhao et al. 2020). Notably, SMC-specific ablation of *Ahr* or *Klf4* also altered the lesion size, fibrous cap, and intermediate VSMC clusters, suggesting that the regulatory function of these genes in the SMC transitioning process would not be specifically confined to the osteochondrogenic phenotype. To date, the key regulatory factors and underlying mechanisms that govern the osteochondrogenic transition of VSMCs have yet to be elucidated.

The roles of the BMP signaling pathway in osteoblast differentiation and implications in atherosclerotic calcification

The TGF-β superfamily comprises TGF-β, BMPs, activin, and other related proteins (Wu, Chen et al. 2016). BMP signaling plays a central role in skeletal system development and homeostasis. BMP signaling is initiated by type I and type II BMP receptors. Binding of BMP ligands leads to the formation of a tetrameric complex composed of homomeric dimers of type I and type II

receptors, which in turn leads to the transphosphorylation of type I receptors. Phosphorylation of type I receptors results in the transduction of signals through either canonical Smad-related or noncanonical p38 mitogen-activated protein kinase (MAPK)-related pathways, which consequently induces the osteogenic transcription factors that lead to osteoblast differentiation (Wu, Chen et al. 2016). Among the 14 types of BMPs, BMP2, BMP4, BMP5, BMP6, BMP7, and BMP9 are known to have osteogenic activity (Abula, Muneta et al. 2015; Luu, Song et al. 2007). BMP2 and BMP7 have been widely studied, and recombinant proteins are currently being tested in human clinical trials for various bone-related defects (Kanakaris and Giannoudis 2008; Razzouk and Sarkis 2012). Short-term expression of BMP2 is necessary and sufficient to induce bone formation (Noël, Gazit et al. 2004), and BMP7 induces the expression of osteoblastic markers, such as ALP, and accelerates mineralization (Gu, Zhang et al. 2004; Shen, Whittaker et al. 2010; Tsuji, Cox et al. 2010). BMP-3 is a "noncanonical" BMP ligand that transduces its signaling through the type IIB activin receptor (AcvrIIB) and Smad2/3-related pathway to oppose the osteogenic function of other BMPs (Kokabu, Gamer et al. 2012).

Smad molecules constitute the canonical arm of TGFβ/BMP signaling. The vertebrate has eight Smads, which can be divided into three subtypes: the receptor-regulated Smads (R-Smads, Smad1, Smad2, Smad3, Smad5, and Smad8), the co-mediator Smad (Co-Smad, Smad4), and the inhibitory Smads (I-Smads, Smad6 and Smad7) (Miyazawa and Miyazono 2017). Upon BMP

ligand binding, the heteromeric BMP receptor complex phosphorylates Smad1/5/8. Phosphorylated Smad1/5/8 forms heteromeric complexes with Smad4 and eventually translocates into the nucleus where it acts as a transcription factor or repressor (Wu, Chen et al. 2016). During osteoblast differentiation, the Smad1/5/8-Smad4 complex forms a transcription complex with RUNX2 and other molecules to initiate the expression of multiple osteoblast-related genes (Wu, Chen et al. 2016).

p38 MAPKs constitute noncanonical arms of the TGFβ/BMP signaling pathway. MAPKs are a family of enzymes that respond to various extracellular stimuli such as environmental stress, growth factors, and cytokines. Conventional MAPKs consist of the extracellular signal-regulated kinase 1/2 (ERK1/2) and ERK5, c-Jun amino (N)-terminal kinase 1/2/3, and p38 isoforms (p38α, p38β, p38γ, and p38δ). MAPK signaling constitutes a series of phosphorylation events. Once stimuli reach the cell, MAPKK kinase (MAP3K) is activated and phosphorylates MAPK kinase (MAP2K), which in turn phosphorylates and activates MAPKs. In the TGFβ/BMP signaling pathway, p38α/β exerts its osteogenic potential by inducing expression or increasing activity through the phosphorylation of some key osteogenic transcription factors such as DLX5, RUNX2, and OSX (Rodríguez-Carballo, Gámez et al. 2016).

TGFβ/BMP signaling can be fine-tuned through multiple mechanisms. Various ECM proteins, such as noggin, chordin, gremlin, and follistatin, can competitively bind BMPs to prevent receptor activation (Abe, Yamamoto et al.

2000; Gazzerro, Gangji et al. 1998; Wan, Pomerantz et al. 2007). I-Smads inhibit TGFβ/BMP signaling in multiple steps. Among the two I-Smads, Smad6 preferentially inhibits BMP signaling, whereas Smad7 inhibits both BMP and TGF-β signaling. I-Smads can prevent the phosphorylation and nuclear translocation of R-Smads, promote R-Smad degradation, and promote receptor degradation via the ubiquitin-proteasome degradation pathway (Miyazawa and Miyazono 2017). The latter is achieved by the E3 ubiquitin ligase Smuf1/2. Smuf1 can widely target BMP signaling machineries, such as BMP type I receptors, Smad1/5, RUNX2, and MKK2, leading to ubiquitin-proteasome degradation (Wu, Chen et al. 2016). Another E3 ubiquitin ligase, Arkadia, can degrade the suppressors of TGFβ/BMP signaling, such as Smad6/7 and c-Ski/SnoN, which in turn promotes the osteoblastic phenotype (Arkadia). Small ubiquitin-related modifier (SUMO) and ubiquitin-conjugating enzyme 9 (Ubc9) target Smad4 for degradation and counteract BMP2-induced osteoblast differentiation (Shimada, Suzuki et al. 2008; Yukita, Hosoya et al. 2012). Other mechanisms, such as transcriptional repressors (Ski/SnoN, Tob), microRNAs (mi133, mi30, mi141, mi542-3p, mi20a, mi140, mi199a), and epigenetic regulation, are also involved in the regulation of TGFβ/BMP signaling (Wu, Chen et al. 2016).

In the atherosclerotic milieu, BMPs are expressed in various cells, including endothelial cells, foam cells, and VSMCs. Several endothelial dysfunction-causing factors, such as oxidative stress, turbulent blood flow, and hypoxia, have been reported to increase BMP expression in endothelial cells

(Johnson, Leopold et al. 2006). Among BMPs, BMP2 and BMP4 have been reported to accelerate the osteogenic differentiation of VSMCs, whereas BMP7 can inhibit the induction of p21 and upregulation of Smad6/7 (Durham, Speer et al. 2018).

Thioredoxin-interacting protein (TXNIP)

Thioredoxin-interacting protein (TXNIP) was originally discovered as a target gene of vitamin D3 in HL-60 cells and was named vitamin D3-upregulated protein 1 (VDUP1) (Chen and DeLuca 1994). TXNIP acts as a key regulator of the cellular redox system by interacting with the redox scavenger protein thioredoxin (Trx). TXNIP binds to the reduced form of Trx with its two cysteine residues through a disulfide bond, thereby acting as an endogenous inhibitor of Trx (Patwari, Higgins et al. 2006). TXNIP belongs to the α-arrestin protein family and contains two arrestin-like domains: PxxP and PPxY sequence. The former is a binding motif for SH3-domain-containing proteins, and the latter is a binding motif for the WW domain. Thus, TXNIP can interact with many proteins such as importin-α, transcriptional corepressors SMRT-mSin3-HDAC, Jab1, E3 ubiquitin ligase itch, Mybbp1a, NOD-like receptor protein 3 (NLRP3), and Trx. Collectively, these results suggest that TXNIP may act as a scaffolding protein in various signaling pathways, thus mediating multiple cellular processes (Yoshihara, Masaki et al. 2014).

A large body of evidence supports the notion that TXNIP is a crucial metabolic regulator, particularly in lipid metabolism. Research on the HcB-19/deem mutant mouse strain suggests that TXNIP can be a causative gene for familial combined hyperlipidemia in mice, which is characterized by hypertriglyceridemia, hypercholesterolemia, elevated levels of plasma apolipoprotein B, and increased secretion of triglyceride-rich lipoprotein (Bodnar, Chatterjee et al. 2002). In addition, under fasting conditions, *Txnip*$^{-/-}$ mice showed fatal abnormalities similar to fatty acid utilization disorders, including reduced survival rate, severe bleeding, dyslipidemia, fatty liver, hypoglycemia, and hepatic and renal dysfunction (Oka, Liu et al. 2006). In this context, *Txnip*$^{-/-}$ mice showed impaired Krebs cycle-mediated fatty acid utilization and defective β-oxidation-mediated acetyl-CoA catabolism, suggesting that TXNIP plays a crucial role in fatty acid utilization (Oka, Liu et al. 2006). In human studies, TXNIP has been found as a highly glucose-responsive gene in human intact pancreatic islets and breast cancers (Shalev, Pise-Masison et al. 2002; Turturro, Friday et al. 2007), and this glucose-mediated upregulation of TXNIP can elicit glucotoxicity and β-cell apoptosis (Minn, Hafele et al. 2005).

TXNIP is also involved in inflammatory processes. Studies have reported that TXNIP directly interacts with and activates NLRP3, a key component of the NLRP3 inflammasome (Yoshihara, Masaki et al. 2014). In macrophages and pancreatic islet cells, the mechanism of ROS-sensitive activation of the inflammasome is explained by the interaction of TXNIP and NLRP3, as ROS

can liberate TXNIP from Trx, allowing it to interact with NLRP3 (Zhou, Tardivel et al. 2010). In contrast, other studies have reported direct IL-1β induction rather than IL-1β processing in hyperglycemia-induced activation of TXNIP (Koenen, Stienstra et al. 2011). In addition, inflammasome activation in the BM-derived macrophages of *Txnip*$^{-/-}$ mice did not result in significant differences in IL-1β secretion (Masters, Dunne et al. 2010). The aforementioned findings collectively suggest that the regulation of inflammatory processes by TXNIP is complex and can be achieved in a cell type- and context-dependent manner.

Accumulating evidence suggests that upregulation of TXNIP can promote apoptosis, although the proapoptotic effect of TXNIP seems to be cell type-dependent (Kim, Suh et al. 2007). Studies have proposed that ASK1 links TXNIP with the apoptotic process. ASK1 is a regulatory protein activated by various stressors, which subsequently induces apoptosis through the JNK and p38 MAPK pathways. TXNIP inhibits the interaction between Trx and ASK1, thereby liberating ASK1-induced apoptosis (Xiang, Seki et al. 2005). Cellular ASK1 levels are controlled by the ubiquitination-degradation pathway, which is related to the direct binding of the reduced form of Trx. Thus, TXNIP can inhibit ASK1 degradation by reducing Trx interaction with ASK1 (Liu and Min 2002). Therefore, TXNIP links the cellular redox state to cellular homeostasis and survival.

In addition to these functions, TXNIP plays a central role in natural killer (NK) cell development (Lee, Kang et al. 2005). TXNIP also plays a role in

cancer biology and stress-related responses involving redox regulation (Kim, Suh et al. 2007). By exploiting the multifunctional role of TXNIP in various physiological and pathological processes, it can be used as a potential target protein for the diagnosis and treatment of various diseases.

Objective

Calcification is a characteristic phenomenon of atherosclerosis which often constitute a majority of plaque components in advanced atherosclerotic lesions. Although the exact role of atherosclerotic calcification on plaque rupture has not yet been precisely defined, it can directly lead to thrombosis in the form of a "calcified nodule," which was reported to be related to cardiac death, acute coronary syndrome, and target-lesion revascularization in patients who underwent the installation of drug-eluting stents. The osteochondrogenic switch of VSMCs is known to be a pivotal cellular process in atherosclerotic calcification. Recent studies on the mice atherosclerotic lesions using scRNA-seq combined with a lineage-tracing system transcriptomically characterized VSMC-derived osteochondrogenic cluster, and showed transitioning process of VSMCs toward the osteochondrogenic cluster.

The mechanisms of the osteochondrogenic transition of VSMCs have been elucidated to some extent, but most are related to well-known processes with regard to osteoblast differentiation. In addition, although some previous studies have shown that SMC-specific ablation of some factors (e.g., *Ahr* and *Klf4*) can modulate VSMC-derived osteochondrogenic clusters, the effect of

this factor was not specifically confined to the osteochondrogenic phenotype, altering other lesion properties such as lesion size, fibrous cap, and intermediate VSMC clusters. To date, the key upstream regulatory factors and underlying mechanisms that govern the osteochondrogenic transition of VSMCs have yet to be elucidated.

In the present study, I attempted to identify the critical regulator of atherosclerotic calcification that governs osteochondrogenic phenotypic modulation of VSMCs. By analyzing the public human scRNA-seq database and endarterectomized atheroma samples, I found that TXNIP was downregulated in the VSMCs of human calcified atherosclerotic lesions. Using three different mouse models (TXNIP ablation in global, SMC-specific, and hematopoietic cells) combined with scRNA-seq analysis and primary VSMC culture experiments, I demonstrated the role of TXNIP as attenuating atherosclerotic calcification by suppressing BMP signaling to inhibit the transition of the modulated VSMCs toward an osteochondrogenic population.

INTRODUCTION

Atherosclerosis currently accounts for most of the worldwide mortality as a major underlying pathological process responsible for serious cardiovascular events (e.g., myocardial infarction, heart failure, and stroke) (Bentzon, Otsuka et al. 2014; Libby 2021). During the progression of atherosclerosis, fibrous materials and calcium gradually accumulate in atherosclerotic lesions, which often constitute the majority of plaque components. In particular, atherosclerotic calcification is a characteristic phenomenon of atherosclerosis. The coronary artery calcium score is highly correlated with the total atherosclerotic plaque burden and can aid in the prediction of patients at high risk for adverse cardiac events (Alexopoulos and Raggi 2009; Greenland, Bonow et al. 2007). Although the exact role of atherosclerotic calcification on plaque rupture/thrombosis has not yet been precisely defined (Alexopoulos and Raggi 2009), atherosclerotic calcification can lead to thrombosis in the form of a "calcified nodule," which is histologically characterized by an erupted calcified mass with a disrupted fibrous cap (Virmani, Kolodgie et al. 2000). The calcified nodules were reported to be related to cardiac death and acute coronary syndrome, and were suspected to be a principal cause of reoperation (i.e., target-lesion revascularization) in patients who underwent the installation of drug-eluting stents (Sugane, Kataoka et al. 2021). Thus, atherosclerotic calcification could cause serious clinical complications in certain circumstances; additionally, specific interventions for atherosclerotic calcification may be required.

Contrary to the previous view of passive and unregulated process, vascular calcification is now considered as an "active" process recapitulating bone morphogenesis (Johnson, Leopold et al. 2006; Durham, Speer et al. 2018). Several cell types, such as vascular smooth muscle cells (VSMCs), pericytes, vessel-residing or circulating stem cells are known to contribute to vascular calcification. These cells acquire an osteochondrogenic phenotype expressing key osteochondrogenic transcription factors, such as RUNX2, SP7, and SOX9, through stimulation by cytokines, such as bone morphogenic proteins (BMPs) in combination with various microenvironment factors (e.g., inflammation, apoptosis, necrosis, oxidative stress, and mitochondrial dysfunctions) (Johnson, Leopold et al. 2006). In the setting of atherosclerosis, VSMCs can adopt multiple phenotypes, such as macrophage/foam cell-like, osteochondrogenic cell-like, mesenchymal stem cell-like, and myofibroblast-like cell-like types through a process called "phenotypic transition" (Grootaert and Bennett 2021). Lineage-tracing studies provided direct evidence that VSMCs are a major source of osteochondrogenic cells in atherosclerotic lesions (Naik, Leaf et al. 2012; Jacobsen, Lund et al. 2017). Moreover, a combination of single-cell RNA-sequencing (scRNA-seq) and a lineage-tracing system directly visualized the process of transitioning VSMCs toward an osteochondrogenic phenotype (Pan, Xue et al. 2020; Kim, Zhao et al. 2020; Alencar, Owsiany et al. 2020). These studies showed that VSMCs first give rise to "intermediate cell" (i.e., modulated VSMC) cluster expressing gene markers, such as *Ly6a* (*Sca1*), *Lum*, and *Lgals3*, and then transform into "osteochondrogenic" clusters,

which are enriched with bone and cartilage formation and collagen-producing genes.

Thioredoxin-interacting protein (TXNIP, or thioredoxin-binding protein2 [TBP2]), initially known as a negative regulator of thioredoxin, is a member of the α-arrestin protein family containing two arrestin-like domains that are responsible for protein-protein interaction. TXNIP is reported to interact with various proteins such as E3 ubiquitin ligase, importin-α, histone deacetylase, Jab1, Mybbp1a, and NOD-like receptor Protein 3 (NLRP3), as well as Trx, implying that TXNIP may act as a scaffolding protein in various signaling pathways (Yoshihara, Masaki et al. 2014). This feature also explains the multifunctional role of TXNIP in various physiological and pathological processes such as proliferation, apoptosis, NK cell development, inflammasome activation, fatty acids, and glucose metabolism (Kim, Suh et al. 2007; Qayyum, Haseeb et al. 2021). The genetic ablation of *Txnip* reduced the oxidative inflammatory response in the VSMCs and mitigated the atherosclerotic burden in *ApoE*$^{-/-}$ mice (Byon, Han et al. 2015); additionally, human studies have reported a relationship between *TXNIP* polymorphism and hypertension and arterial stiffness (Ferreira, Omae et al. 2021; Alvim, Santos et al. 2012). Collectively, these studies suggest that TXNIP is deeply involved in the pathophysiological course of the vascular system. To identify the core regulatory factor of atherosclerotic calcification, I determined from a previous public transcriptome database (GSE159677) that *TXNIP* is significantly downregulated in the VSMCs of human calcified atherosclerotic lesions

(Alsaigh, Evans et al. 2020). In this regard, I set out experiments to test whether TXNIP has a modulatory role in atherosclerotic calcification. Importantly, the genetic ablation of *Txnip* increased the osteochondrogenic differentiation of VSMCs by enhancing BMP signaling. Thus, I propose TXNIP as a crucial regulator of the osteochondrogenic differentiation of VSMCs in the atherosclerotic milieu.

MATERIALS and METHODS

Animal models

Txnip$^{-/-}$ (*Txnip* KO) and their littermate control *Txnip*$^{+/+}$ (WT) mice (C57BL6/J background) were obtained from the Korea Research Institute of Bioscience and Biotechnology (Lee, Kang et al. 2005). For the bone marrow transplantation experiment, recipient C57BL/6J WT mice were obtained from the Central Lab. Animal, Inc. (Seoul, Korea). *Tagln*-cre mice (B6.Cg-Tg(Tagln-cre)1Her/J, strain no. 017491) and *Txnip*$^{flox/flox}$ mice (B6;129-*Txnip*^{tm1Rlee}/J, strain no. 016847) were obtained from the Jackson Laboratory (Bar harbor, ME, USA). To generate SMC-specific ablation of *Txnip* by Cre-mediated recombination under *Tagln* promotor, *Tagln*-Cre mice, and *Txnip*$^{flox/flox}$ mice were bred to give *Tagln*-Cre; *Txnip*$^{flox/flox}$ mice (SMC^{KO}). Their littermates that did not have *Tagln*-Cre were used as the control group (SMC^{WT}). For primary VSMC culture experiments, three to five week old C57BL6/J WT mice were used.

Because wild type C57BL/6 mice do not develop atherosclerotic calcifications, it is necessary to induce atherosclerosis by 15 to 20 weeks of high fat diet (HFD) feeding on *Ldlr*$^{-/-}$ background mice to interrogate atherosclerotic calcification, which requires time-consuming mice mating process [Venegas-Pino, Banko et al. 2013]. Previous study reported that adeno-associated virus-mediated PCSK9 overexpression followed by >15 weeks of HFD in C57BL/6 mice accumulate calcium within the atherosclerotic lesion (Goettsch, Hutcheson et al. 2016). So I induced atherosclerosis by a single

injection of adeno-associated virus serotype 8 (AAV8) encoding m*PCSK9* (rAAV8/D377Y-mPCSK9), followed by 16 weeks of HFD (Research Diet, cat. D12079B). At the time point of the AAV8 injection, WT, *Txnip* KO, SMC^{WT}, and SMC^{KO} mice were 8–10 weeks old, and the mice in the bone marrow transplantation experiment were 14–16 weeks in age due to recovery periods. A previous study reported that upon AAV8-PCSK9 injection, female mice showed impaired liver *PCSK9* transduction with insufficient hypercholesterolemia (Vozenilek, Blackburn et al. 2018). In addition, to exclude possible hormonal effects (e.g., estrogen), I used only male mice in all the experiments. All the animal experiments were approved by the Institutional Animal Care and Use Committee (IACUC) of Seoul National University (approval numbers: SNU-180612 and 210517).

Bone marrow transplantation

Bone marrow (BM) cells from WT or *Txnip* KO mice were injected intravenously into lethally irradiated (500 rad twice, 3 h interval) WT mice. Subsequently, the mice were fed water containing antibiotics (7.6% enrofloxacin) and monitored for six weeks, until the transplanted BM was effectively reconstructed. The transplantation of BM cells was verified by blood PCR. The primer pairs for detecting genotypes were as follows. WT: 5'-ATTCCCCTTCCAGGTGGA-3' and 5'-TTGAAATTGGCTCTGT-3' to detect the 478 bp band, *Txnip* KO: 5'-GCAAAGACCAGACCGTTC AT-3' and 5'-GAAGCCAATGAAACCCA-3' to detect the 593 bp band.

Necropsy, tissue preparations, and histological staining of atherosclerotic lesions

The mice were sacrificed by CO_2 gas inhalation, and blood was obtained through cardiac puncture to measure the serum total cholesterol, triglycerides, HDL, LDL, and Ca^{2+} concentrations. The mice were perfused with phosphate-buffered saline (PBS) through the heart to eliminate blood. The hearts and whole aortas were collected. After peri-adventitial tissue removal, the hearts and aortas were briefly fixed in 10% neutralized formalin for 2 h. The hearts were molded in optimal cutting temperature (OCT) compounds for cryosectioning of the aortic sinus. The aortas were opened longitudinally and pinned onto the plate in a "Y" shape for *en-face* analysis.

The cryosections perpendicular to the aortic sinus were made sequentially from the sinotubular junction (start point; just before the aortic cusps appear) to the point where all the aortic cusps met (end point). Highly calcified parts are prone to produce artifacts (e.g. folding) during sectioning. To complement this experimental pitfall, approximately 7 μm of 70–80 serial sections spanning 490–560 μm of the aortic sinus were produced, and 5 points of regular intervals (approximate 100 μm) from the start to the end of the aortic sinus sections were measured and averaged for quantification. Oil Red O (for lipids), Alizarin Red S (for calcium), Masson's trichrome (for collagen), and Alcian blue (for glycosaminoglycan ECM) staining were carried out according to the general procedures. MOMA-2, SM22α, ACAN, and CHAD proteins were visualized

by immunostaining on cryosections. For the HRP detection method (MOMA-2 and SM22α), the sections were pretreated with H_2O_2 to deplete endogenous peroxidase. For the fluorescence detection method (ACAN and CHAD), auto fluorescence signals were quenched using a TrueBlack® Lipofuscin Autofluorescence Quencher (Biotium, cat. 23007) prior to the blocking step. The primary antibodies against anti-MOMA-2 (Abcam, cat. ab33451; 1:400 dilution), SM22α (Abcam, cat. ab10135; 1:200 dilution), ACAN (Proteintech, cat. 13880-1-AP; 1:200 dilution), and CHAD (Atlas Antibodies, cat. HPA018241; 1:200 dilution) were incubated at 4 °C overnight. Anti-rat (VECTOR, cat. MP-7444-15) and anti-goat (cat. MP-7405) HRP-conjugated secondary antibodies were applied to appropriately matched primary antibodies. Subsequently, the signals were detected using DAB peroxidase (VECTOR, cat. SK-4105). Anti-rabbit Alexa 488 fluorescent secondary antibodies (Jackson ImmunoResearch, cat. 711-545-152; 1:400 dilution) was applied to ACAN and CHAD. The signals were analyzed using a confocal fluorescence microscope (Zeiss, LSM800). For the quantification of immunostaining, three regular interval points from the start to the end of the aortic sinus sections were measured and averaged.

qRT-PCR

The total RNA was extracted from the mouse aorta or adventitial layer-removed atherosclerotic lesions using the Hybrid-R™ kit (GeneAll, cat. 305-101), according to the manufacturer's instructions. Complementary DNA was

synthesized from 200–1,000 ng of total RNA using a QuantiTect Reverse Transcription kit (Qiagen, cat. 205311), and then analyzed by qPCR using a Rotor-Gene SYBR Green PCR kit (Qiagen, cat. 204074). The sequences of primers for detecting indicated mouse mRNA were listed in Table 1.

Table1. Mouse qRT-PCR primers used in the study

Gene	Forward (5'-3')	Reverse (5'-3')
Bglap	GCAATAAGGTAGTGAACAGACTCC	GTTTGTAGGCGGTCTTCAAGC
Bmp2	CACACAGGGACACACCAACC	CAAAGACCTGCTAATCCTCAC
Bmp4	GCCGAGCCAACACTGTGAGGA	GATGCTGCTGAGGTTGAAGAGG
Hmbs	AAGGGCTTTTCTGAGGCACC	AGTTGCCCATCTTTCATCACTG
Ibsp	CACCCCAAGCACAGACTTTT	TCGTCGCTTTCCTTCACTTT
Id1	CCTAGCTGTTCGCTGAAGGC	GTAGAGCAGGACGTTCACCT
Id2	ATGAAAGCCTTCAGTCCGGTG	AGCAGACTCATCGGGTCGT
Id3	CGACCGAGGAGCCTCTTAG	GCAGGATTTCCACCTGGCTA
Id4	CAGTGCGATATGAACGACTGC	GACTTTCTTGTTGGGCGGGAT
Lum	CTCTTGCCTTGGCATTAGTCG	GGGGGCAGTTACATTCTGGTG
Ly6a	GCTATGGAGTCCCATTTGAG	AGGAAGTCTTCACGTTGACC
Myh11	CATCCTGACCCCACGTATCAA	ATCGGAAAAGGCGCTCATAGG
Sp7	AGAGGTTCACTCGCTCTGACG	TTGCTCAAGTGGTCGCTTCTG
Txnip	CGAGTCAAAGCCGTCAGGAT	TTCATAGCGCAAGTAGTCCAAAGT

β-actin	CGCCACCAGTTCGCCATGGA	TACAGCCCGGGGAGCATCGT

Preparation of scRNA-seq experiment

For the scRNA-seq experiment, I used the regions from the aortic sinus to the arch, as this area consists of advanced plaques that are expected to be rich in calcification. The cardiac muscles and peri-adventitial tissues were removed. The aortas were subsequently incubated for 12 min in enzymatic solutions consisting of PBS with Ca^{2+} and Mg^{2+} containing 1 mg/ml of collagenase II (Worthington, cat. CLS-2) and 0.17 mg/ml of elastase (Worthington, cat. LS002279) to remove the adventitia. After the physical separation of the adventitia, the lumen was opened, and the aortic valves were removed. The aortic tissues consisting of plaque and media were cut into 2–5 mm pieces and incubated at 37 °C for 70 min with gentle shaking in a PBS solution (Ca^{2+} and Mg^{2+}) containing DNase I (90 U/mL, Sigma-Aldrich, cat. DN25), collagenase I (675 U/mL, cat. C0130), collagenase XI (187.5 U/mL, cat. C7657), hyaluronidase (90 U/mL, cat. H1115000). The resulting single-cell suspensions were filtered through a 70 μm cell strainer, stained with propidium iodide (PI), and sorted on a BD FACS Aria III instrument. After excluding the debris and doublets using forward/side scatter parameters, the PI-negative live cells were subjected to scRNA-seq experiments. To ensure a sufficient cell number and biological reproducibility, four mice were pooled for each WT and *Txnip* KO genotype.

Pre-processing of the scRNA-seq data

Approximately 20,000 pooled cells (WT and *Txnip* KO each) from adventitia-removed atherosclerotic lesions were partitioned into gel bead-in-emulsion (GEMs) to target a single-cell resolution of 10,000 cells. The cDNA libraries were constructed using the Single Cell 3' Reagent Kit v3 (10x Genomics) and sequenced on the Illumina® system according to the manufacturer's instructions. The 10X Genomics libraries were de-multiplexed and quantified using the CellRanger program (ver. 1) following the manufacturer's instructions. The scRNA-seq data are available in the Sequence Read Archive (SRA) repository under the accession number SRP346850. The gene expression level of each barcode was calculated using the "quant" module of CellRanger with GRCh38 and mm10 (ver. 3.1.0). Low-quality cells were filtered out using the nFeature, nCount, and percent.mt (Figure S3B and C) in the same manner as other datasets.

Analysis of scRNA-seq data

A total of 17,826 (6,564 for WT and 11,262 for *Txnip* KO) viable cells were preprocessed using "preprocess_cds()," and then integrated using "align_cds()" in the monocle 3 package (Butler, Hoffman et al. 2018). The sample batch corrections were performed using the same function. The scRNA-seq data of WT and *Txnip* KO mice were visualized through UMAP using default settings in monocle 3. Clustering based on UMAP embedding was performed with proper resolution, which can characterize each cell cluster. To estimate the

proportions of cells in each cluster, the scale factor (10,000 cells) was multiplied by each genotype. Cluster specific marker gene was defined as specificity ≥ 0.3 and ordered by marker_score using "top_markers()" function in monocle 3.

To integrate the normal VSMCs into WT/*Txnip* KO scRNA-seq data, the scRNA-seq data of 79 aortic arch (AA) and 64 descending thoracic aorta (DT) cells in normal mice were collected from GSE117963 in GEO (Dobnikar, Taylor et al. 2018). To integrate the smooth muscle cell lineage traced atherosclerotic lesional cells into WT/*Txnip* KO scRNA-seq data, scRNA-seq data of atherosclerotic plaque cells containing ZsGreen1-labeled VSMCs (*ROSA26*$^{ZsGreen1/+}$; *Ldlr*$^{-/-}$; *Myh11-CreER*^{T2}) were sourced from GSE155513 (Pan, Xue et al. 2020). The preprocessing of scRNA-seq was conducted in the same manner as the other datasets. The integrations were performed using the "align_cds" function of monocle3 package in R. The top 5 genes of each cell type was selected by the "top_markers" function.

For the further analysis of VSMC-derived cells, VSMCs, modulated VSMCs, and osteochondrogenic clusters were selected and re-aligned using the monocle3 package in R. Subclustering was performed in the same manner as the previous clustering method. The comparison of gene expression levels between WT and *Txnip* KO mice was performed using "FindMarkers" in the Seurat package. DEGs were defined as |average log2 fold change| ≥ 0.2 and adjusted p value < 0.05. The functional enrichment analysis for each gene set was performed using "enricher()" in the clusterProfiler package with the

KEGG pathway database. The significantly associated function of each gene set was defined as a q-value < 0.2. To estimate the activity of Smad1 and Smad4 regulons (defined as transcription factor-target relationship), I used the DoRoTheA program and followed the instructions (Garcia-Alonso, Holland et al. 2019). The confidence levels A, B, and C target genes were only included in the regulon. To estimate the activity of Wnt/β-catenin regulons, gene sets consisting of Wnt/β-catenin targets were collected from previous studies and are described in Table 2.

Table 2. Gene list of the analyzed Wnt/β-catenin regulon. Among the known target genes of Wnt/β-catenin signaling (referenced from: https://web.stanford.edu/group/nusselab/cgi-bin/wnt/target_genes), genes reported as direct targets of Wnt/β-catenin signaling in mammalian species were selected.

Axin2	*Ccnd1*	*Cdc25*	*Cdx1*	*Cldn1*	*Ctla4*	*Fgf18*	*Fosl1*
Fst	*Fzd7*	*Gbx2*	*Gja1*	*Id2*	*Jun*	*Krt1*	*Lef1*
Lgr5	*Myc*	*Mycbp*	*Neurod 1*	*Nrcam*	*Ovol1*	*Pitx2*	*Ppard*
Sp5	*Tbx1*	*Tbx3*	*Tcf4*	*Tcf7*	*Tert*	*Tnfrsf19*	*Vcan*
Vegfa							

In situ hybridization

In situ hybridizations of *Ly6a*, *Myh11*, and *Chad* were performed on paraffin-embedded aortic sinus tissues using RNAscope® 2.5HD Duplex Assay (Advanced Cell Diagnostics, cat. 322435). This assay enables co-detections of two different transcripts using C1 (green signal) and C2 (red signal) channels. Probes for *Ly6a* (RNAscope® Probe-Mm-Ly6a-C2; cat. 427571-C2), *Myh11* (Probe-Mm-Myh11; cat. 316101), and *Chad* (Probe-Mm-Chad; cat. 484881) were used. The experiments were conducted according to the manufacturer's instructions. *Polr2a & Ppib* (constitutively expressed genes of mouse) and *DapB* (constitutively expressed genes of *E. coli*) were used as positive and negative control probes, respectively. Three points of regular intervals from the start to the end of the aortic sinus sections were measured and averaged for quantification.

Analysis of human scRNA-seq data GSE159766

The scRNA-seq data GSE159677 consisted of type VII calcified atherosclerotic plaque cores matched with the adjacent proximal regions of three human patients. Downsampling was performed to reduce data bias due to differences in the cell number (# cells per sample = 2,500). The *MYH11* and *ACTA2* positive cluster cells (VSMCs) were collected from GSE159677. The selected VSMCs were processed by the same procedure in the mouse data. Four subclusters (VSMCs, modulated VSMCs, osteochondrogenic, and fibroblast-like) were characterized by the markers in the mouse scRNA-seq data.

Immunostaining of human atherosclerotic lesion samples

Endarterectomized atherosclerotic plaque tissues from the carotid artery region, which harbored calcification were obtained from patients after the receipt of written informed consent in accordance with the Declaration of Helsinki. The study protocol was approved by the Institutional Review Board of Hanyang University Hospital, Seoul, Korea (IRB number: 2021-11-027-001). The tissue samples were fixed in 10% neutral buffered formalin, processed in a routine procedure, and embedded in paraffin. Serial sections (3 μm) were obtained and subjected to either hematoxylin & eosin staining or immunostaining. For the immunostaining of TXNIP and α-SMA, antigen retrieval was performed using a Tris-EDTA buffer (pH 9.0; Abcam, cat. ab93864). Endogenous peroxidase was depleted by incubation with H_2O_2. TXNIP (Abcam, cat. ab188865; 1:200 dilution; 0.25mg/ml concentration), rabbit monoclonal IgG (Cell signaling, cat. #3900; 1:2000 dilution; 0.25mg/ml concentration), and α-SMA (Agilent, cat. M0851; 1:200 dilution) primary antibodies were incubated overnight at 4 °C. Anti-rabbit (VECTOR, cat. MP-7401), and anti-mouse (cat. MP-7402) HRP-conjugated secondary antibodies were applied to the appropriate slides, and the signals were produced through DAB peroxidase (VECTOR, cat. SK-4105). To quantify the intensity of TXNIP staining, images of two to three × 400 field were taken in the medial side (marked by *α*-SMA on the serial sections) of the periphery of the calcified area or non-calcified area. The staining intensity was evaluated using the ImageJ software (ver. 1.53e, NIH).

Primary VSMC culture experiment

Aortas ranging from the arch to the abdominal region were obtained from 3 to 5 weeks of WT (C57BL6/J) mice. For adventitia removal, the aortas were incubated for 12 min in enzymatic solutions consisting of PBS with Ca^{2+} and Mg^{2+} containing 1 mg/ml of collagenase II (Worthington, cat. CLS-2) and 0.17 mg/ml of elastase (cat. LS002279). The endothelium was removed by gentle scraping. The resulting medium was fully digested into single cells using the same enzymatic combination as that used for adventitia removal. The cultured VSMCs were maintained in DMEM/high glucose supplemented with sodium pyruvate and L-glutamine (GE Healthcare Hyclone™, cat. SH30243.01) supplemented with 10% fetal bovine serum (FBS), penicillin (50 U/ml), and streptomycin (50 μg/mL) in a 5% CO_2 atmosphere at 37 °C. Three or four passaged cells were used for the experiments. *Txnip* siRNA (Bioneer, AccuTarget™ Genome-wide Predesigned siRNA No. 56338-3) or negative control siRNA (Bioneer, AccuTarget™ Negative Control siRNA, cat. SN-1012) were delivered into the cultured VSMCs using Lipofectamine RNAiMAX reagent (Thermo Fisher, cat. 13778075). For osteodifferentiation, the cultured VSMCs were grown in an "osteogenic cocktail," consisting of 0.25 mM L-ascorbic acid, 10 mM β-glycerophosphate, and 0.4 mM H_2O_2 in DMEM/high glucose without sodium pyruvate and L-glutamine (WELGENE, cat. LM001-03) supplemented with 10% FBS and penicillin/streptomycin. The medium was changed every 2 or 3 days. Under these conditions, osteodifferentiation

was achieved in approximately 14 days. At the end point, the extent of osteodifferentiation was visualized by Alizarin Red staining and quantified using the cetylpyridinium chloride extraction method. BMP2 (R&D Systems, cat. 355-BM), or K02288 (MedChemExpress, cat. HY-12278) were used at the indicated concentrations and times.

Immunoblotting

The proteins from whole cell lysates were extracted from primary cultured VSMCs using the Cytobuster^{TM} protein extraction reagent (Millipore, cat. 71009) with a protease inhibitor cocktail (GenDEPOT, cat. P3100), and a phosphatase inhibitor cocktail (GenDEPOT, cat. P3200). To analyze the cytoplasmic and nuclear fractions of β-catenin and Smad4, the cytoplasmic and nuclear proteins were compartmentalized using the NE-PER Nuclear and Cytoplasmic Extraction Reagents kit (Thermo, cat. 78833). The proteins were separated by 10% sodium dodecyl sulfate-polyacrylamide gel electrophoresis (SDS-PAGE) and transferred to nitrocellulose membranes. The membranes were blocked with 5% skim milk. Anti-TXNIP (Abcam, cat. ab188865; 1:500 dilution), β-catenin (Santa Cruz Biotechnology, cat. sc-17791; 1:200 dilution), α-tubulin (Cell Signaling, cat. CST2144; 1:1000 dilution), Lamin B1 (cat. ab16048; 1:1000 dilution), p-Smad1/5/9 (cat. CST13920; 1:500 dilution), Smad1 (cat. CST6944; 1:1000 dilution), Smad4 (cat. sc-7966; 1:200 dilution), Smad5 (cat. sc-101151; 1:200 dilution), Smad6 (cat. sc-25321; 1:200 dilution), Smad7 (cat. sc-365846; 1:100 dilution), p38 (cat. sc-7149; 1:200 dilution), p-

p38 (cat. CST4511; 1:500 dilution), and GAPDH (cat. sc-365062; 1:500 dilution) primary antibodies were incubated at 4 °C overnight. Subsequently, anti-mouse or anti-rabbit HRP-linked secondary antibodies (Cell Signaling, cat. CST7076 and CST7074) were incubated with the appropriate primary antibody host. The signals were produced using a chemiluminescent HRP substrate (Merck Millipore, cat. WBKLS0500) and analyzed using ImageQuant LAS 4000 Mini (GE Healthcare). If necessary, the membranes were stripped using Restore™ Western Blot Stripping Buffer (Thermo Fisher, cat. 21059), followed by additional blotting.

Statistical analysis

Statistical analyses were performed using GraphPad Prism software ver. 7. All the data are presented as mean ± standard deviation. To compare the two groups, the Shapiro-Wilk normality tests were performed first to test whether the data follows a Gaussian distribution. In the case of comparing the intensity of TXNIP staining in human atheroma immunostaining data, a paired Student's t-test (two-tailed) was used. In the rest of the analysis comparing two groups, an unpaired Student's t-test (two-tailed) was applied for parametric data and the Mann–Whitney *U*-test (two-tailed) for non-parametric data. To compare more than two groups, a one-way ANOVA was applied for parametric data and the Kruskal–Wallis test for non-parametric data, followed by a post hoc analysis specified by the GraphPad Prism software. The statistical significance

was set at $P \leq 0.05$. The exact n values and statistical methods are specified in the figure legends.

RESULTS

Genetic ablation of *Txnip* in mice markedly increased atherosclerotic calcification.

To elucidate the role of TXNIP in atherosclerotic calcification, I first examined the phenotypical changes in the atherosclerotic lesions of *Txnip* knockout mice (*Txnip*$^{-/-}$; *Txnip* KO). Atherosclerosis was induced by the overexpression of gain-of-function PCSK9 mutant using adeno-associated virus (AAV) with 16 weeks of a high-fat diet (HFD) (*Figure 1A*). This method enabled me to avoid time-consuming mouse mating processes, and also provided a proper model for interrogating atherosclerotic calcification, as AAV-mediated PCSK9 overexpression followed by >15 weeks of HFD in C57BL/6 mice is reported to accumulate calcium within the lesion (Goettsch, Hutcheson et al. 2016). After induction of atherosclerosis, mice were subjected to serum lipid profiling and preparation of serial cryosections of the aortic sinus (7 μm interval, total 70–80 sections) (*n* of WT/*Txnip* KO = 11/8). The atherosclerotic burdens of aortas were analyzed by making *en face* preparation (aortic arch–upper thoracic) and serial cryosections (lower thoracic and abdominal) (*n* = 6/5). The aortas of remaining mice (*n* = 5/3) were used for qRT-PCR (*Figure 1A*). WT and *Txnip* KO mice showed different lipid profiles (*Figure 1B*), probably because of the altered liver lipid metabolism in *Txnip* KO mice as previously reported (Park, Song et al. 2021; Chutkow, Patwari et al. 2008). There was no significant difference in body weight between two groups (WT = 42.75 ± 4.03g, *Txnip* KO = 39.85 ± 3.97g, *P* = 0.1382). Throughout the aorta, *Txnip* KO mice

showed decreased Oil Red O (ORO)-stained lesion area compared to WT mice (*Figure 1C*). In the aortic sinus region, both WT and *Txnip* KO mice showed advanced atherosclerotic lesions (e.g. fibroatheroma) with calcifications (*Figure 1D–H*). Unlike the aorta, there was no significant difference in the lesion size of aortic sinus region between WT and *Txnip* KO mice (*Figure 1D*). We assume that this discrepancy is partly due to saturation of the lesion development, since atherosclerosis generally develops first in the aortic sinus in murine atherosclerosis model (Venegas-Pino, Banko et al. 2013). The atherosclerotic lesions of *Txnip* KO mice were observed to have fewer macrophages (*Figure 1E*). There were no notable differences in the lesional SM22α-positive area (*Figure 1F*), nor necrotic core size between WT and *Txnip* KO mice (*Figure 1G*). We quantified the plaque calcification using Alizarin Red staining. Notably, the atherosclerotic lesions of *Txnip* KO mice carried significantly higher amounts of plaque calcification compared to WT, as measured by both the ratio to lesion size and absolute area (*Figure 1H*). Also, the atherosclerotic lesions of *Txnip* KO mice showed significantly higher expressions of bone related marker gene *Ibsp* (bone sialoprotein) and *Alpl* (alkaline phosphatase) (*Figure 1I*). Serum concentrations of Ca^{2+} were similar between WT and *Txnip* KO mice (WT = 11.37 ± 0.51 mg/dL, *Txnip* KO = 11.26 ± 1.31 mg/dL, $P = 0.7934$), indicating the absence of endocrinological effects on calcification-rich phenotype of *Txnip* KO mice.

A

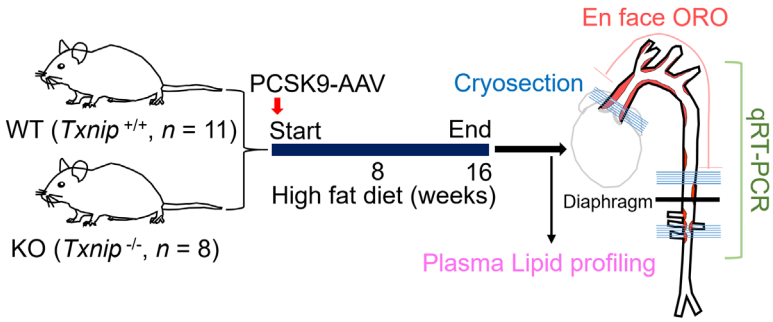
En face ORO
PCSK9-AAV
Cryosection
WT (Txnip +/+, n = 11)
Start
End
8
16
High fat diet (weeks)
Diaphragm
qRT-PCR
KO (Txnip -/-, n = 8)
Plasma Lipid profiling

B

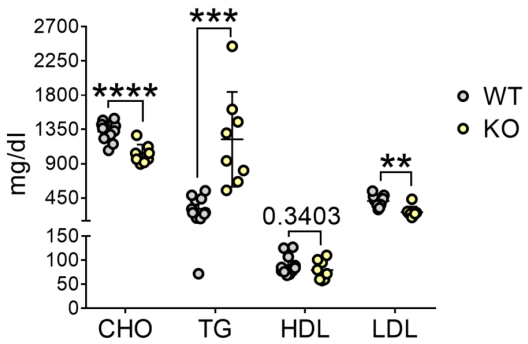
mg/dl
2700
2250
1800
1350
900
450
150
100
50
0
****
***
0.3403
**
WT
KO
CHO
TG
HDL
LDL

C

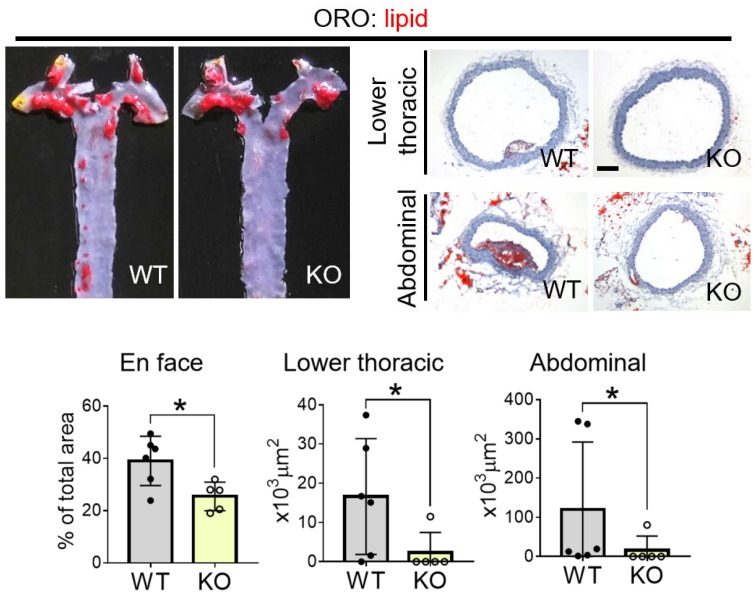
ORO: lipid
WT
KO
Lower thoracic
Abdominal
WT
KO
WT
KO
En face
Lower thoracic
Abdominal
% of total area
x10³µm²
x10³µm²
*
*
*
WT
KO
WT
KO
WT
KO

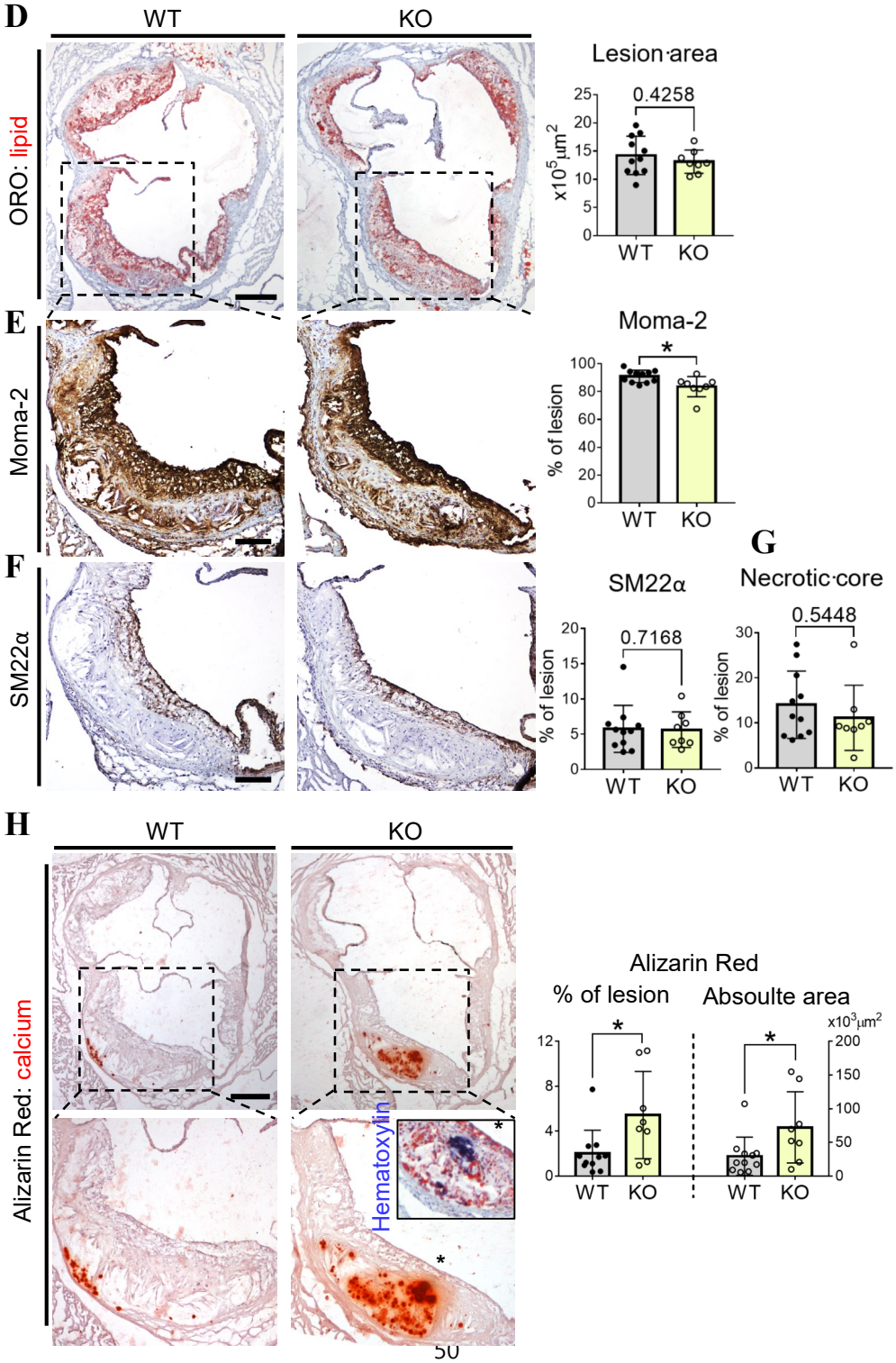
D
WT
KO
ORO: lipid
Lesion area
0.4258
x10^5 µm^2
WT
KO
E
Moma-2
Moma-2
*
% of lesion
WT
KO
F
SM22α
SM22α
0.7168
% of lesion
WT
KO
G
Necrotic core
0.5448
% of lesion
WT
KO
H
WT
KO
Alizarin Red: calcium
Hematoxylin
Alizarin Red
% of lesion
Absoulte area
x10^3 µm^2
WT
KO
WT
KO

I

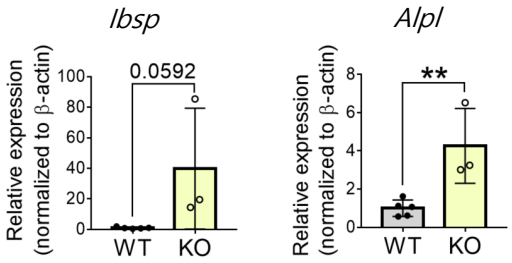

Figure 1 Global knockout of *Txnip* increases atherosclerotic calcification. (*A*) Schematic illustration of the experiment. The mice were injected with PCSK9-AAV and fed HFD for 16 weeks. n = 11/8 for WT/*Txnip* KO. (*B*) Plasma concentrations of total cholesterol (CHO), triglyceride (TG), high-density lipoprotein (HDL), and low-density lipoprotein (LDL). (*C*) The atherosclerotic burden of aortas was analyzed by making *en face* preparation (aortic arch–upper thoracic) and serial cryosections (lower thoracic and abdominal) (n = 6/5). The aortas of remaining mice were used for qRT-PCR (*I*, n = 5/3). (*D–H*) Characterization of atherosclerotic lesions using the 7 μm of perpendicular serial sections (total 70-80 sections) prepared from the aortic sinus. Representative serial sections and quantification results of Oil Red O (ORO) staining (*D*, for lesion size), Moma-2 immunostaining (*E*, for monocyte/macrophage), SM22α immunostaining (*F*, for SM22α positive area), necrotic core area (*G*), and Alizarin red staining (*H*, for calcium). (*I*) qRT-PCR result of *Ibsp* and *Alpl* from atherosclerotic aorta. The scale bars in (*D* and *H*) represent 400 μm; (*E* and *F*) represent 200 μm. The data of CHO and TG in (*B*), the data of en face in (*C*), and the data in (*D*, *E*, and *I*) were analyzed by an unpaired Student's *t*-test (two-tailed). The data of HDL and LDL in (*B*), the data of lower thoracic and abdominal in (*C*), and the data in (*F*, *G*, and *H*) were analyzed using the Mann–Whitney *U*-test (two-tailed). The error bars denote standard deviation. $*P < 0.05$, $**P < 0.01$, $***P < 0.001$, $****P < 0.0001$. In other case, the exact *P* value is specified.

ScRNA-seq analysis revealed that the "osteochondrogenic" cluster enriched with bone- and cartilage-related genes was markedly expanded in *Txnip* KO mice.

For unbiased characterization of the calcification and collagen-rich atherosclerotic phenotype of *Txnip* KO mice in a single-cell level, I performed scRNA-seq using the atherosclerotic lesions of WT and *Txnip* KO mice (*Figure 2A*). Overall sample preparation procedures for scRNA-seq are shown in *Figure 2B*. The regions from the aortic sinus to aortic arch were selected for the experiment because these areas contained mostly advanced atherosclerotic plaques that were expected to be rich in calcifications. The adventitia was removed to focus on cell populations within the plaque. The *in situ* hybridization of *Ly6a* and *Myh11* confirmed the cleanliness of the adventitia, as demonstrated by the absence of adventitial *Ly6a*$^{+}$ cells (*Figure 2C*). A total of 6,564 and 11,262 WT and *Txnip* KO cells passed quality control and proceeded to the generation of single-cell transcriptome (*Figure 2D–E*). The scRNA-seq captured most of the typical atherosclerotic lesion cell clusters (*Figure 2F*). The top five DEGs for each cluster are shown by heatmap in *Figure 2G*. In line with previous reports, I identified a VSMC-derived "pioneer" cluster, which juxtaposed to VSMC cluster known as "modulated VSMC," "*Ly6a*$^{+}$ VSMC," or "intermediate cell state," which expresses *Ly6a* with decreased contractile genes (*Figure 2H*) (Pan, Xue et al. 2020; Shankman, Gomez et al. 2015; Dobnikar, Taylor et al. 2018). This cluster also expressed *Lum*, *Fn1*, and *Lgals3* (*Figure 2I* and *2L*), sharing the transcriptomic signature

of “fibromyocyte” (Kim, Zhao et al. 2020; Wirka, Wagh et al. 2019) and “*Lgals3*$^{+}$ VSMC” (Alencar, Owsiany et al. 2020). Next, I identified a distinct cluster enriched with multiple collagen-producing genes and bone and cartilage-related genes, such as *Ibsp* (bone sialoprotein), *Chad* (chondroadherin), *Acan* (aggrecan), *Sp7* (osterix), *Sox9*, and *Alpl* (*Figure 2G*, *2J–K*, and *M*). I designated this cluster as the “osteochondrogenic cluster,” which shared transcriptomic features of the previously reported “fibrochondrocyte” (Pan, Xue et al. 2020), “chondromyocyte” (Kim, Zhao et al. 2020), and “osteogenic” (Alencar, Owsiany et al. 2020) populations.

Ablation of *Txnip* markedly expanded the osteochondrogenic cluster (*Figure 2N–O*), in line with the calcification-rich phenotype of *Txnip* KO mice. As the osteochondrogenic cluster highly expressed collagen-producing genes and cartilage-related genes, we further characterized theses phenotypes on the histological sections from additional atherosclerosis-induced WT and *Txnip* KO mice (*Figure 2P–Q*, and *S*). Indeed, the atherosclerotic lesion of *Txnip* KO mice showed a higher amount of lesional collagen (*Figure 2P*) and Alcian blue-positive glycosaminoglycans (i.e., extracellular matrix of cartilage, *Figure 2Q*). Immunostaining of the osteochondrogenic marker ACAN and CHAD proteins confirmed the transcriptional differences between WT and *Txnip* KO at the protein level (*Figure 2R–S*). ACAN and CHAD-positive areas also co-localized with the collagen-rich and calcified areas in the serial sections (*Figure 2S*).

A

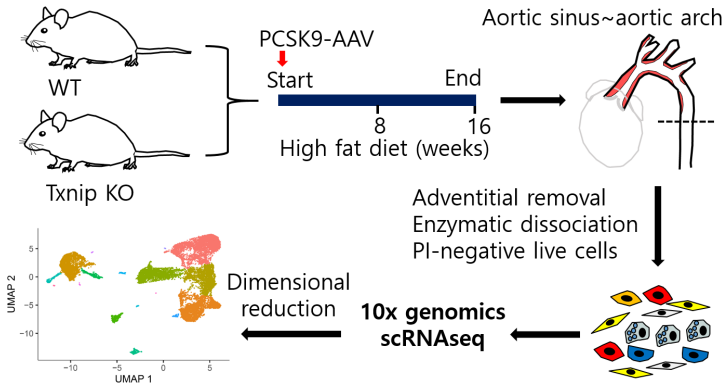
WT
Txnip KO
PCSK9-AAV
Start
End
8
16
High fat diet (weeks)
Aortic sinus~aortic arch
Adventitial removal
Enzymatic dissociation
PI-negative live cells
10x genomics
scRNAseq
Dimensional
reduction
UMAP 1
UMAP 2

B

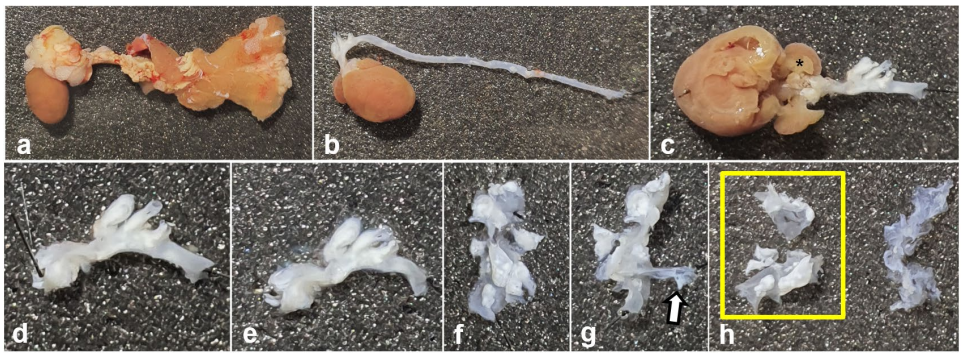
a
b
c
d
e
f
g
h

C

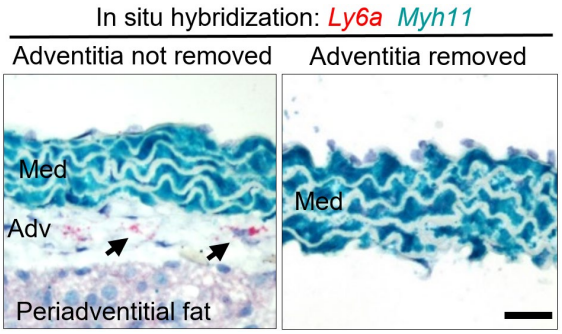
In situ hybridization: Ly6a Myh11
Adventitia not removed
Adventitia removed
Med
Adv
Periadventitial fat
Med

D

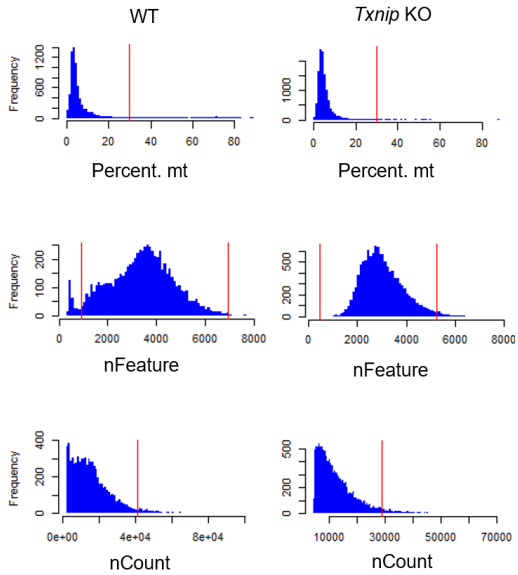

E

QC metrics	WT		*Txnip* KO	
	min	max	min	max
percent.mt %		30		30
nFeatures	900	6,932	453	5,217
nCounts	905	41,917	1053	29,046

Table. Threshold for the viable cells

QC metrics	WT		*Txnip* KO	
	Filtered	Survived	Filtered	Survived
percent.mt %	341	6,845	38	11,814
nFeatures	297	6,889	199	11,653
nCounts	262	6,924	516	11,336
All filter	622	6,564	590	11,262

Table. Filtration results

F

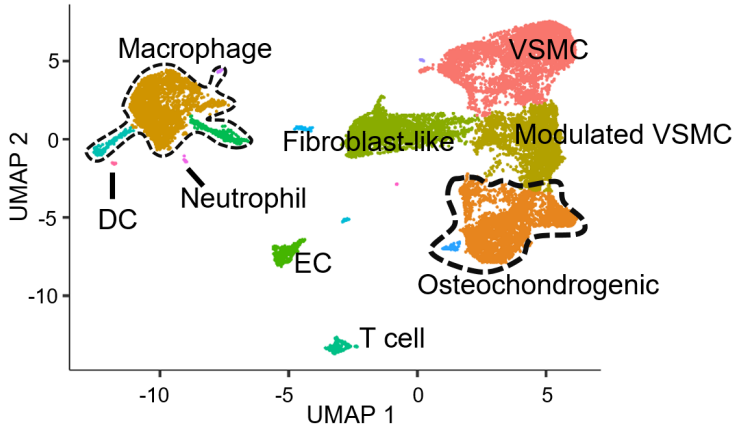

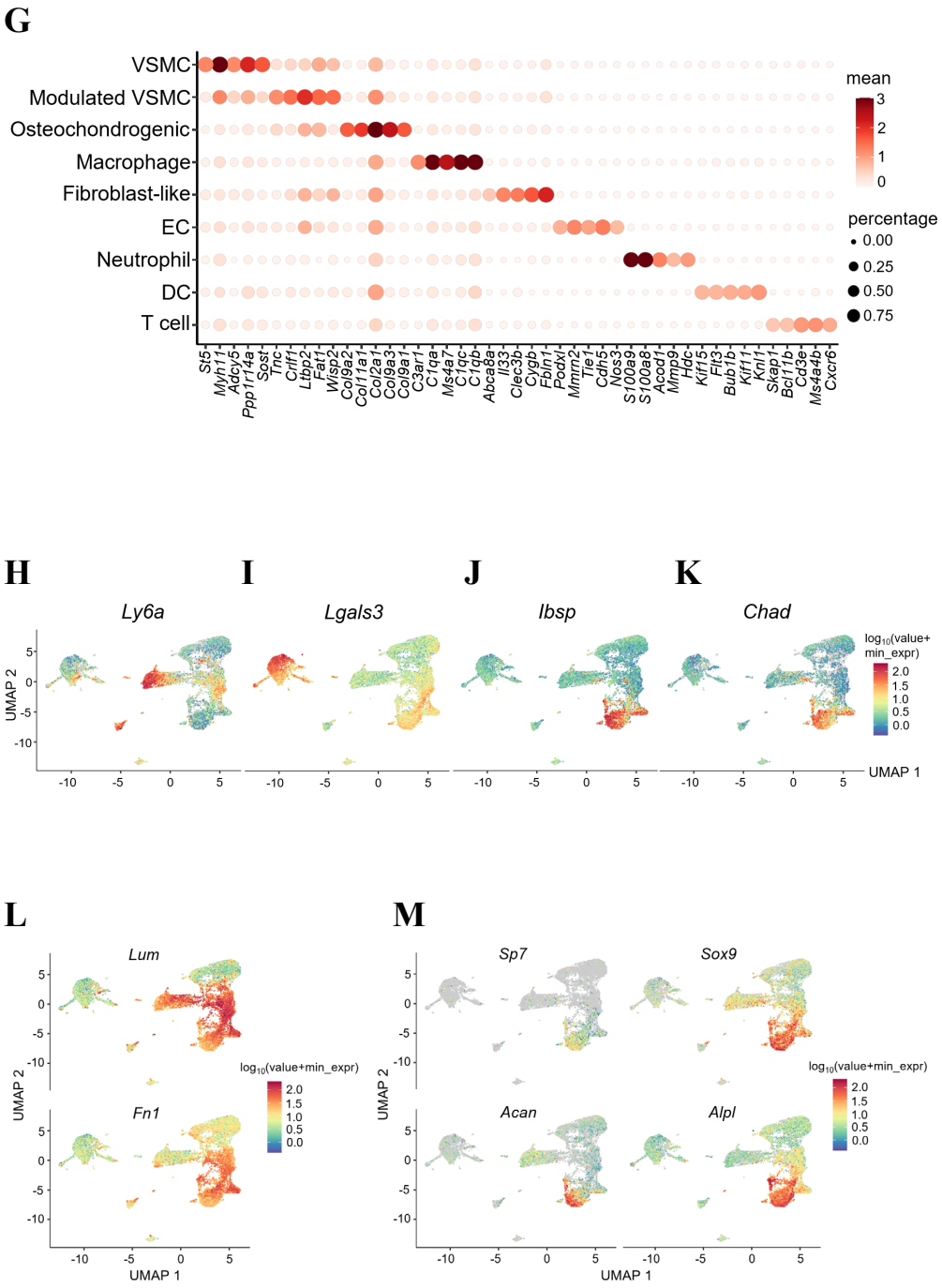
G
VSMC
Modulated VSMC
Osteochondrogenic
Macrophage
Fibroblast-like
EC
Neutrophil
DC
T cell
St5 Myh11 Adcy5 Ppp1r14a Sost Tnc Crlf1 Ltbp2 Fat1 Wisp2 Col9a2 Col11a1 Col2a1 Col9a3 Col9a1 C3ar1 C1qa Ms4a7 C1qc C1qb Abca8a Il33 Clec3b Cygb Fbln1 Podxl Mmrn2 Tie1 Cdh5 Nos3 S100a9 S100a8 Acod1 Mmp9 Hdc Kif15 Flt3 Bub1b Kif11 Knl1 Skap1 Bcl11b Cd3e Ms4a4b Cxcr6
mean
3
2
1
0
percentage
0.00
0.25
0.50
0.75
H
Ly6a
I
Lgals3
J
Ibsp
K
Chad
log10(value+min_expr)
2.0
1.5
1.0
0.5
0.0
UMAP 2
UMAP 1
5
0
-5
-10
L
Lum
Fn1
M
Sp7
Sox9
Acan
Alpl

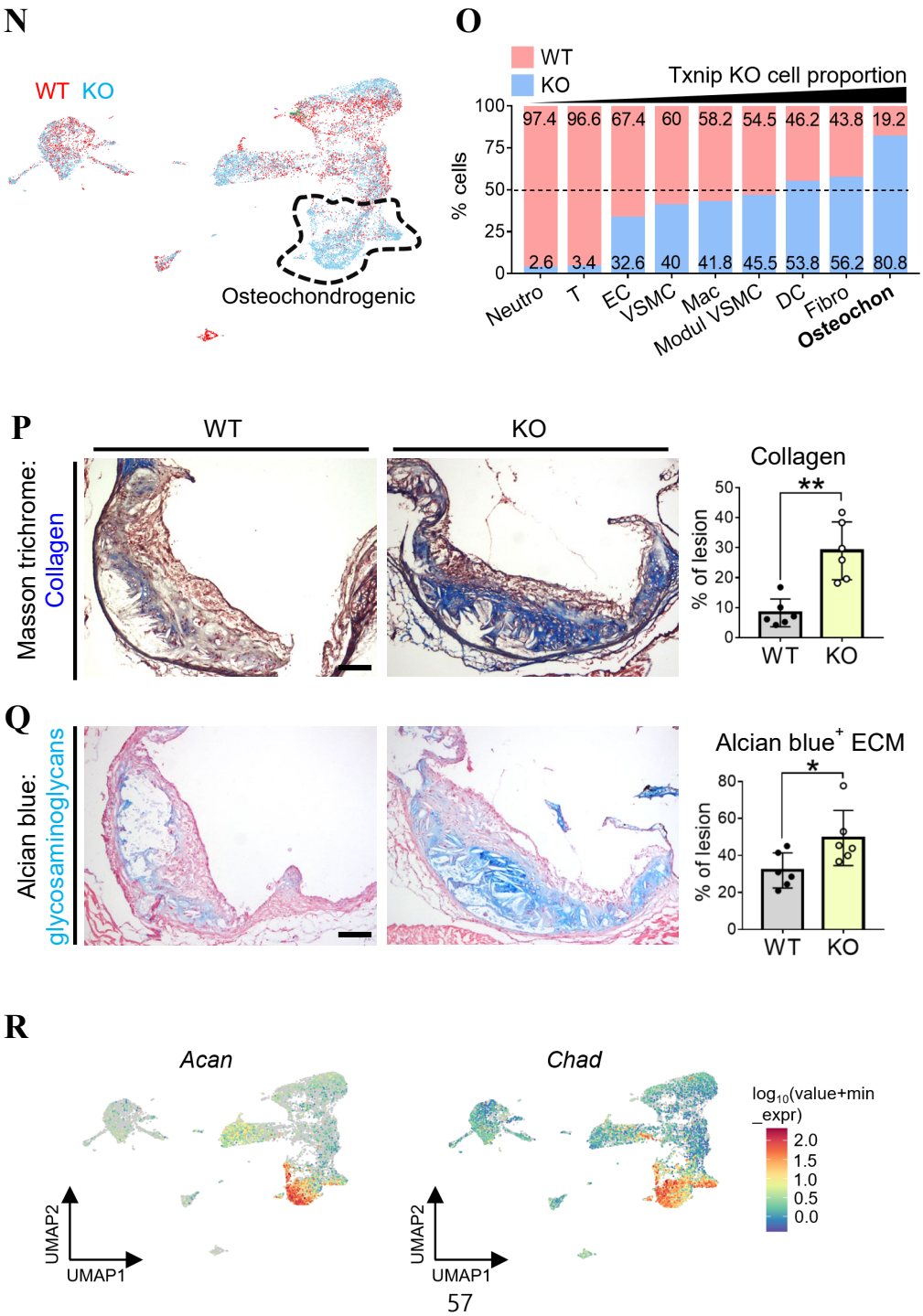
N
WT KO
Osteochondrogenic
O
WT
KO
Txnip KO cell proportion
% cells
100
75
50
25
0
97.4
96.6
67.4
60
58.2
54.5
46.2
43.8
19.2
2.6
3.4
32.6
40
41.8
45.5
53.8
56.2
80.8
Neutro
T
EC
VSMC
Mac
Modul VSMC
DC
Fibro
Osteochon
P
WT
KO
Masson trichrome:
Collagen
Collagen
% of lesion
**
WT
KO
Q
Alcian blue:
glycosaminoglycans
Alcian blue+ ECM
% of lesion
*
WT
KO
R
Acan
Chad
log10(value+min_expr)
2.0
1.5
1.0
0.5
0.0
UMAP2
UMAP1
UMAP2
UMAP1

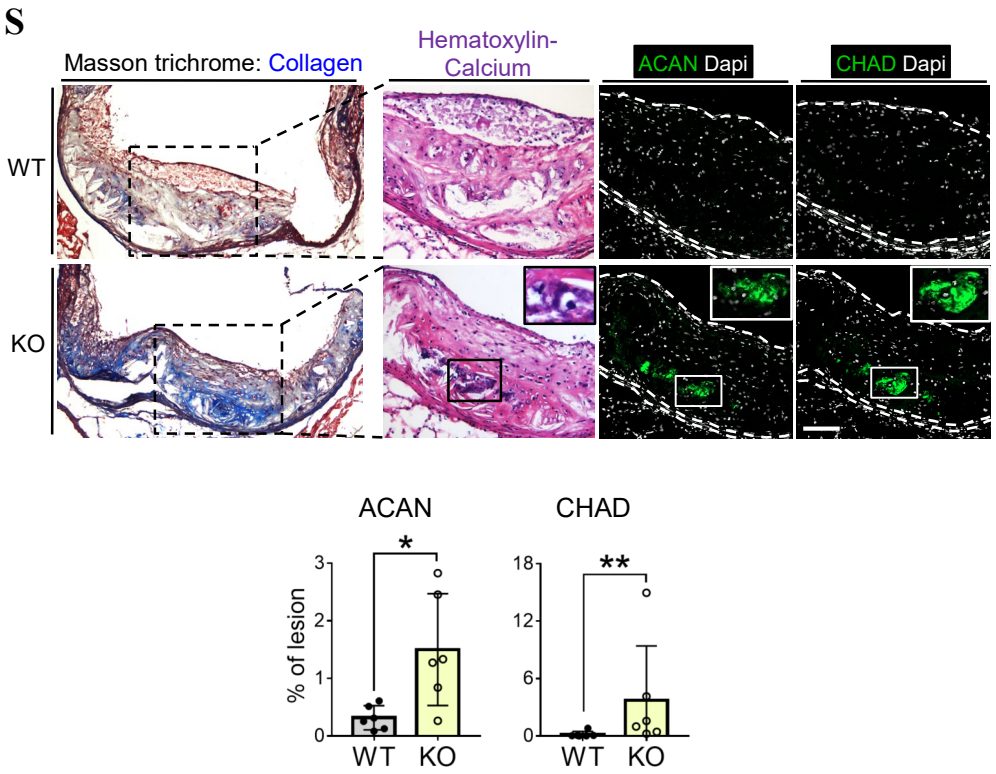

Figure 2 ScRNA-seq analysis reveals the osteochondrogenic cluster enriched with bone- and cartilage-related genes, which is markedly expanded in *Txnip* KO mice. (*A*) Overall experimental procedure. The atherosclerotic plaques of four mice from each WT and *Txnip* KO were pooled. After adventitial removal, the atherosclerotic lesion cells were enzymatically dissociated, and propidium iodide (PI)-negative cells were subjected to scRNA-seq. (*B*) Representative photographs showing sample preparation procedure. (a) Harvesting of the heart and aorta. (b) Periadventitial tissue removal. (c) Opening of the aortic sinus and removal of the aortic part below the aortic arch. (d) Removal of the heart tissue, including the aortic valves. (e) Enzymatic digestion for adventitial removal (f) Opening of the lumen. (g) Stripping of the adventitia. (h) Completion of the adventitial removal. Resulting adventitia-removed atherosclerotic lesion (marked by yellow box) was used for scRNA-seq experiment. (*C*) Confirmation of adventitial removal using *in situ* hybridization of *Ly6a* (red signal, marks adventitial *Ly6a*$^{+}$ cells) and *Myh11*

(green signal, marks medial SMCs). The scale bar represents 50 μm. (*D–E*) Histograms (*D*) and tables (*E*) showing the sample filtration results prior to dimensional reduction and integration of WT and *Txnip* KO scRNA-seq data. Low-quality cells were filtered out using nFeature (the number of expressed genes in each cell), nCount (total UMI counts in each cell), and percentage (percentage of the mitochondrial gene UMI counts) parameters. (*F*) UMAP visualization of integrated WT and *Txnip* KO scRNA-seq data. EC, endothelial cells. DC, dendritic cells. (*G*) Top five DEGs for each cluster. (*H–M*) Feature plots for *Ly6a*, *Lgals3*, *Ibsp*, *Chad, Lum, Fn1, Sp7, Sox9, Acan and Alpl*. (*N*) WT, and *Txnip* KO cells were separately visualized using UMAP. (*O*) The bar graphs showing the proportions of WT and *Txnip* KO for each cluster. (*P* and *Q*) Representative serial sections and quantification results of Masson trichrome staining (*P*, for collagen), Alcian blue (*Q*, for glycosaminoglycan ECM) on the aortic sinus of WT and *Txnip* KO. $n = 6/6$ for WT/*Txnip* KO. (*R*) Feature plots for *Acan* and *Chad*. (*S*) Representative serial section images showing the Masson trichrome staining, Hematoxylin and Eosin (H&E) staining, and immunostaining of the ACAN and CHAD on the aortic sinus sections of WT and *Txnip* KO. ACAN and CHAD-positive areas were quantified ($n = 6/6$ for WT/*Txnip* KO). Scale bar = 100 μm. The data in (*P* and *Q*), and the data of ACAN in (*S*) were analyzed by an unpaired Student's *t*-test (two-tailed). The data of CHAD in (S) by Mann–Whitney *U*-test (two-tailed). The error bars denote standard deviation. $*P < 0.05$, $**P < 0.01$.

Hematopoietic deficiency of TXNIP did not affect atherosclerotic calcification.

Although VSMCs are known to play a major role in atherosclerotic calcification, immune cells, such as macrophages/foam cells can directly affect the calcification via producing matrix vesicles (New, Goettsch et al. 2013) or providing a nucleating site through cell death/apoptosis, and also indirectly by creating a microenvironment facilitating calcification by inflammatory cytokines or secreting BMPs (Johnson, Leopold et al. 2006). Accordingly, I tested whether the hematopoietic absence of TXNIP could affect atherosclerosis using a bone marrow (BM) transplantation mouse model. The BM cells of WT or *Txnip* KO mice were transplanted into lethally irradiated WT mice (hereafter named BM^{WT} and BM^{KO} mice for each group). After six weeks of BM reconstruction, the mice were injected with PCSK9-AAV and fed HFD for 16 weeks (*Figure 3A*). I confirmed the transplantation of WT and *Txnip* KO BM cells by blood PCR (*Figure 3B*). The lipid profiles of BM^{WT} and BM^{KO} mice were comparable, except for a slight elevation of plasma low-density lipoprotein (LDL) in BM^{KO} mice (*Figure 3C*). I did not observe any notable differences between the BM^{WT} and BM^{KO} mice in the lesion size, macrophage contents, plaque calcification, or collagen content (*Figure 3D–H*).

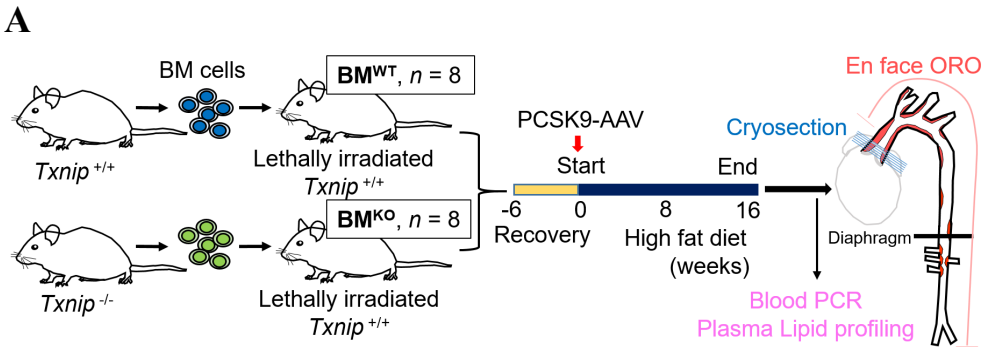
A
BM cells
Txnip +/+
BMWT, n = 8
Lethally irradiated
Txnip +/+
Txnip -/-
BMKO, n = 8
Lethally irradiated
Txnip +/+
PCSK9-AAV
Start
End
-6
0
8
16
Recovery
High fat diet
(weeks)
En face ORO
Cryosection
Diaphragm
Blood PCR
Plasma Lipid profiling

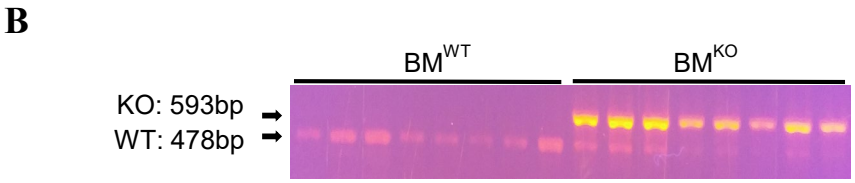
B
BMWT
BMKO
KO: 593bp
WT: 478bp

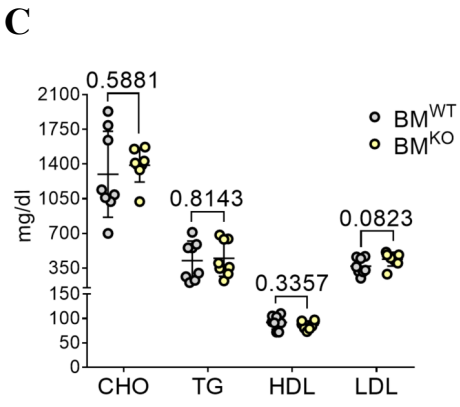
C
0.5881
0.8143
0.3357
0.0823
BMWT
BMKO
mg/dl
2100
1750
1400
1050
700
350
150
100
50
0
CHO
TG
HDL
LDL

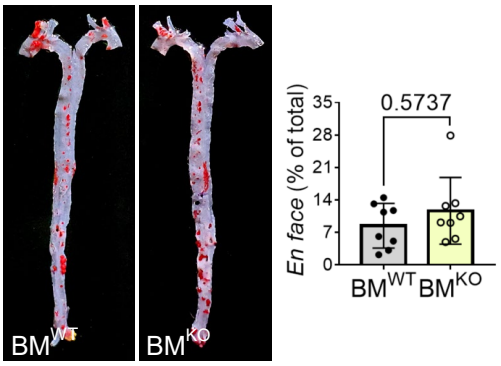
D
BMWT
BMKO
0.5737
En face (% of total)
35
28
21
14
7
0
BMWT
BMKO

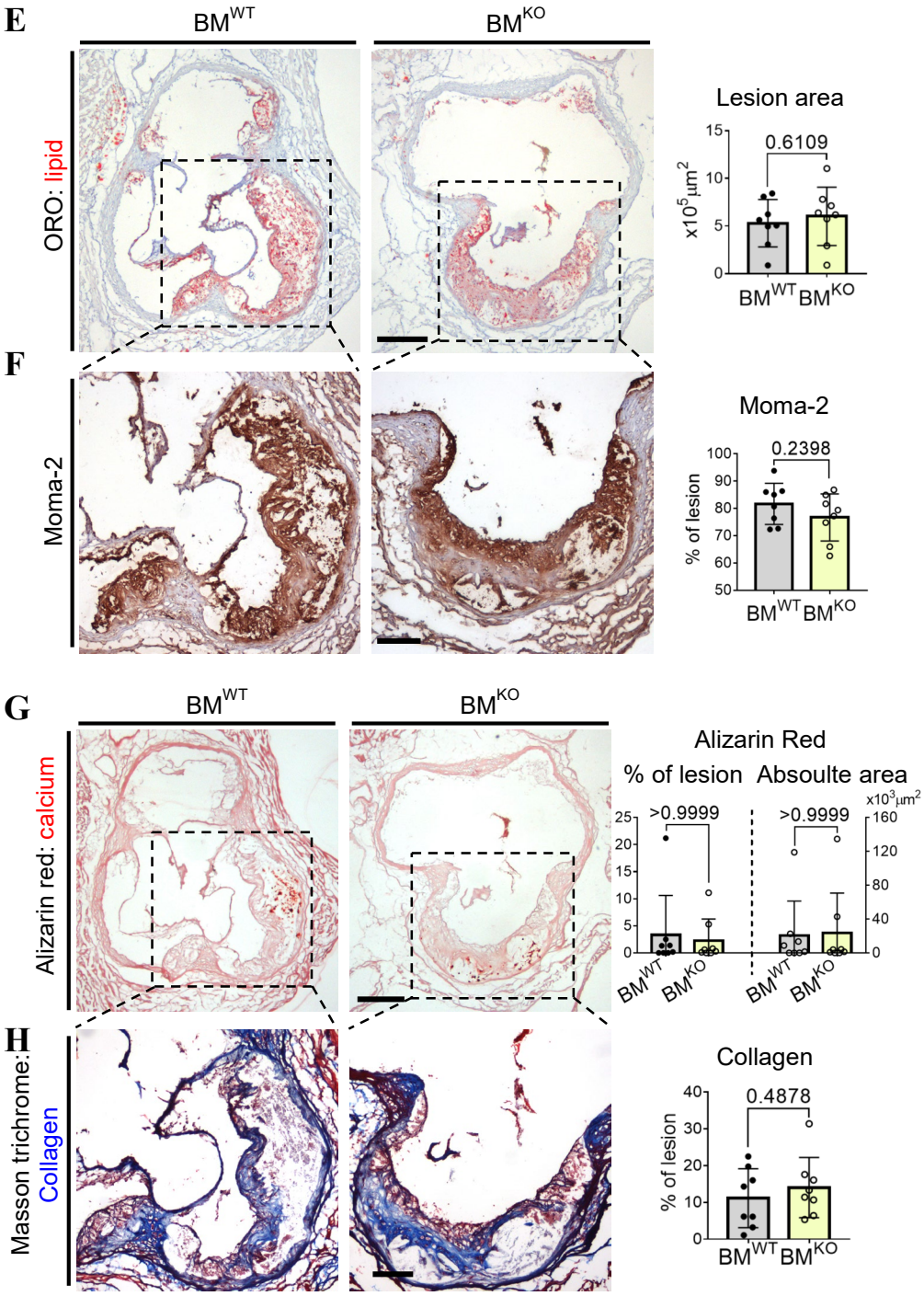
E
BMWT
BMKO
ORO: lipid
Lesion area
0.6109
x10^5 µm^2
BMWT BMKO
F
Moma-2
Moma-2
0.2398
% of lesion
BMWT BMKO
G
BMWT
BMKO
Alizarin red: calcium
Alizarin Red
% of lesion
Absoulte area
x10^3 µm^2
>0.9999
>0.9999
BMWT BMKO
BMWT BMKO
H
Masson trichrome:
Collagen
Collagen
0.4878
% of lesion
BMWT BMKO

Figure 3 Hematopoietic deficiency of TXNIP does not affect the lesion phenotype. (*A*) Schematic illustration of the experiment. BM cells of *WT* or *Txnip* KO mice were transplanted into WT mice. After 6 weeks of recovery, the mice were injected with PCSK9-AAV and fed HFD for 16 weeks. *n* of $BM^{WT}/BM^{KO} = 8/8$. (*B*) Blood PCR result indicating the successful transfusion of the WT and *Txnip* KO BM cells. (*C*) The plasma concentrations of total cholesterol (CHO), triglyceride, high-density lipoprotein (HDL), and low-density lipoprotein (LDL) (*D*) Comparison of the Oil Red O (ORO)-positive areas between BM^{WT} and BM^{KO} on en-face aorta. (*E–H*) Characterization of atherosclerotic lesions using the 7 μm of perpendicular serial sections (total 70-80 sections) prepared from the aortic sinus. Representative serial sections and quantification results of Oil Red O (ORO) staining (*E*, for lesion size), Moma-2 immunostaining (*F*, for monocyte/macrophage), Alizarin red staining (*G*, for calcium), Masson trichrome staining (*H*, for collagen). The scale bars in (*E* and *G*) represent 400 μm; (*F* and *H*) represent 200 μm. The data in (*C*, *E*, *F*, and *H*) were analyzed by an unpaired Student's *t*-test (two-tailed). The data in (*D* and *G*) was analyzed using the Mann–Whitney *U*-test (two-tailed). The error bars denote standard deviation. $*P < 0.05$. In all other cases, the exact *P* values are specified.

The osteochondrogenic cluster is derived from VSMCs.

Since I could not trace the VSMC-derived cells using WT and *Txnip* KO scRNA-seq data set alone (that is, due to the lack of a SMC-lineage tracing reporter system), I integrated WT and *Txnip* KO scRNA-seq data with the data from Pan et al (Pan, Xue et al. 2020). Pan et al. labeled the SMC-lineage cells permanently with ZsGreen1 fluorescence using *Myh11*-CreER^{T2} on *Ldlr* KO background (*ROSA26*$^{ZsGreen1/+}$; *Ldlr*$^{-/-}$; *Myh11-CreER*^{T2}). The integration of two different scRNA-seq data successfully retrieved the most typical atherosclerotic lesion clusters (*Figure 4A–B*). The top five DEGs for each cluster are shown by heatmap in *Figure 4C*. The representative selected marker genes for the VSMC (*Myh11*), modulated VSMC (*Ly6a*), and osteochondrogenic (*Sp7* and *Ibsp*) clusters are shown in *Figure 4D*. When the integrated data were separated according to the ZsGreen1 fluorescence, the modulated VSMCs and osteochondrogenic clusters were almost absent in ZsGreen1 negative cells, implying that these two clusters originated from VSMCs (*Figure 4E*).

A

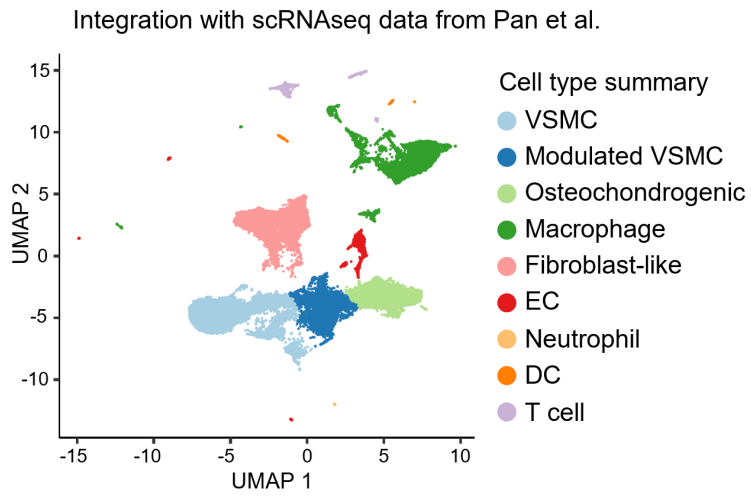
Integration with scRNAseq data from Pan et al.
UMAP 2
UMAP 1
Cell type summary
VSMC
Modulated VSMC
Osteochondrogenic
Macrophage
Fibroblast-like
EC
Neutrophil
DC
T cell

B

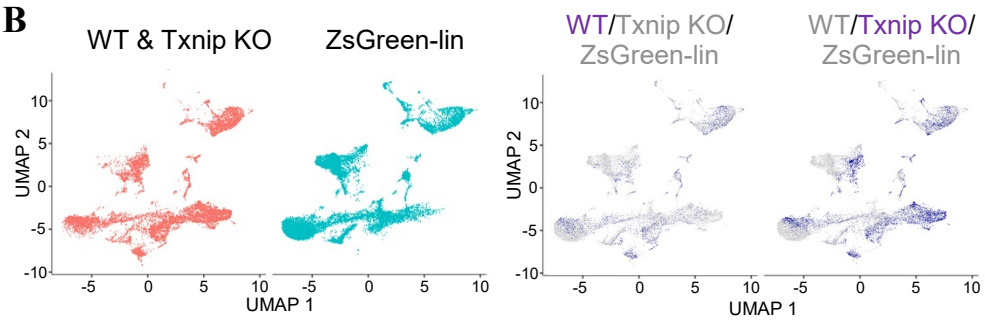
WT & Txnip KO
ZsGreen-lin
WT/Txnip KO/
ZsGreen-lin
WT/Txnip KO/
ZsGreen-lin
UMAP 2
UMAP 1

C

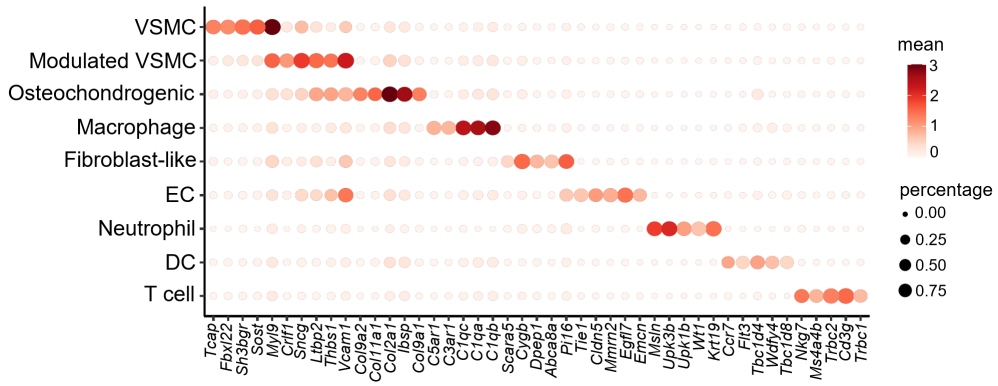
VSMC
Modulated VSMC
Osteochondrogenic
Macrophage
Fibroblast-like
EC
Neutrophil
DC
T cell
Tcap
Fbxl22
Sh3bgr
Sost
Myl9
Crlf1
Sncg
Ltbp2
Thbs1
Vcam1
Col9a2
Col11a1
Col2a1
Ibsp
Col9a1
C5ar1
C3ar1
C1qc
C1qa
C1qb
Scara5
Cygb
Dpep1
Abca8a
Pi16
Tie1
Cldn5
Mmrn2
Egfl7
Emcn
Vsin
Upk3b
Upk1b
Wt1
Krt19
Ccr7
Flt3
Tbc1d4
Wdfy4
Tbc1d8
Nkg7
Ms4a4b
Trbc2
Cd3g
Trbc1
mean
3
2
1
0
percentage
0.00
0.25
0.50
0.75

D

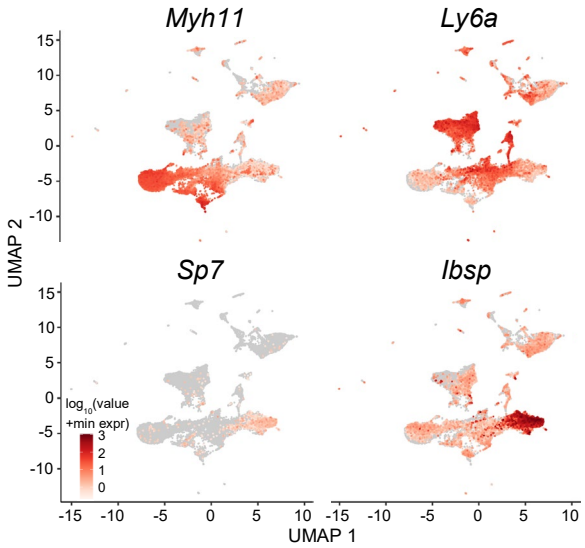
Myh11
Ly6a
Sp7
Ibsp
UMAP 2
UMAP 1
log10(value +min expr)

E

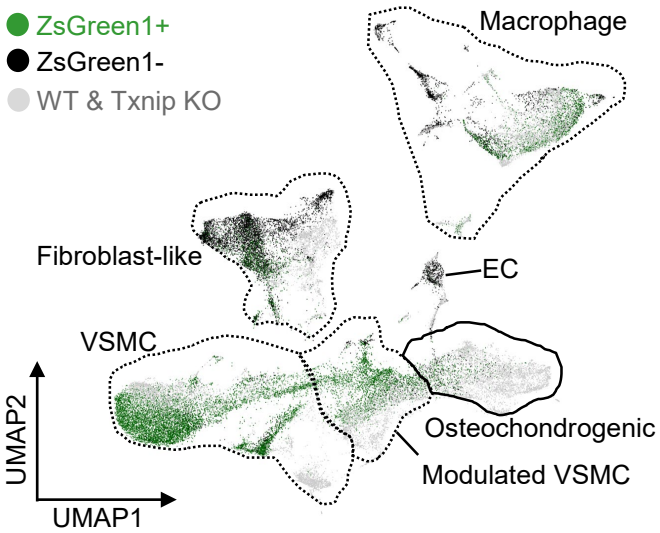
ZsGreen1+
ZsGreen1-
WT & Txnip KO
Macrophage
Fibroblast-like
EC
VSMC
Osteochondrogenic
Modulated VSMC
UMAP2
UMAP1

Figure 4 Integration of the scRNA-seq data reveals the modulated VSMC and osteochondrogenic cluster are VSMC-derived populations. Pan et al. conducted scRNA-seq of atherosclerotic lesions using ZsGreen1-lineage traced SMC (*ROSA26*$^{ZsGreen1/+}$; *Ldlr*$^{-/-}$; *Myh11*-CreER^{T2}). (*A*) UMAP visualization of two integrated scRNA-seq datasets. EC, endothelial cells. DC, dendritic cells. (*B*) The WT & *Txnip* KO and ZsGreen-lin (data of Pan et al.) datasets are shown separately on UMAPs. (*C*) Top five DEGs for each cluster (*D*) Feature plots showing the expression of *Myh11*, *Ly6a*, *Sp7*, and *Ibsp* genes. (*E*) ZsGreen1 fluorescence-positive and -negative cells are shown on UMAP. It is notable that only a few ZsGreen1 negative cells exist in the modulated VSMCs and osteochondrogenic clusters.

Analyzing VSMC-derived cell clusters revealed the enhancement of bone and cartilage formation pathways in *Txnip* KO mice.

I selected the VSMC lineage cells (VSMCs, modulated VSMCs, and osteochondrogenic clusters) for further analysis. The modulated VSMCs were separated into two clusters depending on the *Ly6a* expression level (*Ly6a*^{low} and *Ly6a*^{high} Modul VSMC) (*Figure 5A*). Osteochondrogenic populations were separated into three clusters. The osteochondrogenic cluster (a) occupied a major portion and was contiguous with the *Ly6a*^{high} Modul VSMC cluster (*Figure 5A*). The feature plots for the selected marker genes *Myh11* (VSMC), *Ly6a* & *Lum* (Modul VSMC), *Lgals3* (Modul VSMC ~ osteochondrogenic), *and Ibsp* & *Chad* (osteochondrogenic) are shown in *Figure 5B*. Before proceeding to further analyses, I examined the relationship between normal VSMCs (i.e., VSMCs from undiseased aorta) and VSMC-derived cells of WT and *Txnip* KO from atherosclerotic lesions. For this, I integrated the scRNA-seq data of Dobnikar et al. (GSE1179763, Dobnikar, Taylor et al. 2018), which consisted of normal VSMCs from the aortic arch (AA) and distal thoracic aorta (DT) into WT and *Txnip* KO dataset. The AA and DT cells were confined to the VSMC cluster, and showed few or no expression of the Modul VSMCs or osteochondrogenic cluster-related markers (*Figure C–E*), confirming that Modul VSMC and the osteochondrogenic cluster were atherosclerosis-related cell populations.

The proportion of *Ly6a*^{high} Modul VSMCs was similar between the WT and *Txnip* KO mice, whereas all three osteochondrogenic clusters were markedly

increased in the *Txnip* KO mice (*Figure 5D*). To localize the VSMC-derived cell populations and confirm the proportional differences between WT and *Txnip* KO, I performed *in situ* hybridization. The experiment was validated by probing *Polr2a* & *Ppib* (positive control; constitutively expressed genes of mouse) and *DapB* (negative control; constitutively expressed genes of *E. coli*) on WT atherosclerotic lesions (*Figure 5G*). I observed medial cells that gained *Ly6a* expression and lost *Myh11* expression, which represented the cells of the Modul VSMC cluster (*Figure 5H*). In line with the scRNA-seq data, WT and *Txnip* KO mice showed comparable medial $Ly6a^{+}Myh11^{+}$ cell numbers (*Figure 5H*). The $Chad^{+}$ cells were mostly localized within the lesions, which showed a cartilage-like morphology (*Figure 5I–J*). The $Ly6a^{+}$ cells were occasionally observed adjacent to the $Chad^{+}$ cells. Atherosclerotic lesions of *Txnip* KO mice had a significantly higher number of $Chad^{+}$ cells than those of WT mice (*Figure 5I–J*).

To gain insight into the underlying process by which TXNIP regulates atherosclerotic calcification, I first sought DEGs between WT and *Txnip* KO for VSMC-derived cells (that is, tying VSMC, Modul VSMC, and osteochondrogenic clusters). The bone- and cartilage-related genes, such as *Comp* (cartilage oligomeric matrix protein), *Sparc* (secreted protein acidic and cysteine rich), *Hapln1* (hyaluronan and proteoglycan link protein 1), *Ibsp*, *Acan*, and various collagen-producing genes, were highly upregulated in VSMC-derived cells of *Txnip* KO (*Figure 5K*). Correctly so, *Txnip* occupied the top position of the WT-enriched genes. Next, I performed a gene ontology

pathway analysis using the DEGs of VSMC-derived cells of WT and *Txnip* KO. The pathways, such as “skeletal system development,” “ossification,” “chondrocyte differentiation,” “extracellular matrix organization,” “bone development,” and “cartilage development” were enriched in the VSMC-derived cells of *Txnip* KO (*Figure 5L*).

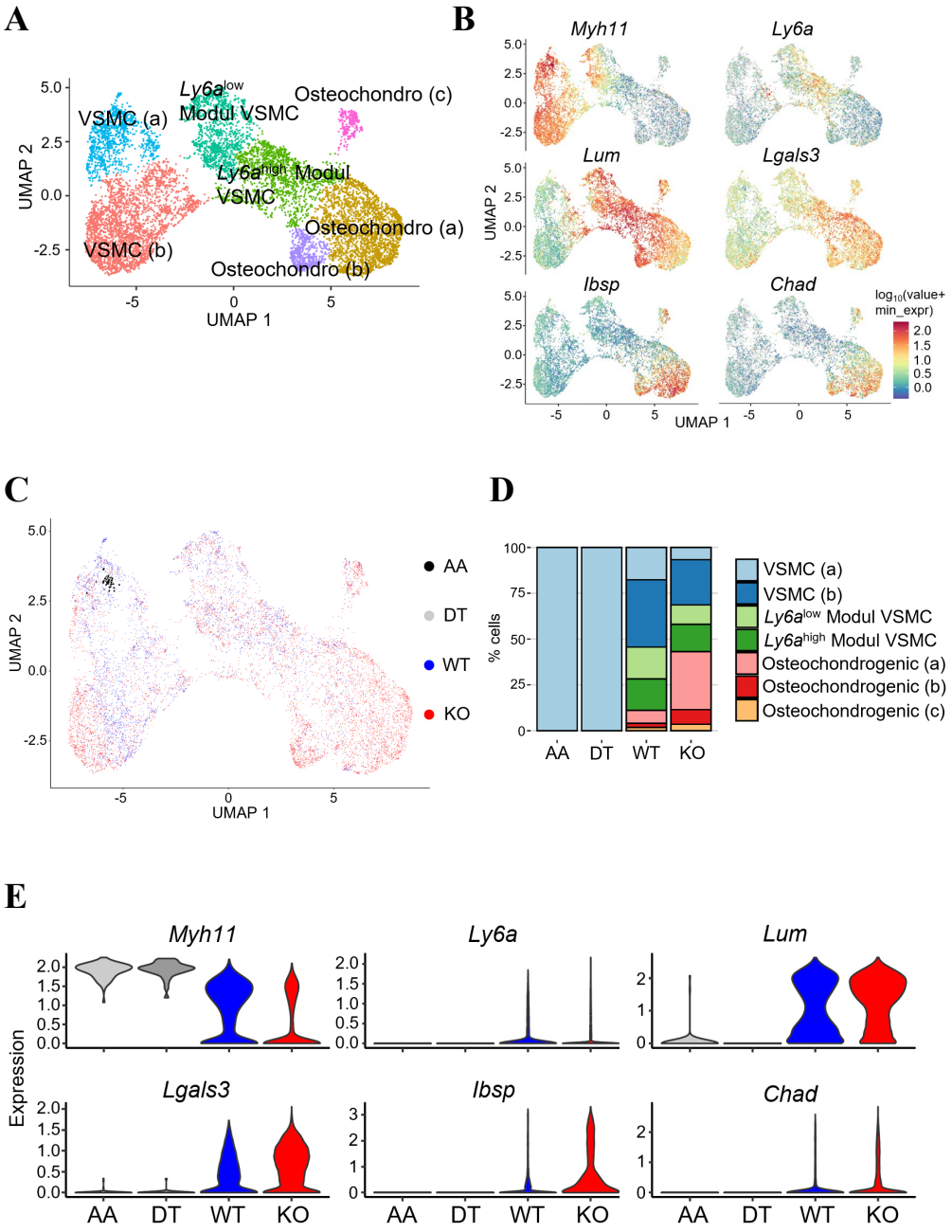
A
VSMC (a)
Ly6a^low Modul VSMC
Osteochondro (c)
Ly6a^high Modul VSMC
Osteochondro (a)
VSMC (b)
Osteochondro (b)
UMAP 1
UMAP 2
B
Myh11
Ly6a
Lum
Lgals3
Ibsp
Chad
log10(value+ min_expr)
C
AA
DT
WT
KO
D
% cells
VSMC (a)
VSMC (b)
Ly6a^low Modul VSMC
Ly6a^high Modul VSMC
Osteochondrogenic (a)
Osteochondrogenic (b)
Osteochondrogenic (c)
E
Expression

F

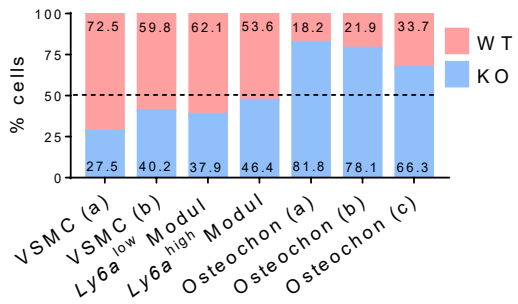

G

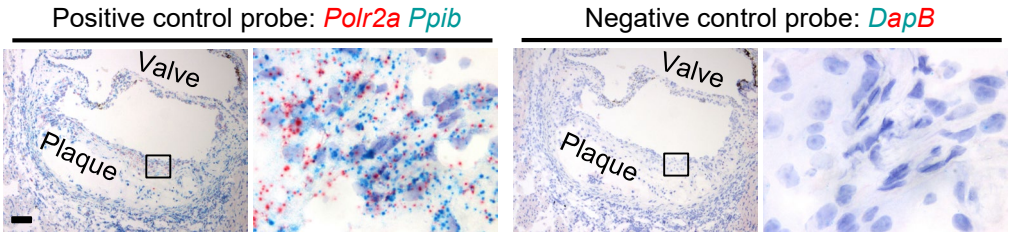

H

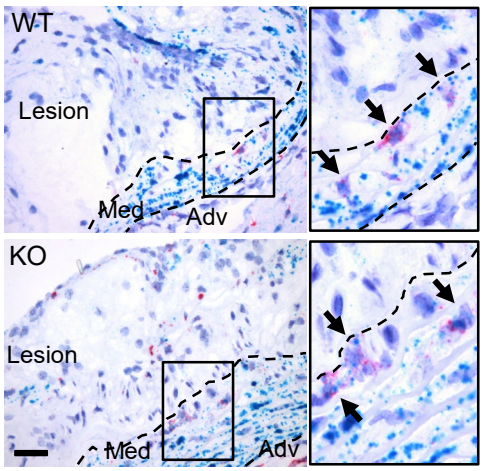

I

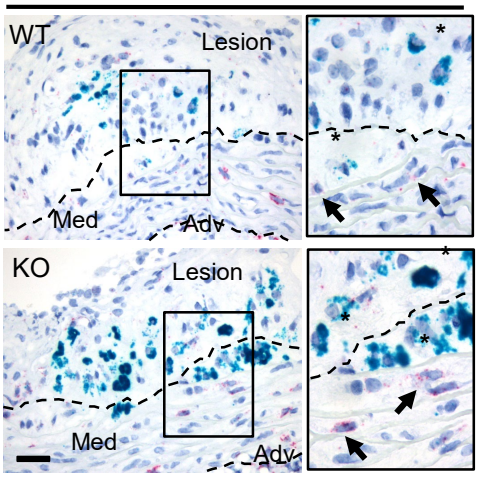

Medial *Ly6a*$^{+}$*Myh11*$^{+}$ cells

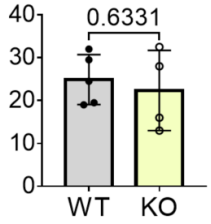

Chad^{+} cells

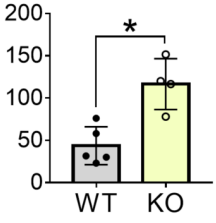

J

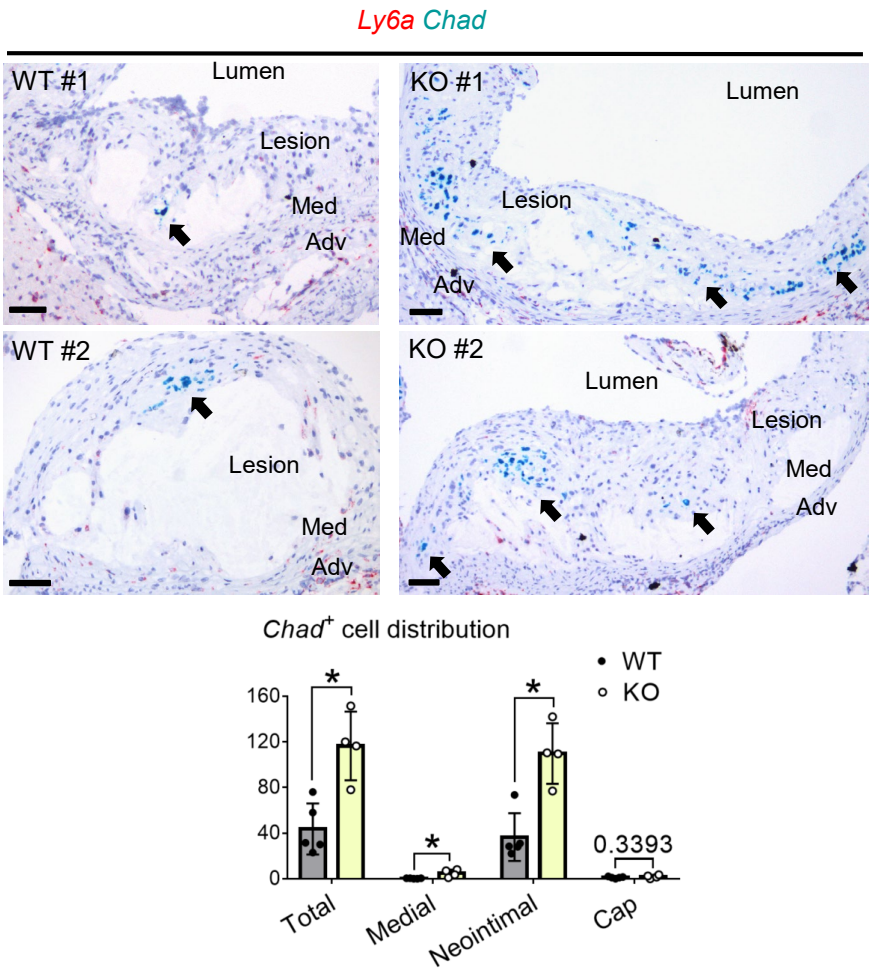
Ly6a Chad
WT #1
Lumen
Lesion
Med
Adv
KO #1
Lumen
Lesion
Med
Adv
WT #2
Lesion
Med
Adv
KO #2
Lumen
Lesion
Med
Adv
Chad+ cell distribution
WT
KO
160
120
80
40
0
*
*
*
0.3393
Total
Medial
Neointimal
Cap

K

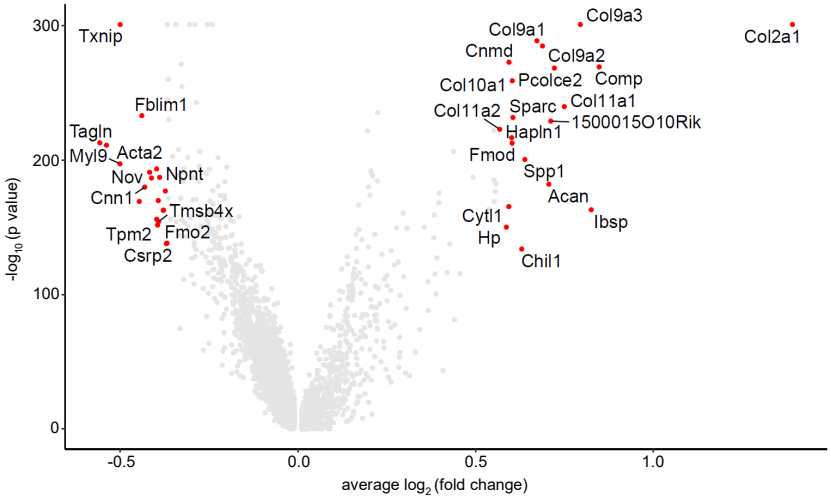
Txnip
Fblim1
Tagln
Myl9
Acta2
Nov
Npnt
Cnn1
Tmsb4x
Tpm2
Fmo2
Csrp2
Col9a3
Col9a1
Col2a1
Cnmd
Col9a2
Col10a1
Pcolce2
Comp
Col11a2
Sparc
Col11a1
1500015O10Rik
Hapln1
Fmod
Spp1
Acan
Cytl1
Ibsp
Hp
Chil1
300
200
100
0
-log10 (p value)
-0.5
0.0
0.5
1.0
average log2 (fold change)

L

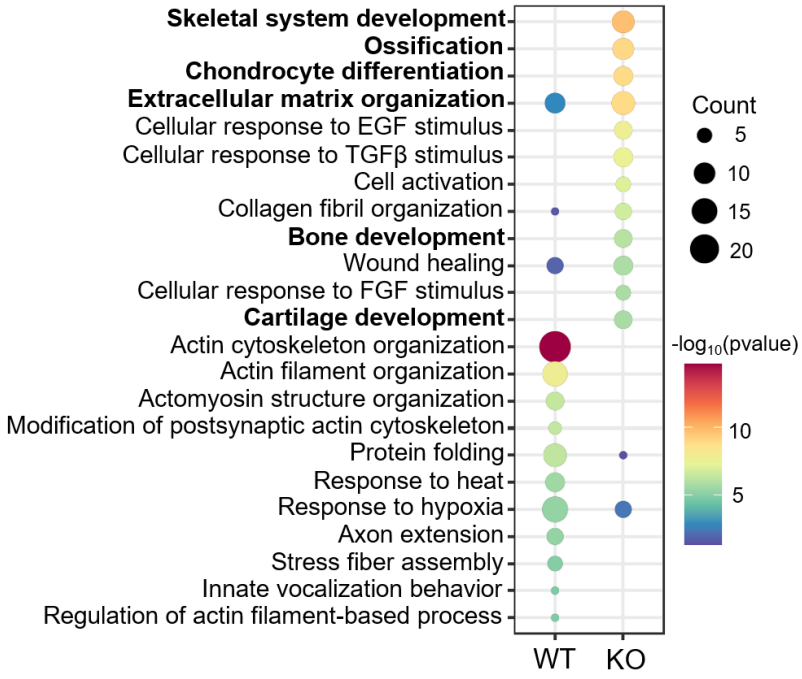
Skeletal system development
Ossification
Chondrocyte differentiation
Extracellular matrix organization
Cellular response to EGF stimulus
Cellular response to TGFβ stimulus
Cell activation
Collagen fibril organization
Bone development
Wound healing
Cellular response to FGF stimulus
Cartilage development
Actin cytoskeleton organization
Actin filament organization
Actomyosin structure organization
Modification of postsynaptic actin cytoskeleton
Protein folding
Response to heat
Response to hypoxia
Axon extension
Stress fiber assembly
Innate vocalization behavior
Regulation of actin filament-based process
WT
KO
Count
5
10
15
20
-log10(pvalue)
10
5

Figure 5 Analyzing VSMC-derived cell clusters reveals the enhancement of bone and cartilage formation pathways in *Txnip* KO mice, and the downregulation of *TXNIP* in human calcified atherosclerotic plaques. (*A*) UMAP of sub-clustered VSMC-derived cells. Modul, modulated. (*B*) Feature plots for *Myh11*, *Ly6a*, *Lum*, *Lgals3*, *Ibsp*, and *Chad*. (*C–D*) Normal VSMCs on WT & *Txnip* KO scRNA-seq data. ScRNA-seq data consisting of the aortic arch (AA) and distal thoracic aorta (DT) from normal healthy WT mice (GSE1179763) were integrated into WT and *Txnip* KO mice scRNA-seq data. (*C*) UMAP color labeled by the samples. (*D*) Cell type fraction rate of the samples. (*E*) Violin plots showing expression of representative marker genes *Myh11* (VSMC cluster), *Ly6a*, *Lum* (modulated VSMC cluster), *Lgals3* (modulated VSMC~osteochondrogenic cluster), *Ibsp*, and *Chad* (osteochondrogenic cluster). (*F*) Bar graphs showing the proportions of WT and *Txnip* KO mice for each cluster. (*G*) The *in situ* hybridization experiment was validated by probing *Polr2a* and *Ppib* (positive control) and *DapB* (negative control) on WT atherosclerotic lesions. (*H–J*) Localization of the VSMC-derived clusters and confirmation of the cell proportion using *in situ* hybridization (n = 5/4 for WT/*Txnip* KO). Scale bar = 100 μm. Med, medial layer. Adv, adventitial layer. Detection and quantification of medial $Ly6a^{+}Myh11^{+}$ cells (marked by arrows) representing the Modul SMC cluster (*H*), and $Chad^{+}$ cells (marked with asterisks) representing the osteochondrogenic cluster (*I*). The $Ly6a^{+}$ cells (marked by arrows) were occasionally observed adjacent to $Chad^{+}$ cells. (*J*) Comparison of $Chad^{+}$ cells at each location between WT and *Txnip* KO mice. (*K*) A volcano plot showing DEGs between WT and *Txnip* KO for the VSMC-derived cell population. VSMCs, modulated VSMCs, and osteochondrogenic clusters were tied together as VSMC-derived cells. (*L*) Results of gene ontology pathway analysis using DEGs of VSMC-derived cells from WT and *Txnip* KO. The data in (*H–J*) were analyzed using an unpaired Student's *t*-test (two-tailed). The error bars denote standard deviation. $*P < 0.05$. In other case, the exact P value is specified.

***TXNIP* is downregulated in the modulated VSMCs and osteochondrogenic cells of human calcified atherosclerotic plaques.**

Next, I examined the expressions of TXNIP in the VSMCs of calcified atherosclerotic plaques in humans by reanalyzing the public transcriptome database. Alsaigh et al. (GSE159677, Alsaigh, Evans et al. 2020) conducted scRNA-seq on the atherosclerotic core portion (AC) of endarterectomized type VII calcified plaques matched with the proximal adjacent regions (PA). Reanalyzing the VSMC cluster (*MYH11* and *ACTA2* positive cluster) of GSE159677 gave four clusters: VSMC, modulated VSMC, osteochondrogenic and fibroblast-like cluster (*Figure 6A*). The feature plots for bone and cartilage-related genes *CRTAC1* (cartilage acidic protein 1), *HAPLN1* (hyaluronan and proteoglycan link protein 1), and collagen-producing gene *COL1A1* are shown in *Figure 6B*. *TXNIP* was down regulated in the modulated VSMC (2.87 fold, adjusted *P* value = 9.53×10^{-5}) and the osteochondrogenic cluster (4.35 fold, adjusted *P* value = 4.57×10^{-21}) of AC compared to PA (*Figure 6C*). Subsequently, I observed the expression of TXNIP at the protein level in the human endarterctomized atheroma plaque samples harboring calcification by using immunohistochemistry. TXNIP was diminished in the medial side (marked by α-SMA on the serial sections) of the periphery of the calcified area (*Figure 6D*).

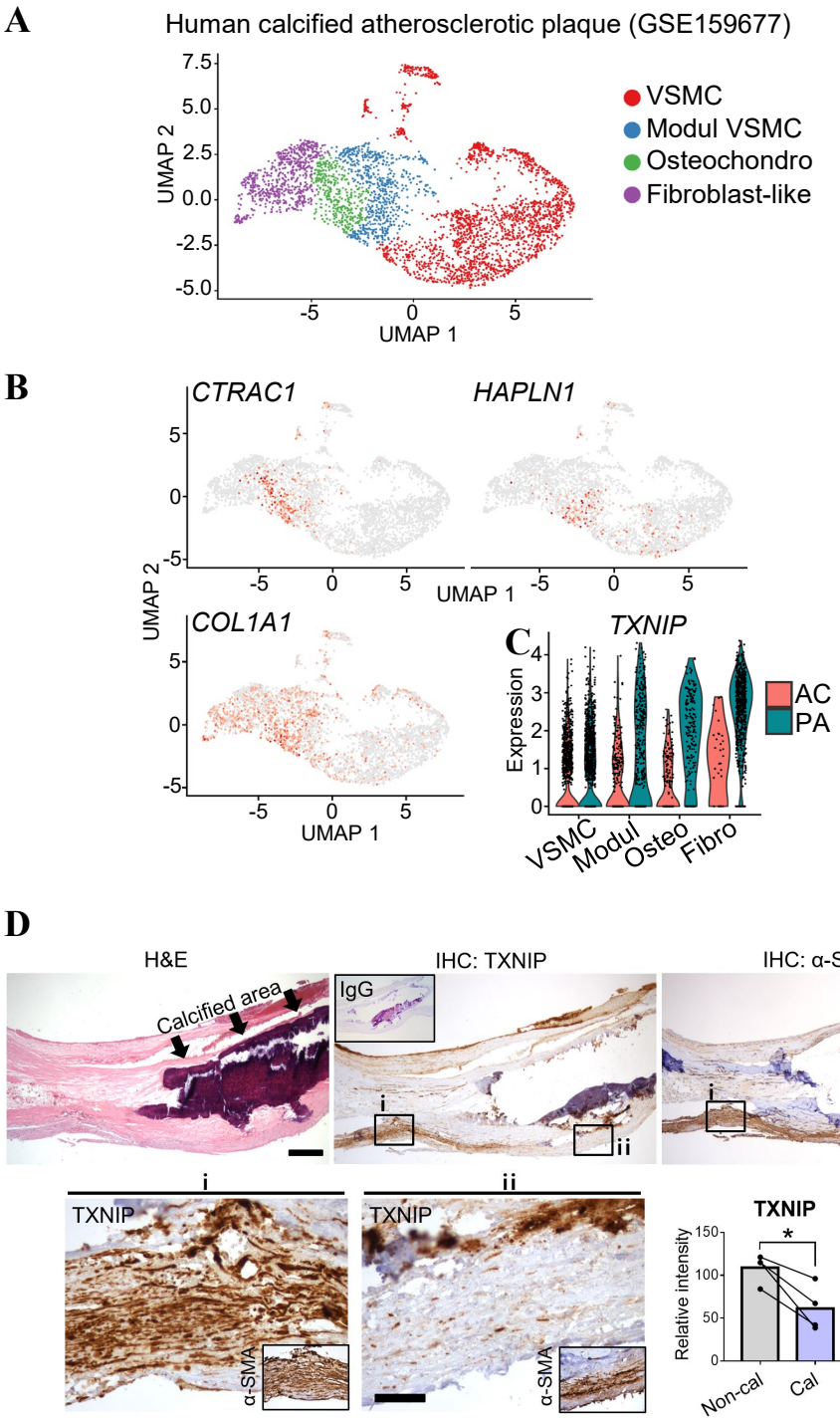
A
Human calcified atherosclerotic plaque (GSE159677)
UMAP 2
UMAP 1
VSMC
Modul VSMC
Osteochondro
Fibroblast-like
B
CTRAC1
HAPLN1
COL1A1
TXNIP
C
Expression
AC
PA
VSMC
Modul
Osteo
Fibro
D
H&E
Calcified area
IHC: TXNIP
IgG
IHC: α-SMA
TXNIP
α-SMA
Relative intensity
Non-cal
Cal

Figure 6 Downregulation of *TXNIP* in the modulated VSMCs and osteochondrogenic cells of human calcified atherosclerotic plaques. (*A–C*) Alsaigh et al. conducted scRNA-seq on the atherosclerotic core portion (AC) of endarterectomized type VII calcified plaques matched with the proximal adjacent regions (PA). VSMC cluster (*MYH11* and *ACTA2* positive cluster) of GSE159677 was reanalyzed. (*A*) UMAP showing reprocessed VSMC cluster. Modul, modulated. (*B*) Feature plots of osteochondrogenic genes *CRTAC1*, *HAPLN1*, and *COL1A1*. (*C*) Violin plots showing the expressions of *TXNIP*. (*D*) Immunohistochemistry of TXNIP in human endartertomized atheroma plaque samples harboring plaque calcification. Medial side was marked by *α*-SMA immunostaining on the serial sections. The scale bars represent 400 μm for low and 50 μm for high magnification. The TXNIP signals between the non-calcified and calcified areas were analyzed by a paired Student's *t*-test (two-tailed, $n = 4$). *$P < 0.05$.

VSMC-specific *Txnip* ablation recapitulates the calcification and collagen-rich plaque phenotype of global *Txnip* KO mice.

To confirm the VSMC-specific inhibitory role of TXNIP in atherosclerotic calcification, I generated mice in which *Txnip* was specifically ablated in SMCs by crossing *Tagln*-Cre and *Txnip*$^{flox/flox}$ mice. *Tagln*-Cre; *Txnip*$^{flox/flox}$ (hereafter named SMC^{KO} mice) and their littermate controls that did not carry the *Tagln*-Cre transgene (hereafter named SMC^{WT} mice) were used. Atherosclerosis was also induced by AAV-mediated *PCSK9* overexpression with 16 weeks of HFD (*Figure 7A*). I analyzed the efficiency and specificity of *Txnip* ablation under the *Tagln* (*SM22α*) promoter. SMC^{KO} mice showed ~90% decreased *Txnip* mRNA expression in the aortic media, whereas the expression of liver and quadriceps muscles was comparable to that in SMC^{WT} mice (*Figure 7B*). In addition, SMC^{KO} showed ~84% decreased *Txnip* mRNA expression in the adventitia, probably because the *Tagln*-Cre mice (B6.Cg-Tg(Tagln-Cre)1Her/J) also showed Cre expression in perivascular adipocytes and their precursors (Chakraborty, Saddouk et al. 2019). TXNIP was successfully eliminated in the SMCs of the aortic media at the protein level in SMC^{KO} mice, whereas the skeletal muscle showed comparable TXNIP level between SMC^{WT} and SMC^{KO} mice (*Figure 7C*). The lipid profiles of the SMC^{KO} mice were comparable to those of SMC^{WT} mice (*Figure 7D*). Unlike *Txnip* KO mice, there were no differences in the lesion size nor macrophage burden between SMC^{WT} and SMC^{KO} mice (*Figure 7E–G*). However, notably, SMC^{KO} mice recapitulated the phenotype of *Txnip* KO mice by showing

increased lesion calcification and amount of collagen (*Figure 7H–I*), confirming the VSMC-specific inhibitory role of TXNIP in atherosclerotic calcification.

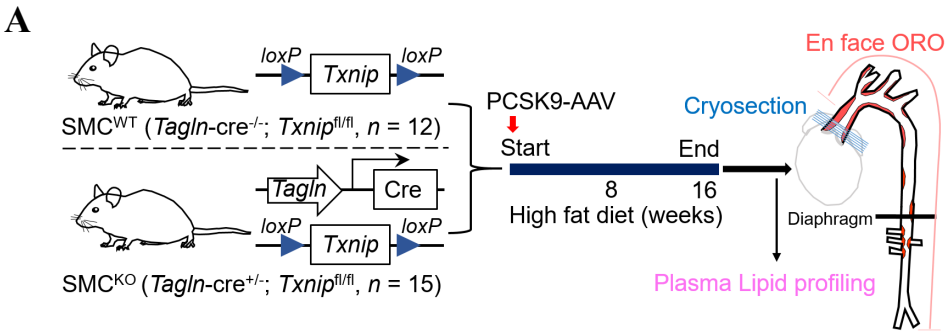
A
loxP
Txnip
loxP
SMC^WT (Tagln-cre^-/-; Txnip^fl/fl, n = 12)
Tagln
Cre
loxP
Txnip
loxP
SMC^KO (Tagln-cre^+/-; Txnip^fl/fl, n = 15)
PCSK9-AAV
Start
End
8
16
High fat diet (weeks)
En face ORO
Cryosection
Diaphragm
Plasma Lipid profiling

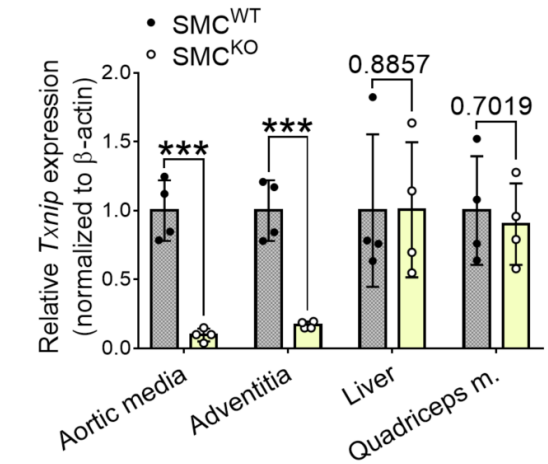
B
SMC^WT
SMC^KO
Relative Txnip expression (normalized to β-actin)
2.0
1.5
1.0
0.5
0.0
***
***
0.8857
0.7019
Aortic media
Adventitia
Liver
Quadriceps m.

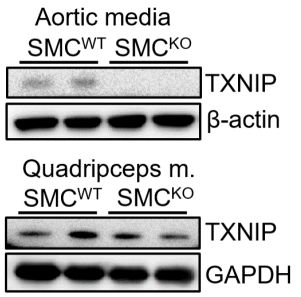
C
Aortic media
SMC^WT SMC^KO
TXNIP
β-actin
Quadripceps m.
SMC^WT SMC^KO
TXNIP
GAPDH

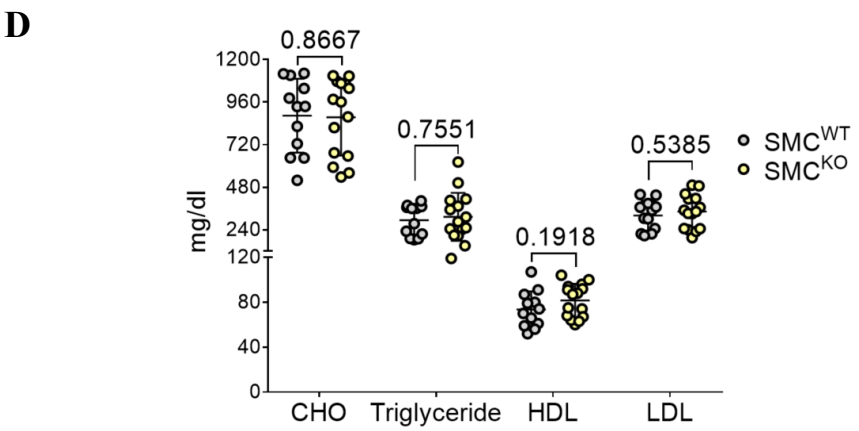
D
0.8667
0.7551
0.1918
0.5385
1200
960
720
480
240
120
80
40
0
mg/dl
CHO
Triglyceride
HDL
LDL
SMC^WT
SMC^KO

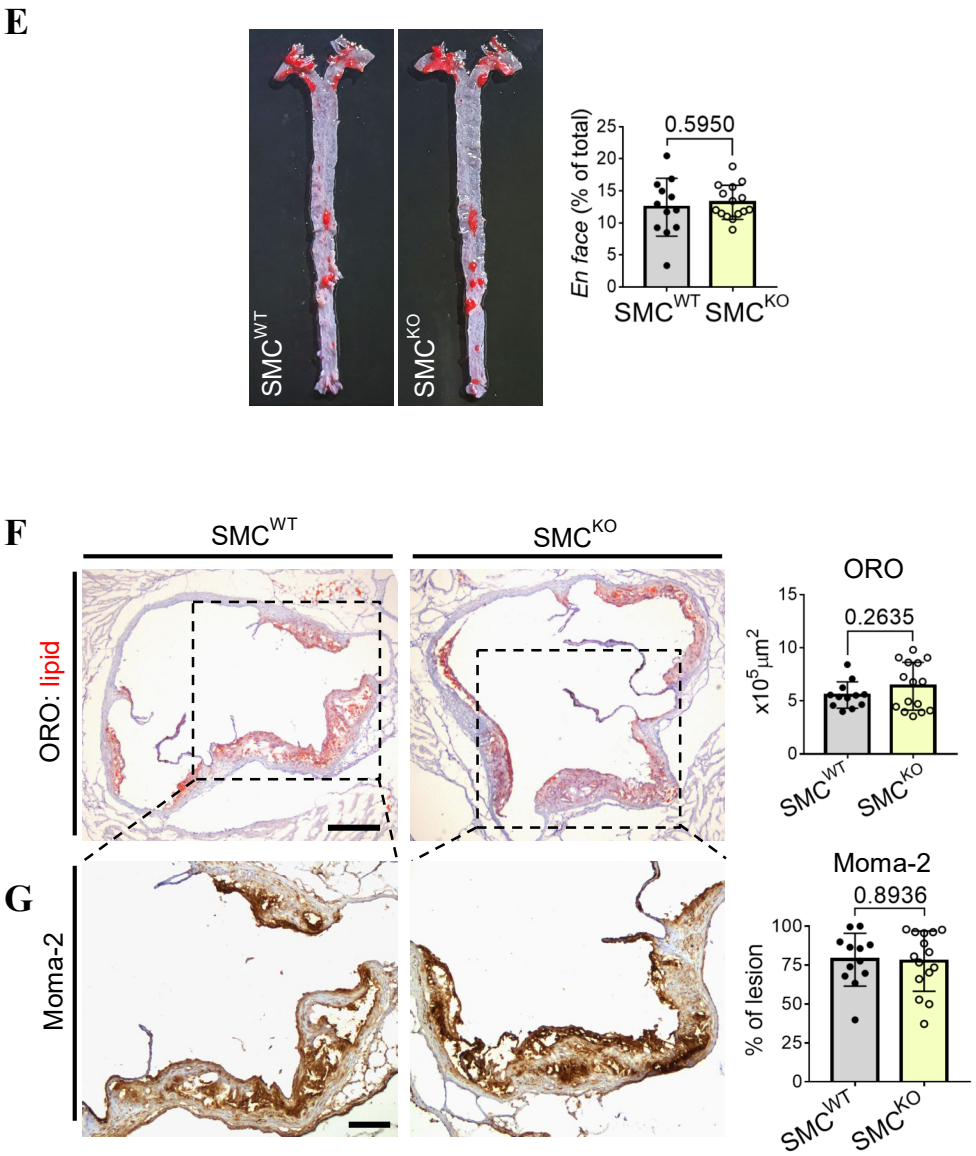
E
SMC^WT
SMC^KO
En face (% of total)
0.5950
25
20
15
10
5
0
SMC^WT SMC^KO
F
SMC^WT
SMC^KO
ORO: lipid
ORO
0.2635
x10^5 µm^2
15
10
5
0
SMC^WT SMC^KO
G
Moma-2
Moma-2
0.8936
% of lesion
100
75
50
25
0
SMC^WT SMC^KO

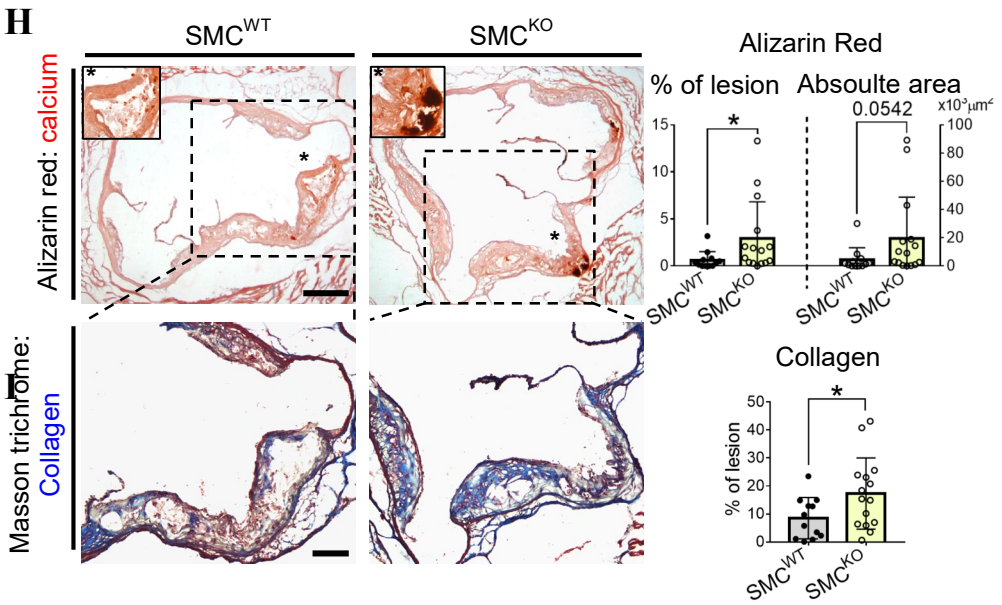

Figure 7 VSMC-specific *Txnip* ablation recapitulates the calcification-rich plaque phenotype of global *Txnip* KO mice. (*A*) Schematic illustration of the experiment. *Tagln*-cre; *Txnip*$^{flox/flox}$ (SMC^{KO}) mice and their littermate controls that did not have *Tagln*-cre (SMC^{WT}) were subjected to atherosclerosis. The mice were injected with PCSK9-AAV and fed HFD for 16 weeks. (*B* and *C*) Validation of SMC-specific ablation of *Txnip*. (*B*) qRT-PCR data showing *Txnip* mRNA expression in the aortic media, adventitia, liver, and quadriceps muscle (n = 4 mice for both groups). *Txnip* expression was normalized to that of *β-actin*. (*C*) Western blot showing TXNIP level in the aortic media and quadriceps muscle. The representative blot images of two mice per group (a total of four mice per group were analyzed). (*D*) The plasma concentrations of the total CHO, triglyceride, HDL, and LDL. (*E*) Comparison of the Oil Red O (ORO)-positive areas between SMC^{WT} and SMC^{KO} on en-face aorta (n of SMC^{WT}/SMC^{KO} mice = 12/14). (*F–I*) Characterization of atherosclerotic lesions using the 7 μm of perpendicular serial sections (total 70-80 sections) prepared from the aortic sinus. Representative serial sections and quantification results of Oil Red O (ORO) staining (*F*, for lesion size), Moma-

2 immunostaining (*G*, for monocyte/macrophage), Alizarin red staining (*H*, for calcium), Masson trichrome staining (*I*, for collagen). *n* of SMC^{WT}/SMC^{KO} mice = 12/15. The scale bars in (*F* and *H*) represent 400 μm; (*G* and *I*) represent 200 μm. The data of the aortic media, adventitia, and quadriceps muscle in (*B*), the data of HDL and LDL of (*D*), and the data in (*E*, *F*, *G,* and *I*) were analyzed by an unpaired Student's *t*-test (two-tailed). All the remaining data were analyzed using the Mann–Whitney *U*-test (two-tailed). The error bars denote standard deviation. $*P < 0.05$, $***P < 0.001$. In all other cases, the exact *P* values are specified.

TXNIP suppression in VSMCs accelerate osteodifferentiation and augments BMP signaling.

Considering that only the proportion of osteochondrogenic clusters was significantly increased in *Txnip* KO mice and the modulated VSMCs were comparable to WT control, the effect of TXNIP in inhibiting osteodifferentiation would have been exerted in the modulated VSMCs. I selected the primary cultured VSMCs by means of the proper *in vitro* model (*Figure 8A*), because cultured VSMCs are reported to mimic *Ly6a*$^{+}$ modulated VSMCs (Dobnikar, Taylor et al. 2018). I verified this finding by examining the expressions of *Ly6a* and *Lum* (upregulated in the modulated VSMC cluster), and the *Myh11* (contractile gene; VSMC marker) along the culture passages. Once (P1) or twice (P2) passaged VSMCs showed significantly increased expression of *Ly6a* and *Lum*, and decreased expression of *Myh11* compared to the initial passage (P0) (*Figure 8B*). P3 to P4 passaged VSMCs were then treated with negative control siRNA (NC) or *Txnip* siRNA (si-*Txnip*) and subjected to osteodifferentiation (*Figure 8A*). Western blotting confirmed > 90% knockdown of TXNIP in protein level by *Txnip* siRNA (*Figure 8C*). The suppression of TXNIP significantly accelerated the osteodifferentiation (*Figure 8D*). I also confirmed the same phenotype in cultured VSMCs from SMC^{WT} and SMC^{KO} (*Figure 8E–F*). Upon osteodifferentiation, TXNIP suppression significantly increased the expression of the key osteogenic transcription factor *Sp7* and the osteochondrogenic cluster-specific genes

Bglap (osteocalcin) and *Ibsp*. In addition, this resulted in conversely decreased *Myh11* expression (*Figure 8G*).

BMP signaling plays a pivotal role in bone and cartilage development,[30] and is also known to be deeply involved in the osteodifferentiation of VSMCs in the setting of atherosclerosis.[7, 8] In atherosclerosis, BMP2 and BMP4 are known to induce osteodifferentiation, and are expressed in various cell types, such as endothelial cells, foam cells, and VSMCs.[7] Indeed, *Bmp2* and *Bmp4* were transcriptionally expressed in almost all the cell types (*Figure 8H*). Notably, the osteochondrogenic cluster showed higher expression of *Bmp2*, suggesting to the possible self-reinforcement of the osteochondrogenic population. Upon osteodifferentiation, I verified the expressions of *Bmp2* and *Bmp4* in cultured VSMCs. In line with the scRNA-seq data, the osteodifferentiation increased *Bmp2* but decreased *Bmp4* expression in cultured VSMCs (*Figure 8I*). Next, I examined the expressions of the inhibitor of DNA binding (Id) proteins, which are transcribed by BMP as a crucial target of BMP signaling.[31] After osteodifferentiation, TXNIP suppression increased the expressions of all classes of Ids (Id1-4), implying up-regulation of BMP signaling by TXNIP suppression (*Figure 8J*).

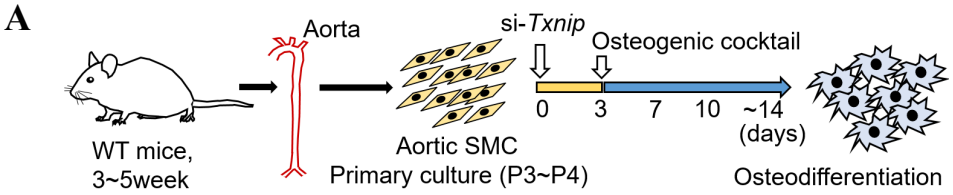
A
Aorta
si-Txnip
Osteogenic cocktail
0
3
7
10
~14
(days)
WT mice,
3~5week
Aortic SMC
Primary culture (P3~P4)
Osteodifferentiation

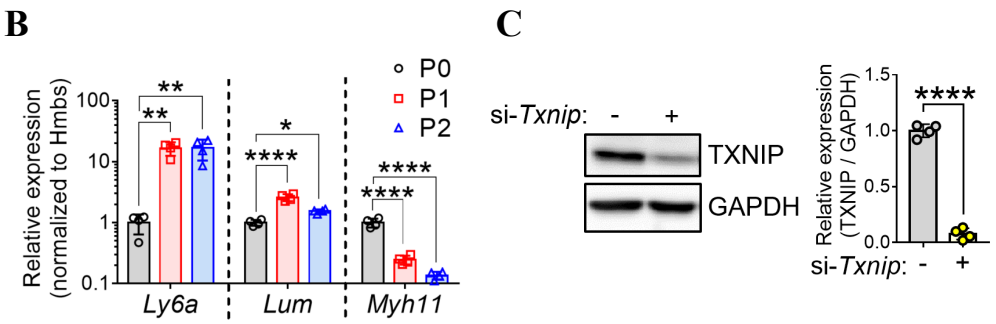
B
Relative expression
(normalized to Hmbs)
P0
P1
P2
Ly6a
Lum
Myh11
C
si-Txnip: - +
TXNIP
GAPDH
Relative expression
(TXNIP / GAPDH)
si-Txnip: - +

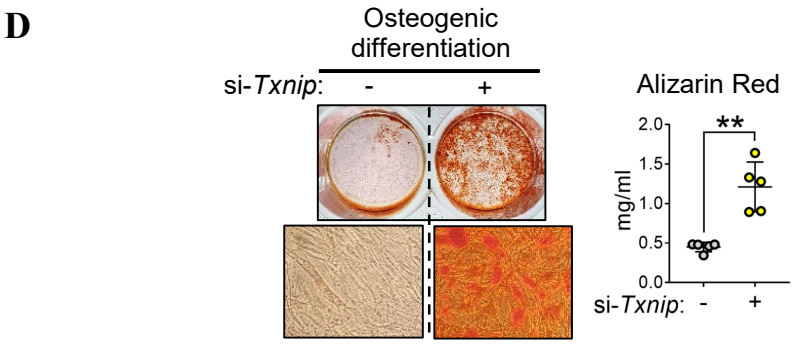
D
Osteogenic
differentiation
si-Txnip: - +
Alizarin Red
mg/ml
si-Txnip: - +

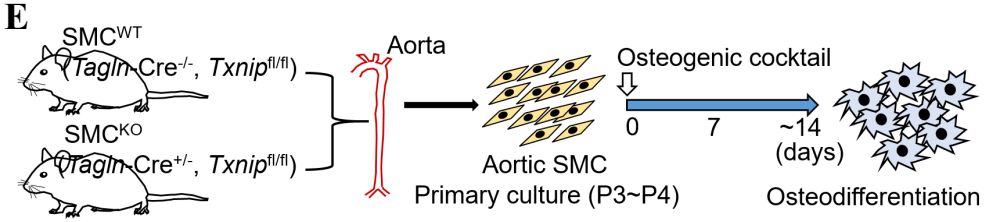
E
SMCWT
(Tagln-Cre-/-, Txnipfl/fl)
SMCKO
(Tagln-Cre+/-, Txnipfl/fl)
Aorta
Aortic SMC
Primary culture (P3~P4)
Osteogenic cocktail
0
7
~14
(days)
Osteodifferentiation

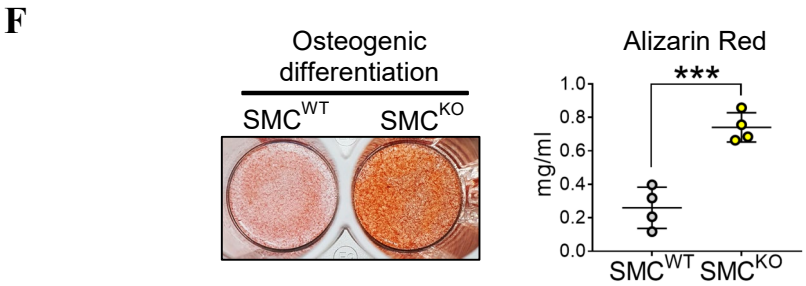
F
Osteogenic
differentiation
SMCWT
SMCKO
Alizarin Red
mg/ml
SMCWT
SMCKO

G

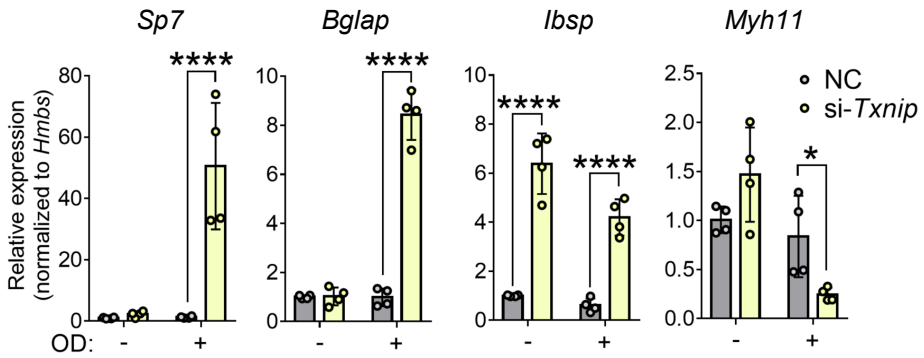
Sp7
Bglap
Ibsp
Myh11
Relative expression
(normalized to Hmbs)
****
****
****
****
*
NC
si-Txnip
OD:
-
+

H

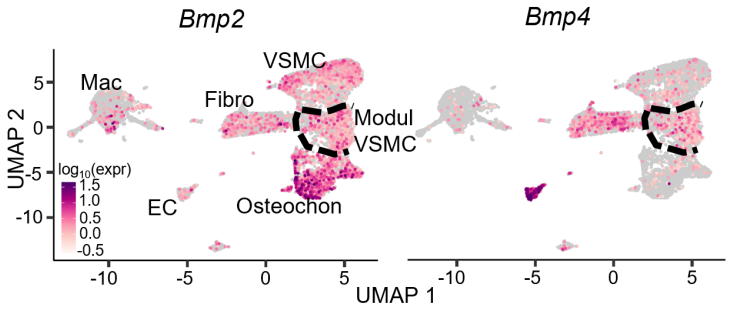
Bmp2
Bmp4
Mac
Fibro
VSMC
Modul
VSMC
EC
Osteochon
log10(expr)
UMAP 2
UMAP 1

I

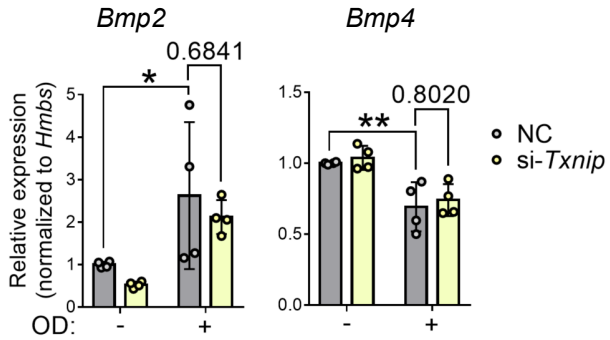
Bmp2
Bmp4
0.6841
0.8020
*
**
Relative expression
(normalized to Hmbs)
NC
si-Txnip
OD:
-
+

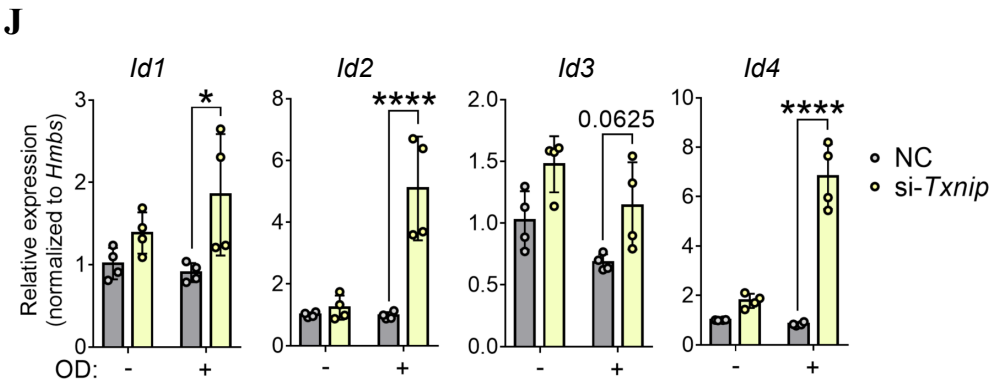

Figure 8 *Txnip* knockdown in VSMCs accelerate osteodifferentiation and augments BMP signaling. (*A*) Schematic illustration of the experiment. The pooled VSMCs from two to three WT mice constituted one biological replicate. Cultured VSMCs were treated with negative control siRNA (NC) or *Txnip* siRNA (si-*Txnip*) and were subjected to osteodifferentiation by "osteogenic cocktail" (β-glycerophosphate, L-ascorbic acid, and H_2O_2) incubation. (*B*) qRT-PCR results showing the changes in gene expressions of *Ly6a* and *Lum* (upregulated in the modulated VSMC cluster), and the *Myh11* (contractile gene; VSMC marker) along the culture passages. $n = 4$. P, passage. (*C*) Western blot confirming knockdown of TXNIP by si-*Txnip*. TXNIP expression was normalized to GAPDH for quantification. $n = 4$. (*D*) Alizarin Red staining results of osteodifferentiation (end point). The staining was quantified by cetylpyridinium chloride extraction. $n = 5$. (*E*) Schematic illustration of the experiment. VSMCs were primary cultured from littermate control of SMC^{WT} and SMC^{KO}. The pooled VSMCs from two to three mice constituted one biological replicate. (*F*) Alizarin Red staining results of osteodifferentiation (end point). The staining was quantified by cetylpyridinium chloride extraction. $n = 4$. (*G*) qRT-PCR results showing the expressions of *Sp7*, *Bglap*, *Ibsp* (which are the osteochondrogenic marker genes), and *Myh11* (which is a contractile gene; VSMC marker) in the NC and si-*Txnip* treated VSMCs with or without osteodifferentiation. $n = 4$. (*H*) Feature plots showing *Bmp2* and *Bmp4* expression in WT and *Txnip* KO scRNA-seq data. Mac, macrophage; Fibro, fibroblast-like; Modul, modulated; Osteochon, osteochondrogenic; EC,

endothelial cell. (*I*) qRT-PCR results showing the expressions of *Bmp2* and *Bmp4* in the NC and si-*Txnip* treated VSMCs with or without osteodifferentiation. $n = 4$. (*J*) qRT-PCR results showing the mRNA expressions of inhibitor of DNA binding (Id) proteins, which are transcribed by BMP as a crucial target of BMP signaling. $n = 4$. (*G*, *I*, and *J*) *Hmbs* was used as a housekeeping gene for qRT-PCR. The data in (*B*) were analyzed using one-way ANOVA, followed by post-hoc test (Dunnett's multiple comparison test). The data in (*C* and *F*) were analyzed by an unpaired Student's *t*-test (two-tailed), and (*D*) were analyzed by a Mann–Whitney *U*-test (two-tailed). The data in (*G*, *I*, and *J*) were analyzed using one-way ANOVA except *Id3*, followed by post-hoc test (Holm-Sidak`s multiple comparison test in the case of *Sp7* and *Id1*; Sidak`s multiple comparison test in the case of the remaining data). The data of *Id3* in (*J*) were analyzed using Kruskal–Wallis test, followed by post-hoc test (Dunn`s multiple comparison test). The error bars denote standard deviation. $*P < 0.05$, $**P < 0.01$, $****P < 0.0001$. In all other cases, the exact *P* values are specified. OD, osteodifferentiation.

TXNIP inhibits osteodifferentiation of VSMCs by suppressing both canonical and non-canonical BMP signaling.

The BMPs transduce their signaling through Smads-involved canonical pathways and p38 mitogen-activated protein kinase (MAPK)-involved non-canonical pathways. In the canonical pathways, the BMP receptors phosphorylate Smad1/5/9 (receptor-activated Smads; R-Smads), and subsequently translocate into the nucleus in interaction with Smad4 (common Smad; Co-Smad) to activate the osteogenic program (Wu, Chen et al. 2016). I examined both canonical and non-canonical BMP signaling under BMP2 stimulation. TXNIP suppression increased the p-Smad1/5/9 levels and increased the total amount of Smad1 and Smad5. When the inhibitory Smads (i-Smads; Smad6 and Smad7) were examined, Smad6 showed comparable level; however, Smad7 was diminished upon TXNIP suppression. Moreover, TXNIP suppression increased p-p38, which is a non-canonical pathway (*Figure 9A*). Next, I compartmentalized the cytoplasmic and nuclear proteins and examined the Smad4. Notably, both nuclear and cytoplasmic fractions of Smad4 were significantly increased upon TXNIP suppression (*Figure 9B*). I checked the activities of Smad1 and Smad4 regulons (Garcia-Alonso, Holland et al. 2019) in the VSMC-derived cell populations of WT & *Txnip* KO scRNA-seq data. Both Smad1 and Smad4 regulon activities were enriched in the ostechondrogenic clusters (*Figure 9C–D*), suggesting that the BMP signaling pathway was upregulated in *Txnip* KO mice. These data collectively indicate that TXNIP suppresses both canonical and non-canonical BMP signaling

pathways. Finally, to test whether the augmentation of BMP signaling under TXNIP suppression is necessary and sufficient for accelerated osteodifferentiation, I used the potent BMP signaling inhibitor K02288 (Sanvitale, Kerr et al. 2013). K02288 (10 μM) induced a near-complete block of both canonical and non-canonical BMP signaling, marked by significant decrease of p-Smad1/5/9 and p-p38 levels (*Figure 9E*). K02288 treatment abrogated the effect of TXNIP suppression on osteodifferentiation (*Figure 9F*).

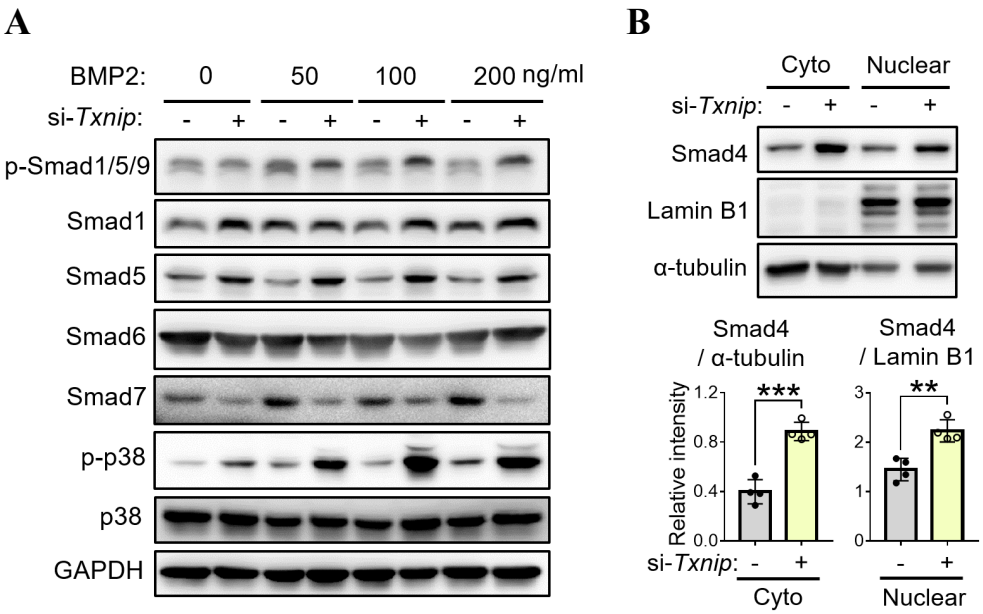
A
BMP2: 0 50 100 200 ng/ml
si-Txnip: - + - + - + - +
p-Smad1/5/9
Smad1
Smad5
Smad6
Smad7
p-p38
p38
GAPDH
B
Cyto Nuclear
si-Txnip: - + - +
Smad4
Lamin B1
α-tubulin
Smad4 / α-tubulin
Smad4 / Lamin B1
Relative intensity
***
**
si-Txnip: - + - +
Cyto
Nuclear

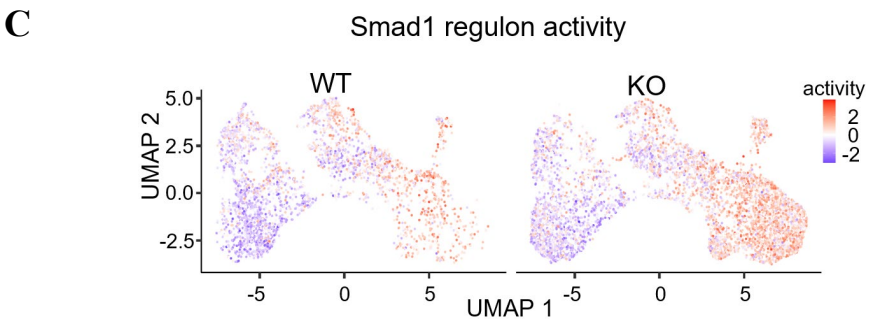
C
Smad1 regulon activity
WT
KO
activity
UMAP 2
UMAP 1

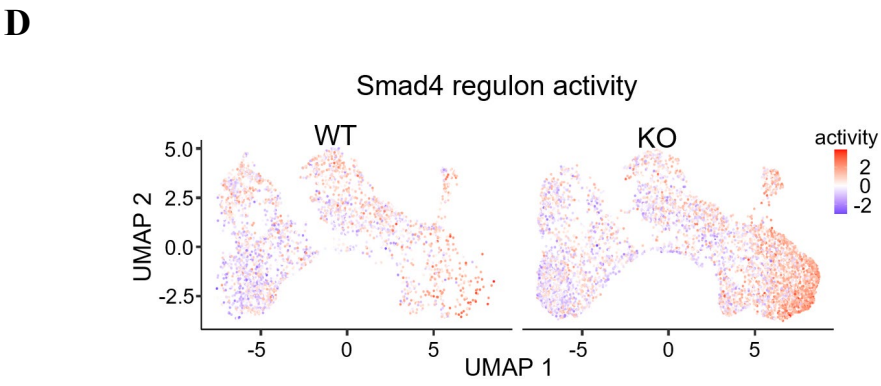
D
Smad4 regulon activity
WT
KO
activity
UMAP 2
UMAP 1

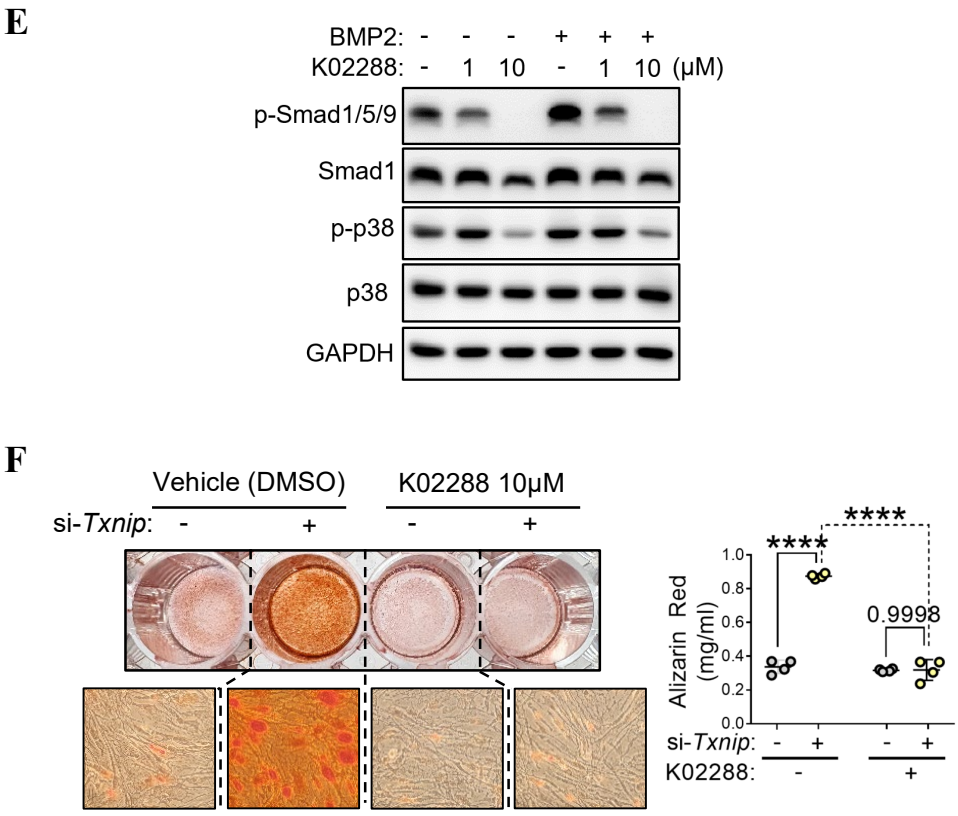

Figure 9 *Txnip* knockdown in VSMCs upregulates both canonical and non-canonical BMP signaling leading to osteodifferentiation. (*A*) Western blot showing canonical and non-canonical BMP signaling upon si-*Txnip* treatment. The results at 16 h after BMP treatment. The representative images for $n = 4$. (*B*) Western blot showing cytoplasmic and nuclear fractions of Smad4 upon *Txnip* siRNA treatment. α-tubulin and Lamin B1 were used as the loading controls for the cytoplasmic and nuclear fractions, respectively. $n = 4$. (*C–D*) Feature plots showing the regulon activities of Smad1 and Smad4 in VSMC-derived cells of WT and *Txnip* KO. (*E*) Western blot showing the validation result of determining the concentration of the BMP signaling inhibitor K02288. Representative images of $n = 2$. (*F*) Alizarin Red staining results showing abrogation of the effect of *Txnip* knockdown on osteodifferentiation. 10 μM of K02288 was treated in advance of siRNA transfection, and was added to the

osteogenic cocktail for every medium replacement. The staining was quantified by cetylpyridinium chloride extraction. $n = 4$. (*G*) Graphical abstract showing the role of TXNIP in atherosclerotic calcification. Osteochondro, osteochondrogenic cells. EC, endothelial cells. Modul, modulated. Mac, macrophages. Myofibro, myofibroblasts. The data in (*B*) were analyzed by an unpaired Student's *t*-test (two-tailed). The data in (*F*) were analyzed using one-way ANOVA, followed by post-hoc test (Sidak`s multiple comparison test). The error bars denote standard deviation. $^{**}P < 0.01$, $^{***}P < 0.001$, $^{****}P < 0.0001$. In other case, the exact *P* value is specified.

Wnt/β-catenin signaling is not involved in the effect of TXNIP on VSMC osteodifferentiation.

Wnt/β-catenin signaling is also reported to be involved in the osteodifferentiation of VSMCs in atherosclerotic calcification (Cai, Sun et al. 2016). I checked the regulon activity of Wnt/β-catenin (*Table 2*). However, I did not find a notable difference in the Wnt/β-catenin regulon activity between WT and *Txnip* KO mice (*Figure 10A*). Also, TXNIP suppression did not alter the nuclear β-catenin levels in cultured VSMCs (*Figure 10B*), suggesting that Wnt/β-catenin signaling is not involved in the effect of TXNIP on VSMC osteodifferentiation.

A

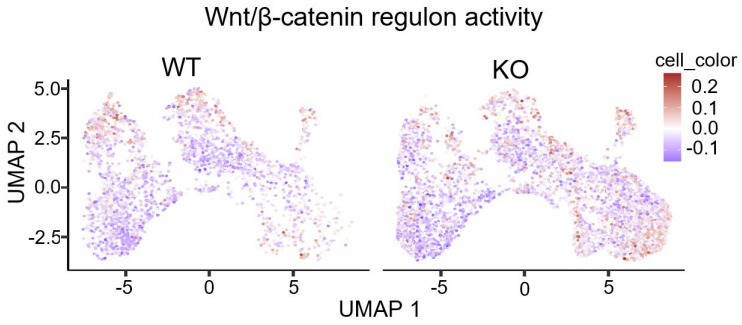

B

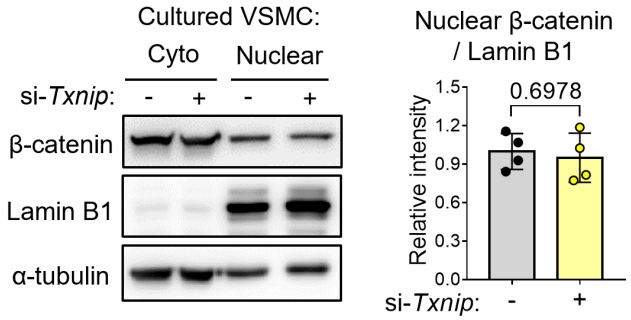

Figure 10 Wnt/β-catenin signaling is not involved in the effect of TXNIP on VSMC osteodifferentiation. (*A*) Feature plots showing Wnt/β-catenin regulon activity in the VSMC-derived cells of WT and *Txnip* KO mice. (*B*) Western blot showing cytoplasmic and nuclear fractions of β-catenin upon *Txnip* siRNA treatment. α-tubulin and Lamin B1 were used as the loading controls for the cytoplasmic and nuclear fractions, respectively. The data in (*B*) were analyzed using the Mann–Whitney *U*-test (two-tailed). The error bars denote standard deviation. The exact *P* value is specified.

DISCUSSION

Recent studies using a combination of lineage-traced reporter mice with the scRNA-seq technique showed generally consistent findings with regard to the process of VSMCs transitioning toward osteochondrogenic clusters (Pan, Xue et al. 2020; Kim, Zhao et al. 2020; Alencar, Owsiany et al. 2020). VSMCs first give rise to the "pioneer" cell population (showing similar transcriptomic profiles albeit named differently by each group: "intermediate cell state", "fibromyocyte", or "*Lgals3*$^{+}$ VSMC" and then transform into the osteochondrogenic population ("fibrochondrocyte", "chondromyocytes", or "osteogenic"). In particular, studies from two independent groups showed that SMC-specific ablation of *Ahr* or *Klf4* can increase (*Ahr*, Kim, Zhao et al. 2020) or decrease (*Klf4*, Alencar, Owsiany et al. 2020) the osteochondrogenic population. Notably, the SMC-specific ablation of *Ahr* or *Klf4* also altered the lesion size and fibrous cap, and altered the intermediate VSMC clusters in the case of *Klf4*, suggesting that the regulatory function of these genes in SMC transitioning would not be specifically confined to the osteochondrogenic phenotype. To date, the key regulatory factors and underlying mechanisms that govern the osteochondrogenic transition of VSMCs are yet to be elucidated.

Here, I confirmed the existence of a distinct osteochondrogenic population that is responsible for atherosclerotic calcification, and demonstrated that TXNIP is a novel regulator of atherosclerotic calcification by "holding" transition of the modulatory VSMCs toward the osteochondrogenic cluster through the suppression of BMP signaling. The regulatory role of TXNIP is

thought to be specific to the transitioning process of modulated VSMCs toward osteochondrogenic cells, which is supported by the following data: (1) a comparable proportion of the modulated VSMC cluster in the scRNA-seq, (2) *Ly6a*$^{+}$*Myh11*$^{+}$ cells of *in situ* hybridization data between WT and *Txnip* KO, and (3) unaltered lesion size and macrophage contents in the SMC^{KO} mice.

In previous studies on AHR and KLF4, the osteochondrogenic cluster was considered a disease-prone cell population, because the amount of osteochondrogenic population was proportional to the lesion size and macrophage content, and inversely proportional to the fibrous cap (Kim, Zhao et al. 2020; Alencar, Owsiany et al. 2020; Shankman, Gomez et al. 2015). However, *Txnip* KO mice showed markedly expanded osteochondrogenic clusters, but reduced macrophage content and unaltered (in case of the aortic sinus region) or reduced (in case of the aorta) lesion size. Furthermore, the SMC-specific ablation of *Txnip* exclusively increased plaque calcification and collagen content, while other phenotypes remained unchanged. Based on the experimental data, enhanced lesional calcification in *Txnip* KO mice appears to be caused by osteochondrogenic phenotypic switch of VSMCs regardless of other lesion features including lipid accumulation and macrophage content. For reference, the possible reasons for the altered phenotypes except calcification in *Txnip* KO mice are as follows: (1) results from the different lipid profiles between WT and *Txnip* KO mice; (2) the absence of TXNIP in endothelial cells, as TXNIP is reported to be involved in the regulation of stress fiber formation, inflammatory response, and angiogenesis of endothelial cells

(Wang, Nigro et al. 2012; Domingues, Boisson-Vidal et al. 2020; Spindel, Burke et al. 2014). The hematopoietic absence of TXNIP was less likely to contribute to the phenotype of *Txnip* KO mice, as I did not observe any notable differences between BM^{WT} and BM^{KO} mice.

Atherosclerotic burdens of BM^{WT}/BM^{KO} mice and SMC^{WT}/SMC^{KO} mice were approximately 40-60% less than that of WT/*Txnip* KO mice on basis of the aortic sinus lesion size. In the case of BM^{WT}/BM^{KO} mice, the difference would come from irradiation treatment, since irradiation is reported to affect atherosclerotic lesion size (Schiller, Kubo et al. 2001). For reference, the lipid profile of BM^{WT} and WT ($Txnip^{+/+}$) mice were comparable. In the case of SMC^{WT}/SMC^{KO} mice, the difference would have been primarily attributable to different lipid profiles. SMC^{WT} showed lower plasma concentrations of CHO (33%), TG (4%), HDL (18%), and LDL (22%) compared to WT mice. It is quite surprising that this differences were observed, because SMC^{WT}/SMC^{KO} and WT/*Txnip* KO mice share same background as C57BL/6J. Since SMC^{WT} mice lack Cre gene ($Txnip^{flox/flox}$) as a control group for SMC^{KO} (*Tagln*-Cre; $Txnip^{flox/flox}$), the differences of lipid profile between SMC^{WT} and WT ($Txnip^{+/+}$) mice probably attributable to unknown genetic background difference between $Txnip^{flox/flox}$ and $Txnip^{+/+}$ mice. Of note, lipid profiles between SMC^{WT} and SMC^{KO}, and BM^{WT} and BM^{KO} were comparable, respectively. Because *Txnip* KO mice showed different lipid profile compared to WT mice, these findings indirectly support the involvement of TXNIP in liver lipid metabolism (Park, Song et al. 2021; Chutkow, Patwari et al. 2008).

SMC^{KO} mice lack TXNIP not only in VSMCs, but also in other smooth muscle cells consisting involuntary non-striated muscle tissue distributed throughout the whole body. Therefore, SMC^{KO} mice may exhibit unexpected phenotypes derived from non-vascular tissue. In addition, it is possible that this unexpected phenotype secondarily affects atherosclerotic lesions of SMC^{KO} mice. Normal and atherosclerosis-induced SMC^{KO} mice did not exhibit any notable differences in the gross organ morphology compared to SMC^{WT} mice. Additional characterization such as histopathological examination, complete blood cell count, serum biochemistry, and/or hormonal profiling can rule out possible unexpected effect of smooth muscle cell ablation of TXNIP other than vascular tissue. Importantly, atherosclerosis is primarily initiated and propagated by blood lipids, immune cells, and in situ proliferation of medial smooth muscle cells (Bentzon, Otsuka et al. 2014). The lipid profiles of SMC^{KO} mice were comparable to SMC^{WT} mice, and *Tagln*-Cre mice used in this experiment (B6.Cg-Tg(Tagln-cre)1Her/J) are reported to not show Cre-leakage in immune cells (Chakraborty, Saddouk et al. 2019). Therefore, it is very unlikely that the smooth muscle cell ablation of TXNIP other than vascular tissue (if present) in SMC^{KO} mice had secondary effects on the atherosclerotic calcification.

Through *in vitro* experiments using cultured VSMCs, I found that the suppression of TXNIP increased both canonical and non-canonical BMP signaling. In canonical signaling, the suppression of TXNIP collectively increased the activated and total amount of R-Smads (Smad1 and Smad5) and

Co-Smad (Smad4), together with decreased Smad7. In the regulation of TGFβ/BMP signaling, i-Smads (Smad6/7) are known to play a key role by interfering with R-Smad phosphorylation at the type I receptors, preventing the nuclear translocation of R-Smads, and promoting the degradation of the receptors or R-Smads by recruiting E3 ubiquitin ligases Smurf1/2 (Wu, Chen et al. 2016; Miyazawa and Miyazono 2017). Therefore, the change in the phosphorylation and total levels of R-Smads upon TXNIP suppression could be a result of decreased Smad7 levels. At the another point, TXNIP belongs to the α-arrestin family and can act as an adaptor molecule for the NEDD4 E3s ubiquitin ligase family to ubiquitinate and degrade several endocytic cargo proteins (Shah and Kumar 2021). As Smuf1/2 belongs to the NEDD4 family, TXNIP might act as an adaptor for Smuf1/2 to degrade R-Smads and Co-Smad. Lastly, TXNIP may interact with or modify the function of other regulatory molecules, such as RING (really interesting new gene) type E3 ubiquitin ligase Arkadia, which can degrade Smad7, or SUMO (small ubiquitin-related modifier) and Ubc9 (ubiquitin conjugating enzyme 9), which can degrade Smad4 (Wu, Chen et al. 2016). In non-canonical signaling, TXNIP suppression increases p38 phosphorylation. p38 MAPK signaling accelerates osteoblast differentiation by increasing the expression and activity of osteoblast-specific transcription factors RUNX2, DLX5, or SP7 (Rodríguez-Carballo, Gámez et al. 2016). A study reported the direct interactions of TXNIP with p38 to inhibit p38 activation in hematopoietic stem cells (Jung, Kim et al. 2016); therefore, TXNIP might also directly suppress p38 activation in VSMCs. On the other

hands, TXNIP may indirectly inhibit p38 activation through Smad7, because Smad7 is reported to downregulate p38 activation in chondrocytes (Iwai, Murai et al. 2008), although opposite effects have also been reported (Miyazawa and Miyazono 2017). Further studies are required to reveal the underlying molecular mechanisms for the observed complex effects of TXNIP on BMP signaling.

Transcriptional expression of TXNIP can be regulated by several factors. Glucose and endoplasmic reticulum stress (ER stress) are representative factors known to induce TXNIP expression. Cellular Ca^{2+} concentration, epigenetic mechanisms, and miRNAs can also regulate TXNIP expression (Shalev 2014). According to the reanalyzed data GSE159677, *TXNIP* was downregulated in the modulated VSMC and the osteochondrogenic cluster of calcified human atherosclerotic lesion, but not in the VSMC cluster. Therefore, the possible explanations for the downregulation of *TXNIP* in the modulated VSMC and the osteochondrogenic cluster can be speculated in two ways. Frist, intimal microenvironment composed of inflammation, lipids, and various cytokines may either directly affect TXNIP expression, or indirectly affect through the aforementioned TXNIP-regulating factors. Second, VSMC-intrinsic mechanism could regulate TXNIP expression. Various molecules such as SRF-MYOCD, KLF4, OCT, and miRNAs as well as epigenetic modifications are involved in the VSMC modulation (Grootaert and Bennett 2021). As phenotypical transitioning occurs in VSMCs, these factors may affect transcriptional expression of TXNIP.

The other remaining questions are as follows. (1) Does the regulatory role of TXNIP in BMP signaling also works in other cell types? BMP signaling not only plays a central role in bone morphogenesis, but is also involved in various physiological and embryogenic processes (Wang, Green et al. 2014). As I did not observe any notable skeletal or developmental anomalies in *Txnip* KO mice, the regulatory effect of TXNIP on BMP signaling is not likely pan-cellular. However, these possibilities still remain. (2) What is the role of TXNIP in other cardiovascular diseases that involve the phenotypic modulation of VSMCs (e.g., medial artery calcification, hypertension, pulmonary arterial hypertension, cerebral microangiopathy, Marfan syndrome) (Frismantiene, Philippova et al. 2018)? Further studies are required to address these questions.

Lastly, here I have made assertion under the premise that osteochondrogenic cluster is the primary cause of atherosclerotic calcification. Osteochondrogenic cells would not the sole source of atherosclerotic calcification, because calcification can occur from the matrix vesicles produced from macrophages, and degenerative deposition of calcium can occur in the necrotic and apoptotic environment (New, Goettsch et al. 2013; Bentzon, Otsuka et al. 2014). However, importantly, previous studies have shown that VSMC-specific deletion of the key osteoblast transcription factor RUNX2 reduced atherosclerotic calcification by 50-80% compared to control groups, suggesting that not total, but a significant contribution of the osteogenic phenotype of VSMCs to atherosclerotic calcification (Lin, Chen et al. 2016; Sun, Byon et al. 2012). This is also supported by the data in this study:

(1) correlation of the alizarin red-positive area and the osteochondrogenic population in WT and *Txnip* KO mice, (2) coincidence of the osteochondrogenic cluster marker ACAN and CHAD-positive area and the calcified area. Therefore, it cannot be said that the osteochondrogenic cells is sole source for the atherosclerotic calcification, but it is certainly contributing to a significant part. The notion that increased atherosclerotic calcification in *Txnip* KO mice is attributable to the osteochondrogenic cell is further supported by the following data: (1) comparable atherosclerotic calcification between BM^{WT} and BM^{KO} mice (i.e. excluding the effect from macrophage-derived matrix vesicles), (2) comparable necrotic core size in WT and *Txnip* KO mice. Interrogating atherosclerotic calcification using the osteochondrogenic cell-specific ablation mice model (e.g. using diphtheria toxin receptor (DTR) driven by osteochondrogenic cell-specific gene), if side effects (e.g. lethality derived from altered bone homeostasis) could be avoided, can verify the exact contribution of osteochondrogenic cells to atherosclerotic calcification.

CONCLUSION

Calcification is a characteristic phenomenon of advanced atherosclerotic lesions. Atherosclerotic calcification can lead to thrombosis in the form of a "calcified nodule," which can also hinder the effect of anti-atherosclerotic treatment (i.e. drug-eluting stents). Here, I present TXNIP as a novel critical regulator of atherosclerotic calcification. The anti-calcification role of TXNIP is mediated by the suppression of BMP signaling in the modulated vascular smooth muscle cells (VSMCs), which is a precursor population of osteochondrogenic cells. By exploiting the regulatory role of TXNIP in the osteochondrogenic transition of VSMCs, TXNIP could be a potential therapeutic target for atherosclerotic calcification.

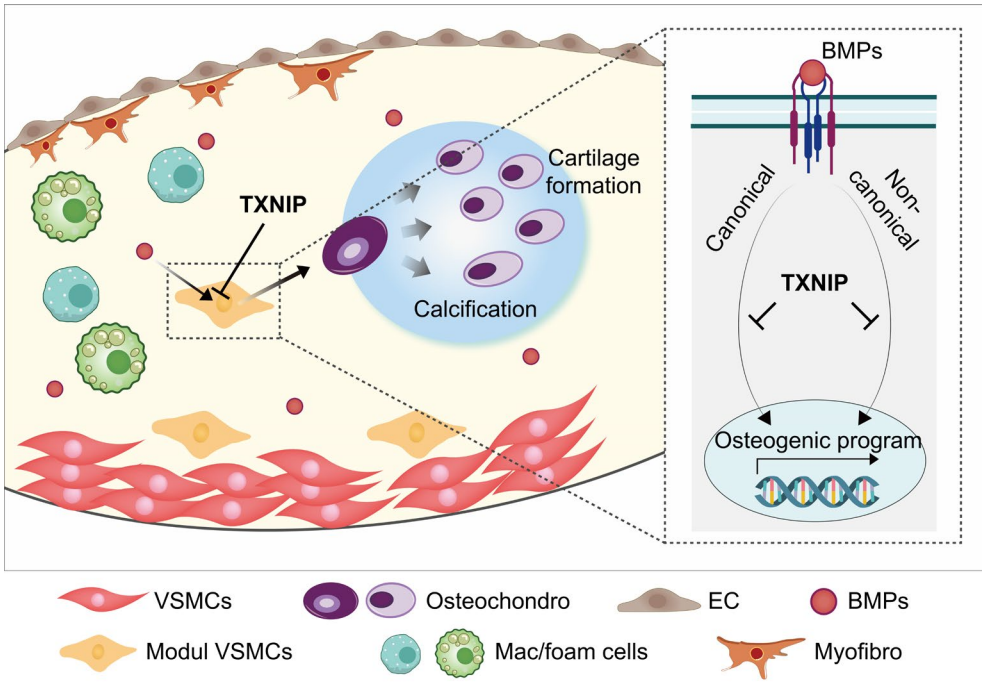

국문초록

동맥경화 칼슘 침착에서 Thioredoxin Interacting Protein 의 역할

우 상 호

지도 교수: 김 대 용

서울대학교 대학원 수의학과 수의병리학 전공

혈관 평활근 세포가 골·연골세포로 표현형 전환을 하는 현상은 동맥경화 칼슘 침착의 핵심 원인으로 알려져 있다. 그러나 아직까지 이 과정을 조절하는 분자적 기전에 대해서는 잘 알려져 있지 않다. 선행 연구들은 세포 내에서 다양한 기능을 하는 단백질인 TXNIP 가 혈관 평활근 세포의 병태생리와 동맥경화 칼슘 침착에 주요한 역할을 할 가능성을 시사해 왔었다. 본 연구에서는 동맥경화 칼슘 침착의 원인이 되는 혈관 평활근 세포의 골·연골세포로의 표현형 전환 과정에서 TXNIP 의 역할을 탐구하였다.

단일 세포 RNA 시퀀싱 분석 기법을 동원하여 *Txnip*$^{-/-}$ 마우스의 동맥경화 표현형이 분석되었다. *Tagln*−Cre; *Txnip*$^{flox/flox}$ 마우스 (평활근 세포 조건부로 *Txnip* 가 결핍된 모델) 및 골수 이식 마우스 (조혈 세포에서 *Txnip* 가 결핍된 모델)의 동맥경화 표현형이 분석되었다. 사람의 칼슘 침착이 있는 동맥 경화 병변의 혈관 평활근 세포에서

TXNIP 의 발현을 알아보기 위하여 공개 단일 세포 시퀀싱 데이터 GSE159677 이 재분석되었다. 사람 동맥내막절제술 시료에 대하여 TXNIP의 발현 양상을 면역 염색으로 살펴보았다. 혈관 평활근 세포 1차 배양을 통하여 생체 외 기전 연구가 수행되었다.

Txnip$^{-/-}$ 마우스의 동맥경화 병변은 *Txnip*$^{+/+}$ 마우스에 비해 크게 증가된 칼슘 및 섬유질 침착을 나타내었다. 후속된 단일 세포 RNA 시퀀싱 분석은 혈관 평활근 세포에서 유래된 조절된 혈관 평활근 세포 및 골·연골세포 집단을 밝혀내었다. 골·연골세포 집단은 *Txnip*$^{+/+}$ 마우스에 비해 *Txnip*$^{-/-}$ 마우스에서 그 비중이 크게 증가되어 있었다. 혈관 평활근 유래 세포 집단에 대한 유전자 경로 분석 결과, *Txnip*$^{-/-}$ 마우스에서 골·연골 형성 관련 경로와 BMP 신호 경로가 활성화되어 있었다. GSE159677 에 대한 분석 결과 사람의 칼슘 침착이 있는 동맥경화 병변의 조절된 혈관 평활근 세포 및 골·연골세포 집단에서 *TXNIP* 의 발현이 유의미하게 감소해 있었다. 사람 동맥내막절제술 시료에 대한 TXNIP 면역 염색 결과, 칼슘 침착 부위 주변의 중간막 부위에서 TXNIP 가 감소해 있었다. *Tagln*−Cre; *Txnip*$^{flox/flox}$ 마우스의 동맥경화 병변 표현형은 칼슘 및 섬유질 침착이 증가된 *Txnip*$^{-/-}$ 동맥경화 병변을 재현하였다. 반면 조혈 세포 특이적인 TXNIP 의 결핍은 동맥 경화 칼슘 침착에 영향을 미치지 않았다. 1 차 혈관 평활근 세포 배양 실험을 통해, TXNIP 의 억제가 골분화를 가속시키며 BMP 신호의 주경로와 부경로 모두를 활성화함이 밝혀졌다. BMP 신호 전달 억제제인 K02288 을 처리하였을 때 골분화에 대한 TXNIP 의 억제 효과가 상쇄되는 것을 확인하였다.

결론적으로, TXNIP 는 혈관 평활근 세포가 골·연골세포 표현형으로 전환하는 과정을 BMP 신호 전달 저해를 통하여 억제함으로써 동맥 경화 칼슘 침착의 조절자로 역할 한다. 본 연구는 동맥경화 병변에 대한

이해도를 높혔으며, 중요하게는 동맥 경화 칼슘 침착의 억제 인자로 기능하는 TXNIP 의 새로운 역할을 규명한 의의를 지닌다.

핵심어: 동맥경화, 칼슘 침착, 혈관 평활근 세포, 표현형 전환, TXNIP, 골·연골세포, BMP

학 번: 2016-21767

REFERENCES

Abe E., Yamamoto M., Taguchi Y., Lecka-Czernik B., O`Brien C. A., Economides A. N., Stahl N., Jilka R. L. and Manolagas S. C. (2000) Essential requirement of BMPs-2/4 for both osteoblast and osteoclast formation in murine bone marrow cultures from adult mice: antagonism by noggin. J Bone Miner Res 15(4):663-673.

Abula K., Muneta T., Miyatake K., Yamada J., Matsukura Yu., Inoue M., Sekiya I., Graf D., Economides A. N., Rosen V. and Tsuji K. (2015) Elimination of BMP7 from the developing limb mesenchyme leads to articular cartilage degeneration and synovial inflammation with increased age. FEBS Lett 589(11):1240-1248.

Alencar G. F., Owsiany K. M., Karnewar S., Sukhavasi K., Mocci G., Nguyen A. T., Williams C. M., Shamsuzzaman S., Mokry M., Henderson C. A., Haskins R., Baylis R. A., Finn A. V., McNamara C. A., Zunder E. R., Venkata V., Pasterkamp G., Björkegren J., Bekiranov S. and Owens G. K. (2020) Stem cell pluripotency genes Klf4 and Oct4 regulate complex SMC phenotypic changes critical in late-stage atherosclerotic lesion pathogenesis. Circulation 142(21):2045-2059.

Alexopoulos N. and Raggi P. (2009) Calcification in atherosclerosis. Nat Rev Cardiol 6(11):681-688.

Alsaigh T., Evans D., Frankel D. and Torkamani A. (2020) Decoding the transcriptome of atherosclerotic plaque at single-cell resolution. Biorxiv [Preprint] Available from doi.org/10.1101/2020.03.03.968123.

Alvim R. O., Santos P. C. J. L., Ferreira N. E., Mill J. G., Krieger J. E. and Pereira A. C. (2012) Thioredoxin interacting protein (TXNIP) rs7212 polymorphism is associated with arterial stiffness in the Brazilian general population. J Hum Hypertens 26(5):340-342.

Basatemur G. L., Jørgensen H. F., Clarke M. C. H., Bennett M. R. and Mallat Z. (2019) Vascular smooth muscle cells in atherosclerosis. Nat Rev Cardiol 16(12):727-744.

Bentzon J. F., Otsuka F., Virmani R. and Falk E. (2014) Mechanisms of plaque formation and rupture. Circ Res 114(12):1852-1866.

Bodnar J. S., Chatterjee A., Castellani L. W., Ross D. A., Ohmen J., Cavalcoli J., Wu C., Dains K. M., Catanese J., Chu M., Sheth S. S., Charugundla K., Demant P., West D. B., Jong P. and Lusis A. J. (2002) Positional cloning of the combined hyperlipidemia gene Hyplip1. Nat Genet 30(1):110.

Boettger T., Beetz N., Kostin S., Schneider J., Krüger M., Hein L. and Braun T. (2009) Acquisition of the contractile phenotype by murine arterial smooth muscle cells depends on the Mir143/145 gene cluster. J Clin Invest 119(9):2634-2647.

Bowman M. A. H., Gawdzik J., Bukhari U., Husain A. N., Toth P. T., Kim G., Earley J. and Mcnally E. M. (2011) S100A12 in vascular smooth muscle accelerates vascular calcification in apolipoprotein E–null mice by activating an osteogenic gene regulatory program. Arterioscler Thromb Vasc Biol 31(2):337-344.

Butler A., Hoffman P., Smibert P., Papalexi E. and Satija R. (2018) Integrating single-cell transcriptomic data across different conditions, technologies, and species. Nat Biotechnol 36(5):411-420.

Byon C. H., Han T., Wu J. and Hui S. T. (2015) Txnip ablation reduces vascular smooth muscle cell inflammation and ameliorates atherosclerosis in apolipoprotein E knockout mice. Atherosclerosis 241(2):313-321.

Cai T., Sun D., Duan Y., Wen P., Dai C., Yang J. and He W. (2016). WNT/β-catenin signaling promotes VSMCs to osteogenic transdifferentiation and calcification through directly modulating Runx2 gene expression. Exp Cell Res 345(2):206-217.

Cao D., Wang Z., Zhang C. L., Oh J., Xing W., Li S., Richardson J. A., Wang D. Z. and Olson E. N. (2005) Modulation of smooth muscle gene expression by association of histone acetyltransferases and deacetylases with myocardin. Mol Cell Biol 25(1):364-376.

Chakraborty R., Saddouk F. Z., Carrao A. C., Krause D. S., Greif D. M. and Martin K. A. (2019) Promoters to study vascular smooth muscle: mistaken identity? Arterioscler Thromb Vasc Biol 39(4):603-612.

Chappell J., Harman J. L., Narasimhan V. M., Yu H., Foote K., Siomns B. D., Bennett M. R. and Jørgensen H. F. (2016) Extensive proliferation of a subset of differentiated, yet plastic, medial vascular smooth muscle cells contributes to neointimal formation in mouse injury and atherosclerosis models. Circ Res 119(12):1313-1323.

Chen K. S. and DeLuca H. F. (1994) Isolation and characterization of a novel cDNA from HL-60 cells treated with 1, 25-dihydroxyvitamin D-3. Biochim Biophys Acta 1219(1):26-32.

Cheng S. L., Behrmann A., Shao J. S., Ramachandran B., Krchma K., Arredondo Y. B., Kovacs A., Mead M., Maxson R. and Towler D. A. (2014) Targeted reduction of vascular Msx1 and Msx2 mitigates arteriosclerotic calcification and aortic stiffness in LDLR-deficient mice fed diabetogenic diets. Diabetes 63(12):4326-4337.

Cheng S. L., Ramachandran B., Behrmann A., Shao J. S., Mead M., Smith C., Krchma K., Arredondo Y. B., Kovacs A., Kapoor K., Brill L. M., Perera R., Williams B. O. and Towler D. A. (2015) Vascular smooth muscle LRP6 limits arteriosclerotic calcification in diabetic LDLR−/− mice by restraining noncanonical Wnt signals. Circ Res 117(2):142-156.

Cherepanova O. A., Gomez D., Shankman L. S., Swiatlowska P., Williams J., Sarmento O. F., Alencar G. F., Hess D. L., Bevard M. H., Greene E. S., Murgai M., Turner S. D., Geng Y. J., Bekiranov S., Connelly J. J., Tomilin A. and Owens G. K. (2016) Activation of the pluripotency factor OCT4 in smooth muscle cells is atheroprotective. Nat Med 22(6):657-665.

Chutkow W. A., Patwari P., Yoshioka J. and Lee R. T. (2008) Thioredoxin-interacting protein (Txnip) is a critical regulator of hepatic glucose production. J Biol Chem 283(4):2397-2406.

Cordes K. R., Sheehy N. T., White M. P., Berry E. C., Morton S. U., Muth A. N., Lee T. H., Miano J. M., Ivey K. N. and Srivastava D. (2009) miR-145 and miR-143 regulate smooth muscle cell fate and plasticity. Nature 460(7256):705-710.

Davis B. N., Chan M. C., Reno K. E., Weisman A. S., Layne M. D., Lagna G. and Akiko H. (2011) Down-regulation of Krüppel-like Factor-4 (KLF4) by microRNA-143/145 is critical for modulation of vascular smooth muscle cell phenotype by transforming growth factor-β and bone morphogenetic protein 4. J Biol Chem 286(32):28097-28110.

Davis B. N., Hilyard A. C., Nguyen P. H., Lagna G. and Hata A. (2008) Induction of microRNA-221 by platelet-derived growth factor signaling is critical for modulation of vascular smooth muscle phenotype. J Biol Chem 284(6):3728-3738.

Deaton R. A., Gan Q. and Owens G. K. (2009) Sp1-dependent activation of KLF4 is required for PDGF-BB-induced phenotypic modulation of smooth muscle. Am J Physiol Heart Circ Physiol 296(4):H1027-H1037.

Dobnikar L., Taylor A. L., Chappell J., Oldach P., Harman J. L., Oerton E., Dzierzak E., Bennett M. R., Spivakov M. and Jørgensen H. F. (2018) Disease-relevant transcriptional signatures identified in individual smooth muscle cells from healthy mouse vessels. Nat Commun 9(1):4567.

Domingues A., Boisson-Vidal C., Rouge P. M., Dizier B., Sadoine J., Mignon V., Vessieres E., Henrion D., Escriou V., Bigey P., Chaussain C., Smadja D. M. and Nivet-Antoine V. (2020) Targeting endothelial thioredoxin-interacting protein (TXNIP) protects from metabolic disorder-related impairment of vascular function and post-ischemic revascularisation. Angiogenesis 23(2):249-264.

Durham A. L., Speer M. Y., Scatena M., Giachelli C. M. and Shanahan C. M. (2018) Role of smooth muscle cells in vascular calcification: implications in atherosclerosis and arterial stiffness. Cardiovasc Res 114(4):590-600.

Feil S., Fehrenbacher B., Lukowski R., Essmann F., Schulze-Osthoff K., Schaller M. and Feil R. (2014) Transdifferentiation of vascular smooth muscle cells to macrophage-like cells during atherogenesis. Circ Res 115(7):662-667.

Ferreira N. E., Omae S., Pereira A., Rodrigues M. V., Miyakawa A. A., Campos L. C. G., Santos P. C. J. L., Dallan L. A., Martinez T. L., Santos R. D., Mill J. G., Krieger J. E. and Pereira A. C. (2021) Thioredoxin interacting protein genetic variation is associated with diabetes and hypertension in the Brazilian general population. Atherosclerosis 221(1):131-136.

Frismantiene A., Philippova M., Erne P. and Resink T. J. (2018) Smooth muscle cell-driven vascular diseases and molecular mechanisms of VSMC plasticity. Cell Signal 52:48-64.

Garcia-Alonso L., Holland C. H., Ibrahim M. M., Turei D. and Saez-Rodriguez J. (2019) Benchmark and integration of resources for the estimation of human transcription factor activities. Genome Res 29(8):1363-1375.

Gazzerro E., Gangji V. and Canalis E. (1998) Bone morphogenetic proteins induce the expression of noggin, which limits their activity in cultured rat osteoblasts. J Clin Invest 102(12):2106-2114.

Goettsch C., Hutcheson J. D., Hagita S., Rogers M. A., Creager M. D., Pham T., Choi J., Mlynarchik A. K., Pieper B., Kjolby M., Aikawa M. and Aikawa E. (2016) A single injection of gain-of-function mutant PCSK9 adeno-associated virus vector induces cardiovascular calcification in mice with no genetic modification. Atherosclerosis 251:109-118.

Gomez D., Shankman L. S., Nguyen A. T. and Owens G. K. (2013) Detection of histone modifications at specific gene loci in single cells in histological sections. Nat Methods 10(2):171-177.

Gomez D., Swiatlowska P. and Owens G. K. (2015) Epigenetic control of smooth muscle cell identity and lineage memory. Arterioscler Thromb Vasc Biol 35(12):2508-2516.

Greenland P., Bonow R. O., Brundage B. H., Budoff M. J., Eisenberg M. J., Grundy S. M., Lauer M. S., Post W. S., Raggi P., Redberg R. F., Rodgers G. P., Shaw L. J., Taylor A. J. and Weintraub W. S. (2007) ACCF/AHA 2007 clinical expert consensus document on coronary artery calcium scoring by computed tomography in global cardiovascular risk assessment and in evaluation of patients with chest pain: a report of the American College of Cardiology Foundation Clinical Expert Consensus Task Force (ACCF/AHA Writing Committee to Update the 2000 Expert Consensus Document on Electron Beam Computed Tomography) developed in collaboration with the Society of Atherosclerosis Imaging and Prevention and the Society of Cardiovascular Computed Tomography. J Am Coll Cardio 49(3):378-402.

Grootaert M. O. J. and Bennett M. R. (2021) Vascular smooth muscle cells in atherosclerosis: time for a re-assessment. Cardiovascular Res 117(11):2326-2339.

Gu K., Zhang L., Jin T. and Rutherford R. B. (2004) Identification of potential modifiers of Runx2/Cbfa1 activity in C2C12 cells in response to bone morphogenetic protein-7. Cells Tissues Organs 176(1-3):28-40.

Iwai T., Murai J., Yoshikawa H. and Tsumaki N. (2008) Smad7 inhibits chondrocyte differentiation at multiple steps during endochondral bone formation and down-regulates p38 MAPK pathways. J Biol Chem 283(40):27154-27164.

Jacobsen K., Lund M. B., Shim J., Gunnersen S., Füchtbauer E. M., Kjolby M., Carramolino L. and Bentzon J. F. (2017) Diverse cellular architecture of atherosclerotic plaque derives from clonal expansion of a few medial SMCs. JCI Insight 2(19):e95890.

Johnson R. C., Leopold J. A. and Loscalzo J. (2006) Vascular calcification: pathobiological mechanisms and clinical implications. Circ Res 99(10):1044-1059.

Jung H., Kim D. O., Byun J. E., Kim W. S., Kim M. J., Song H. Y., Kim Y. K., Kang D. K., Park Y. J., Kim T. D., Yoon S. R., Lee H. G., Choi E. J., Min S. H. and Choi I. (2016) Thioredoxin-interacting protein

regulates haematopoietic stem cell ageing and rejuvenation by inhibiting p38 kinase activity. Nat Commun 7:13674.

Kanakaris N. K. and Giannoudis P. V. (2008) Clinical applications of bone morphogenetic proteins: current evidence. J Surg Orthop Adv. 17(3):133-146.

Kim J. B., Zhao Q., Nguyen T., Pjanic M., Cheng P., Wirka R., Travisano S., Nagao M., Kundu R. and Quertermous T. (2020) Environment-sensing aryl hydrocarbon receptor inhibits the chondrogenic fate of modulated smooth muscle cells in atherosclerotic lesions. Circulation 142(6):575-590.

Kim S. Y., Suh H. W., Chung J. W., Yoon S. R. and Choi I. (2007) Diverse functions of VDUP1 in cell proliferation, differentiation, and diseases. Cell Mol Immunol 4(5):345-351.

Koenen T. B., Stienstra R., Tits L. J., Graaf J. Stalenhoef A. F. H., Joosten L. A. B., Tack C. J. and Netea M. G. (2011) Hyperglycemia activates caspase-1 and TXNIP-mediated IL-1β transcription in human adipose tissue. Diabetes 60(2):517-524.

Kokabu S., Gamer L., Cox K., Lowery J., Tsuji K., Raz R., Economides A., Katagiri T. and Rosen V. (2012) BMP3 suppresses osteoblast differentiation of bone marrow stromal cells via interaction with Acvr2b. Mol Endocrinol 26(1):87-94.

Kramann R., Goesttsch C., Wongboonsin J., Iwata H., Schneider R. K., Kuppe C., Kaesler N., Chang-Panesso M., Machado F. G., Gratwohl S., Madhurima K., Hutcheson J. D., Jain S., Aikawa E. and Humphreys B. D. (2016) Adventitial MSC-like cells are progenitors of vascular smooth muscle cells and drive vascular calcification in chronic kidney disease. Cell Stem Cell 19(5):628-642.

Lee K. N., Kang H. S., Jeon J. H., Kim E. M., Yoon S. R., Song H., Lyu C. Y., Piao Z. H., Kim S. U., Han Y. H., Song S. S., Lee Y. H., Song K. S., Kim Y. M., Yu D. Y. and Choi I. (2005) VDUP1 is required for the development of natural killer cells. Immunity 22(2):195-208.

Li S., Wang D. Z., Wang Z., Richardson J. A. and Olson E. N. (2003) The serum response factor coactivator myocardin is required for vascular smooth muscle development. Proc Natl Acad Sci U S A 100(16):9366-9370.

Libby P. (2021) The changing landscape of atherosclerosis. Nature 592(7855):524-533.

Libby P. and Pasterkamp G. (2015) Requiem for the 'vulnerable plaque'. Eur Heart J 36(43):2984-2987.

Libby P., Buring J. E., Badimon L., Hansson G. K., Deanfield J., Bittencourt M. S., Tokgözoglu L. and Lewis E. F. (2019) Atherosclerosis. Nat Rev Dis Primers 5(1):56.

Lin M. E., Chen T. M., Wallingford M. C., Nguyen N. B., Yamada S., Sawangmake C., Zhang J., Speer M. Y. and Giachelli C. M. (2016) Runx2 deletion in smooth muscle cells inhibits vascular osteochondrogenesis and calcification but not atherosclerotic lesion formation. Cardiovasc Res 112(2):606-616.

Liu Y. and Min W. (2002) Thioredoxin promotes ASK1 ubiquitination and degradation to inhibit ASK1-mediated apoptosis in a redox activity-independent manner. Circ Res 90(12):1259-1266.

Luu H. H., Song W. X., Luo X., Manning D., Luo J., Deng Z. L., Sharff K. A., Montag A. G., Haydon R. C. and He T. C. (2007) Distinct roles of bone morphogenetic proteins in osteogenic differentiation of mesenchymal stem cells. J Orthop Res 25(5):665-677.

Mack C. P. (2011) Signaling mechanisms that regulate smooth muscle cell differentiation. Arerioscler Thromb Vasc Biol 31(7): 1495-1505.

Mackenzie N. C. W., Staines K. A., Zhu D., Genever P. and Macrae V. E. (2014) miRNA-221 and miRNA-222 synergistically function to promote vascular calcification. Cell Biochem Funct 32(2):209-216.

Manabe I. and Owens G. K. (2001) Recruitment of serum response factor and hyperacetylation of histones at smooth muscle–specific regulatory

regions during differentiation of a novel P19-derived in vitro smooth muscle differentiation system. Circ Res 88(11):1127-1134.

Masters S. L., Dunne A., Subramanian S. L., Hull R. L., Tannahill G. M., Sharp F. A., Becker C., Franchi L., Yoshihara E., Chen Z., Mullooly N., Mielke L. A., Harris J., Coll R. C., Mills K. H. G., Mok K. H., Newsholme P., Nuñez G., Yodoi J., Kahn S. E., Lavelle Ed. C. and O'Neill L. A. J. (2010) Activation of the NLRP3 inflammasome by islet amyloid polypeptide provides a mechanism for enhanced IL-1β in type 2 diabetes. Nat Immunol 11(10):897-904.

McDonald O. G., Wamhoff B. R., Hoofnagle M. H. and Owens G. K. (2006) Control of SRF binding to CArG box chromatin regulates smooth muscle gene expression in vivo. J Clin Invest 116(1):36-48.

Minn A. H., Hafele C. and Shalev A. (2005) Thioredoxin-interacting protein is stimulated by glucose through a carbohydrate response element and induces β-cell apoptosis. Endocrinology 146(5):2397-2405.

Misra A., Feng Z., Chandran R. R., Kabir I., Rotllan N., Aryal B., Sheikh A. Q., Ding L., Qin L., Fernández-Hernando C., Tellides G. and Greif D. M. (2018) Integrin beta3 regulates clonality and fate of smooth muscle-derived atherosclerotic plaque cells. Nat Commun 9(1):2073

Miyazawa K. and Miyazono K. (2017) Regulation of TGF-β family signaling by inhibitory Smads. Cold Spring Harb Perspect Biol 9(3):a022095.

Miyazono K. and Miyazawa K. (2002) Id: a target of BMP signaling. Science's STKE 2002(151):pe40.

Mosse P. R., Campbell G. R., Wang Z. L. and Campbell J. H. (1985) Smooth muscle phenotypic expression in human carotid arteries. I. Comparison of cells from diffuse intimal thickenings adjacent to atheromatous plaques with those of the media. Lab Invest 53(5):556-562.

Murray C. J. L. and Lopez A. D. (2013) Measuring the global burden of disease. N Engl J Med 369(5):448-457.

Nagao M., Lyu Q., Zhao Q., Wirka R. C., Bagga J., Nguyen T., Cheng P., Kim J. B., Pjanic M., Miano J. M. and Quertermous T. (2020) Coronary disease-associated gene TCF21 inhibits smooth muscle cell differentiation by blocking the myocardin-serum response factor pathway. Circ Res 126(4):517-529.

Naik V., Leaf E. M., Hu H., Yang H. Y., Nguyen N. B., Giachelli C. M. and Speer M. Y. (2012) Sources of cells that contribute to atherosclerotic intimal calcification: an in vivo genetic fate mapping study. Cardiovasc Res 94(3):545-554.

Nakagawa Y., Ikeda K., Akakabe Y., Koide M., Uraoka M., Yutaka K-T., Kurimoto-Nakano R., Takahashi T., Yamada H., Okigaki M. and Matsubara H. (2010) Paracrine osteogenic signals via bone morphogenetic protein-2 accelerate the atherosclerotic intimal calcification in vivo. Arterioscler Thromb Vasc Biol 30(10):1908-1915.

Nakashima Y., Wight T. N. and Sueishi K. (2008) Early atherosclerosis in humans: role of diffuse intimal thickening and extracellular matrix proteoglycans. Cardiovasc Res 79(1):14-23.

New S. E. P., Goettsch C., Aikawa M., Marchini J. F., Shibasaki M., Yabusaki K., Libby P., Shanahan C. M., Croce K. and Aikawa E. (2013) Macrophage-derived matrix vesicles: an alternative novel mechanism for microcalcification in atherosclerotic plaques. Circ Res 113(1):72-77.

Noël D., Gazit D., Bouquet C., Apparailly F., Bony C., Plence P., Millet V., Turgeman G., Perricaudet M., Sany J. and Jorgensen C. (2004) Short-term BMP-2 expression is sufficient for in vivo osteochondral differentiation of mesenchymal stem cells. Stem Cells 22(1):74-85.

Oka S. i., Liu W., Masutani H., Hirata H., Shinkai Y., Yamada S. I., Yoshida T., Nakamura H. and Yodoi J. (2006) Impaired fatty acid utilization in thioredoxin binding protein-2 (TBP-2)-deficient mice: a unique animal model of Reye syndrome. FASEB J. 20(1):121-123.

Owens G. K. (1995) Regulation of differentiation of vascular smooth muscle cells. Physiol Rev 75(3):487-517.

Pan H., Xue C., Auerbach B., Fan J., Bashore A. C., Cui J., Yang D. Y., Trignano S. B., Liu W., Shi J., Ihuegbu C. O., Bush E. C., Worley J., Vlahos L., Laise P., Solomon R. A., Connolly E. S., Califano A., Sims P. A., Zhang H., Li M. and Reilly M. P. (2020) Single-cell genomics reveals a novel cell state during smooth muscle cell phenotypic switching and potential therapeutic targets for atherosclerosis in mouse and human. Circulation 142(21):2060-2075.

Park H. S., Song J. W., Park J. H., Lim B. K., Moon O. S., Son H. Y., Lee J. H., Gao B., Won Y. S. and Kwon H. J. (2021) TXNIP/VDUP1 attenuates steatohepatitis via autophagy and fatty acid oxidation. Autophagy 17(9):2549-2564.

Patwari P., Higgins L. J., Chutkow W. A., Yoshioka J. and Lee R. T. (2006) The interaction of thioredoxin with Txnip: evidence for formation of a mixed disulfide by disulfide exchange. J Biol Chem 281(31):21884-21891.

Qayyum N., Haseeb M., Kim M. S. and Choi S. (2021) Role of thioredoxin-interacting protein in diseases and its therapeutic outlook. Int J Mol Sci 22(5):2754.

Qiu P., Feng X. H. and Li L. (2003) Interaction of Smad3 and SRF-associated complex mediates TGF-β1 signals to regulate SM22 transcription during myofibroblast differentiation. J Mol Cell Cardiol 35(12):1407-1420.

Razzouk S. and Sarkis R. (2012) BMP-2: biological challenges to its clinical use. N Y State Dent J 78(5):37.

Rodríguez-Carballo E., Gámez B. and Ventura F. (2016) p38 MAPK signaling in osteoblast differentiation. Front Cell Dev Biol 4:40.

Sanvitale C. E., Kerr G., Chaikuad A., Ramel M. C., Mohedas A. H., Reichert S., Wang Y., Triffitt J. T., Cuny G. D., Yu P. B., Hill C. S. and Bullock A. N (2013) A new class of small molecule inhibitor of BMP signaling. PloS One 8(4):e62721.

Sato Y., Finn A. V. and Virmani R. (2021) Calcified nodule: A rare but important cause of acute coronary syndrome with worse clinical outcomes. Atherosclerosis 318:40-42.

Schiller N. K., Kubo N., Boisvert W. A. and Curtiss L. K. (2001) Effect of γ-irradiation and bone marrow transplantation on atherosclerosis in LDL receptor-deficient mice. ATVB 21(10):1674-1680.

Shah S. S. and Kumar S. (2021) Adaptors as the regulators of HECT ubiquitin ligases. Cell Death Differ 28(2):455-472.

Shalev A. (2014). Minireview: Thioredoxin-interacting protein: regulation and function in the pancreatic β-cell. Mol Endocrinol 28(8):1211-1220.

Shalev A., Pise-Masison C. A., Radonovich M., Hoffmann S. C., Hirshberg B., Brady J. N. and Harlan D. M. (2002) Oligonucleotide microarray analysis of intact human pancreatic islets: identification of glucose-responsive genes and a highly regulated TGFβ signaling pathway. Endocrinology 143(9):3695-3698.

Shankman L. S., Gomez D., Cherepanova O. A., Salmon M., Alencar G. F., Haskins R. M., Swiatlowska P., Newman A. A. C., Greene E. S., Straub A. C., Isakson B., Randolph G. J. and Owens G. K. (2015) KLF4-dependent phenotypic modulation of smooth muscle cells has a key role in atherosclerotic plaque pathogenesis. Nat Med 21(6):628-637.

Shen B., Wei A., Whittaker S., Williams L. A., Tao H., Ma D. D. F. and Diwan A. D. (2010) The role of BMP-7 in chondrogenic and osteogenic differentiation of human bone marrow multipotent mesenchymal stromal cells in vitro. J Cell Biochem 109(2):406-416.

Shi X., Gao J., Lv Q., Cai H., Wang F., Ye R. and Liu X. (2020) Calcification in atherosclerotic plaque vulnerability: friend or foe?. Front Physiol 11:56.

Shimada K., Suzuki N., Ono Y., Tanaka K., Maeno M. and Ito K. (2008) Ubc9 promotes the stability of Smad4 and the nuclear accumulation of Smad1 in osteoblast-like Saos-2 cells. Bone 42(5):886-893.

Spindel O. N., Burke R. M., Yan C. and Berk B. C. (2014) Thioredoxin-interacting protein is a biomechanical regulator of Src activity: key role in endothelial cell stress fiber formation. Circ Res 114(7):1125-1132.

Sugane H., Kataoka Y., Otsuka F., Nakaoku Y., Nishimura K., Nakano H., Murai K., Honda S., Hosoda H., Matama H., Doi T., Nakashima T., Fujino M., Nakao K., Yoneda S., Tahara Y., Asaumi Y., Noguchi T., Kawai K. and Yasuda S. (2021) Cardiac outcomes in patients with acute coronary syndrome attributable to calcified nodule. Atherosclerosis 318:70-75.

Sun Y., Byon C. H., Yuan K., Chen J., Mao X., Heath J. M., Javed A., Zhang K., Adnerson P. G. and Chen Y. (2012) Smooth muscle cell–specific Runx2 deficiency inhibits vascular calcification. Circ Res 111(5):543-552.

Tsaousi A., Mill C. and George S. J. (2011) The Wnt pathways in vascular disease: lessons from vascular development. Curr Opin Lipidol 22(5):350-357.

Tsubakihara Y., Hikita A., Yamamoto S., Matsushita S., Matsushita N., Oshima Y., Miyazawa K. and Imamura T. (2015) Arkadia enhances BMP signalling through ubiquitylation and degradation of Smad6. J Biochem 158(1):61-71.

Tsuji K., Cox K., Gamer L., Graf D., Economides A. and Rosen V. (2010) Conditional deletion of BMP7 from the limb skeleton does not affect bone formation or fracture repair. J Orthop Res 28(3):384-389.

Turturro F., Friday E. and Welbourne T. (2007) Hyperglycemia regulates thioredoxin-ROS activity through induction of thioredoxin-interacting protein (TXNIP) in metastatic breast cancer-derived cells MDA-MB-231. BMC Cancer 7:96.

Venegas-Pino DE., Banko N., Khan M. I., Shi Y. and Werstuck GH. (2013) Quantitative Analysis and Characterization of Atherosclerotic Lesions in the Murine Aortic Sinus. JoVE 82:e50933.

Virmani R., Kolodgie F. D., Burke A. P., Farb A. and Schwartz S. M. (2000) Lessons from sudden coronary death: a comprehensive morphological classification scheme for atherosclerotic lesions. Arterioscler Thromb Vasc Biol 20(5):1262-1275.

Vozenilek A. E., Blackburn C. M. R., Schilke R. M., Chandran S., Castore R., Klein R. L. and Woolard M. D. (2018) AAV8-mediated overexpression of mPCSK9 in liver differs between male and female mice. Atherosclerosis 278:66-72.

Wan D. C., Pomerantz J. H., Brunet L. J., Kim J. B., Chou Y. F., Wu B. M., Harland R., Blau H. M. and Longaker M. T. (2007) Noggin suppression enhances in vitro osteogenesis and accelerates in vivo bone formation. J Biol Chem 282(36): 26450-26459.

Wang H., Zhao H., Zhu H., Li Y., Tang J., Li Y. and Zhou B. (2021) Sca1+ cells minimally contribute to smooth muscle cells in atherosclerosis. Circ Res 128(1):133-135.

Wang R. N., Green J., Wang Z., Deng Y., Qiao M., Peabody M., Zhang Q., Ye J., Yan Z., Denduluri S., Idowu O., Li M., Shen C., Hu A., Haydon R. C., Kang R., Mok J., Lee M. J., Luu H. L. and Shi L. L. (2014) Bone morphogenetic protein (BMP) signaling in development and human diseases. Genes Dis. 1(1):87-105.

Wang X. Q., Nigro P., World C., Fujiwara K., Yan C. and Berk B. C. (2012) Thioredoxin interacting protein promotes endothelial cell inflammation in response to disturbed flow by increasing leukocyte adhesion and repressing Kruppel-like factor 2. Circ Res 110(4):560-568.

Wang Z., Wang D. Z., Hockemeyer D., McAnally J., Nordheim A. and Olson E. N. (2004) Myocardin and ternary complex factors compete for SRF to control smooth muscle gene expression. Nature 428(6979):185-189.

Wirka R. C., Wagh D., Paik D. T., Pjanic M., Nguyen T., Miller C. L., Kundu R., Nagao M., Coller J., Koyano T. K., Fong R., Woo Y. J., Liu B., Montgomery S. B., Wu J. C., Zhu K., Chang R., Alamprese M., Tallquist M. D., Kim J. B. and Quertermous T. (2019) Atheroprotective roles of smooth muscle cell phenotypic modulation and the TCF21

disease gene as revealed by single-cell analysis. Nat Med 25(8):1280-1289.

Woldt E., Terrand J., Milh M., Matz R. L., Bruban V., Coudane F., Foppolo S., Asmar Z. E., Chollet M. E., Ninio E., Bednarczyk A., Thiersé D., Schaeffer C., Dorsselaer A. V., Boudier C., Wahli W., Chambon P., Metzger D., Herz J. and Boucher P. (2012) The nuclear hormone receptor PPARγ counteracts vascular calcification by inhibiting Wnt5a signalling in vascular smooth muscle cells. Nat Commun 3:1077.

Wu M., Chen G. and Li Y. P. (2016) TGF-β and BMP signaling in osteoblast, skeletal development, and bone formation, homeostasis and disease. Bone Res 4:16009.

Xiang G., Seki T., Schuster M. D., Witkowski P., Boyle A. J., See F., Martens T. P., Kocher A., Sondermeijer H., Krum H. and Itescu S. (2005) Catalytic degradation of vitamin D up-regulated protein 1 mRNA enhances cardiomyocyte survival and prevents left ventricular remodeling after myocardial ischemia. J Biol Chem 280(47):39394-39402.

Yoshida T. and Hayashi M. (2014) Role of Krüppel-like factor 4 and its binding proteins in vascular disease. J Atheroscler Thromb 21(5):402-413.

Yoshida T., Sinha S., Dandré F., Wamhoff B. R., Hoofnagle M. H., Kremer B. E., Wang D. Z., Olson E. N. and Owens G. K. (2003) Myocardin is a key regulator of CArG-dependent transcription of multiple smooth muscle marker genes. Circ Res 92(8):856-864.

Yoshida T., Yamashita M. and Hayashi M. (2012) Krüppel-like factor 4 contributes to high phosphate-induced phenotypic switching of vascular smooth muscle cells into osteogenic cells. J Biol Chem 287(31):25706-25714.

Yoshihara E., Masaki S., Matsuo Y., Chen Z., Tian H. and Yodoi J. (2014) Thioredoxin/Txnip: redoxisome, as a redox switch for the pathogenesis of diseases. Front Immunol 4:514.

Yukita A., Hosoya A., Ito Y., Katagiri T., Asashima M. and Nakamura H. (2012) Ubc9 negatively regulates BMP-mediated osteoblastic differentiation in cultured cells. Bone 50(5):1092-1099.

Zhou R., Tardivel A., Thorens B., Choi I. and Tschopp J. (2010) Thioredoxin-interacting protein links oxidative stress to inflammasome activation. Nat Immunol 11(2):136-140.

감사의 글

학부생 실습 시절 현미경으로 병변 조직을 보고 많은 흥미를 느껴 병리학실에 처음 문을 두드렸었던 기억이 납니다. 대학원 입학 이후 7 년이라는 적지 않은 시간이 흘렀으며 그동안 많은 배움과 변화의 과정이 있었고, 본 학위 논문이 좋은 결실로 마무리되어 정말 기쁩니다. 이 과정들 동안 제가 좋은 결실을 맺도록 힘써주시고 지도해주신 김대용 교수님께 진심으로 감사의 말씀을 드립니다.

연구를 함에 있어 여러 난관들이 필연적으로 발생하기 마련이지만, 돌이켜보면 저에게는 상당히 흥미롭고 재미있는 시간들이었습니다. 이 자리를 빌어 저에게 지적 자극과 영감을 주시고 아낌없는 지원을 해주신 최재훈 교수님께 진심으로 감사드립니다. 또한 귀한 시간을 내어 학위 논문을 심사해주시고 아낌없는 조언들을 해 주신 김용백 교수님, 이소영 교수님, 최양규 교수님께 감사드립니다.

본 논문에서 “나 (I)”라는 표현을 사용하였지만, 연구가 형태를 갖추어 결과로 나오기까지 다른 수많은 사람들의 도움이 있었습니다. 본 연구가 결실을 맺도록 생물정보학 부분을 맡아 저와 함께 많은 노력을 해주신 경동수 박사님께 이 자리를 빌어 감사드립니다. 함께 생활하며 저에게 많은 도움을 준 두민이형, 정섭이, 경희 누나, 그리고 성현이에게 고맙다는 말 전합니다. 또한 바쁜데도 불구하고 시간을 내어 실험을 도와주고 조언을 준 한양대의 승현이, 규성이형, 민규, 기병이형에게도 고맙다는 말 전합니다. 끝으로 여기에 다 적지 못한 저에게 도움을 주었던 모든 분들에게 감사를 전하고 싶습니다.

마지막으로 지금과 같은 제 자신이 있도록 항상 저를 지지해주고 응원해주신 우리 가족 아빠, 어머니, 그리고 동생 상경이에게 사랑한다는 말 전합니다.